

**Fluorescence based studies on  
neuronal processes**

Dissertation for the award of the degree  
"Doctor rerum naturalium"  
of the Georg-August University Göttingen  
submitted by

**Sabrina Schröder**

from Kirch Lengern, Germany  
Göttingen, 2014



I hereby declare that the Ph.D. thesis entitled "Fluorescence based studies on neuronal processes" has been written independently and with no other sources and aids than quoted.

Göttingen, June, 2014



Members of the Thesis Committee :

**Prof. Dr. Peter Jomo Walla (Referee)**

Workgroup Biomolecular Spectroscopy and Single Molecule Detection  
Max-Planck Institute for biophysical Chemistry, Göttingen

and

Department Biophysical Chemistry  
Institute for physical and theoretical Chemistry  
Technische Universität Carola-Wilhelmina zu Braunschweig

**Prof. Dr. Ulf Diederichsen (Referee)**

Institute for Organic and Biomolecular Chemistry  
University of Göttingen

**Prof. Dr. Jörg Enderlein**

Single Molecule Spectroscopy and Imaging for Biophysics and Complex Systems  
University of Göttingen



# Contents

<b>1</b>	<b>Motivation &amp; Summary</b>	<b>1</b>
<b>2</b>	<b>Introduction</b>	<b>3</b>
2.1	Presynaptic Processes . . . . .	3
2.2	SNARE proteins: The fusion machinery . . . . .	3
2.2.1	Synaptotagmin-1: triggering exocytosis . . . . .	4
2.2.2	Two models explain the role of calcium in exocytosis . . . . .	6
2.3	Methods in optical spectroscopy . . . . .	8
2.3.1	The basic principle of fluorescence . . . . .	8
2.3.2	Förster-resonance-energy-transfer (FRET) . . . . .	9
2.3.3	Fluorescence-correlation-spectroscopy . . . . .	11
2.3.4	Optical trapping . . . . .	15
2.4	Lasers . . . . .	17
2.5	Physical Chemistry . . . . .	19
2.5.1	1 <sup>st</sup> order kinetics . . . . .	19
2.5.2	Hill equation . . . . .	20
2.5.3	Adsorption isotherms . . . . .	20
<b>3</b>	<b>Material and Methods</b>	<b>22</b>
3.1	Material . . . . .	22
3.1.1	Chemicals . . . . .	22
3.1.2	Proteins . . . . .	22
3.1.3	Antibodies . . . . .	23
3.1.4	Phospholipids and cholesterol . . . . .	24
3.1.5	Further fluorescence dyes and components . . . . .	24
3.1.6	Buffers . . . . .	25
3.1.7	Software . . . . .	26
3.1.8	Instruments . . . . .	26
3.2	Methods . . . . .	28
3.2.1	Determination of calcium concentration . . . . .	28
3.2.2	SDS PAGE and Western Blot . . . . .	28
3.2.3	Reconstitution of proteins into SUVs . . . . .	28
3.2.4	Reconstitution of $\Delta$ N-complex into LUVs . . . . .	29
3.2.5	General FCCS experiments . . . . .	30
3.2.6	Optical trapping experiments . . . . .	30
3.2.7	TPE confocal fluorescence microscopy setup . . . . .	31

<b>4</b>	<b>Results</b>	<b>33</b>
4.1	Synaptotagmin-1 is a distance regulator . . . . .	33
4.1.1	Synaptotagmin-1 binding depends on ionic strength conditions and liposome concentration . . . . .	34
4.1.2	ATP can enhance liposome tethering . . . . .	40
4.1.3	Synaptotagmin-1 acts as a distance regulator when bound to $\text{PiP}_2$ and is affected by electrostatic screening through ATP . . . . .	43
4.1.4	Synaptotagmin-1 induced distance regulation is affected by synaptobrevin 2 . . . . .	51
4.1.5	The concentration of $\text{PiP}_2$ and $\text{Ca}^{2+}$ determine the amount of tethered liposomes . . . . .	56
4.1.6	Syntaxin 1A circumvents synaptotagmin-1 dependent distance regulation . . . . .	58
4.1.7	Both $\text{C}_2$ domains of synaptotagmin-1 are required to maintain proper distance regulation . . . . .	60
4.2	Optical trapping . . . . .	65
4.2.1	Characterization of the setup . . . . .	65
4.2.2	Characterization of the effective focal volume . . . . .	66
4.2.3	Validation of optically trapped LUVs . . . . .	69
4.2.4	Oregon green lifetime . . . . .	71
4.2.5	Adsorption isotherms of synaptotagmin-1 SUVs . . . . .	73
4.2.6	Distance regulation in optical trapping . . . . .	77
4.2.7	Fusion of SUVs to optically trapped LUVs . . . . .	80
<b>5</b>	<b>Discussion</b>	<b>88</b>
5.1	Synaptotagmin-1 is a distance regulator . . . . .	88
5.1.1	The influence of ionic strength conditions and liposome concentration . . . . .	88
5.1.2	The influence of anionic lipid concentration and ATP . . . . .	90
5.1.3	Analyzing the role of $\text{PiP}_2$ and ATP with the Hill model . . . . .	92
5.1.4	The role of $\text{PiP}_2$ in distance regulation . . . . .	94
5.1.5	The role of the different functional domains of synaptotagmin-1 . . . . .	95
5.1.6	Circumvention of synaptotagmin-1 based distance regulation . . . . .	97
5.1.7	Distance regulation in the recycling and/or reserve pool . . . . .	98
5.1.8	Summary of findings . . . . .	100
5.2	Optical trapping . . . . .	101
5.2.1	Optical trapping conditions . . . . .	101
5.2.2	Applications of optical trapping . . . . .	103
5.2.3	Summary of findings . . . . .	105
<b>6</b>	<b>Outlook</b>	<b>106</b>
<b>7</b>	<b>Appendix</b>	<b>108</b>
7.1	Error analysis . . . . .	108
7.1.1	Fraction bound $f_{bound}$ . . . . .	108
7.1.2	Linear regression . . . . .	108
7.1.3	Normalized fluorescence lifetime changes . . . . .	108

---

7.1.4	Characterization of the setup . . . . .	109
7.1.5	Langmuir coefficient . . . . .	109
7.1.6	Diffusion coefficient . . . . .	109
7.2	Matlab codes . . . . .	110
7.2.1	MatLab codes for displaying time trace . . . . .	110
7.2.2	MatLab codes for FCS . . . . .	111
7.2.3	MatLab codes for fluorescence lifetime analysis . . . . .	111
7.3	Abbreviations and Symbols . . . . .	112



# Chapter 1

## Motivation & Summary

Synaptotagmin-1 is a calcium dependent trigger of the SNARE-fusion machinery that ultimately upon stimulation executes signal transmission between neurons. However, the actual mechanistic function and the role of different calcium binding domains of synaptotagmin-1 still remain unclear. The original motivation for this study was therefore based on interesting findings and suggestions of three previous publications addressing the role of synaptotagmin-1 in exocytosis [121, 119, 83]. In one of these studies, it has been proposed that the triggering function of synaptotagmin-1 is based on a membrane distance regulation mechanism [119]. In addition, it has been shown that *cis*-membrane binding of synaptotagmin-1 is favoured over *trans*-binding [121], but that fusion nonetheless can be enhanced by ATP [83]. It remains unclear whether ATP prevents *cis*-binding directly or acts at a later stage by just pushing the equilibrium further towards the fused state. Furthermore, the role of synaptotagmin-1 in exocytotic priming and triggering is still elusive [49]. Here, two models have been proposed with each of them accounting for conflicting findings that have been made in the past [49]. The authors of the above mentioned articles used different fluorescence techniques like fluorescence anisotropy [83], Förster-resonance-energy-transfer [119] and Fluorescence-cross-correlation-spectroscopy (FCCS) [121]. The present study aims to find further evidence for or against a distance regulation function of synaptotagmin-1 with the help of additional FCCS studies combined with fluorescence lifetime analysis. In fact, the results presented in this thesis demonstrate that synaptotagmin-1 can act as a distance regulator when bound to  $\text{PiP}_2$  by synchronous alterations in tethering and membrane distance shortening. Here, synchronous tethering to an opposing lipid bilayer is furthermore achieved by the  $\text{C}_2\text{B}$  domain of synaptotagmin-1. Calcium ions, which are necessary for tethering, trigger this  $\text{PiP}_2$  dependent distance regulation function. Despite the cooperative behaviour of synaptotagmin-1 towards binding  $\text{Ca}^{2+}$  in the presence of  $\text{PiP}_2$  [118], a reduction of the intermembrane distance occurs proportional to tethering. However, high  $\text{PiP}_2$  concentrations increase the base level of tethering. Moreover, the distance regulation function of synaptotagmin-1 is circumvented by the presence of syntaxin 1A.

In addition, a new approach to study tethering and fusion processes by optical trapping is introduced. This method reveals the first way of studying exocytotic processes at plasma membrane (PLM) analogues without introducing

any artifacts like an enhanced surface tension. It is demonstrated that optical trapping of large unilamellar vesicles ( $d= 110$  nm) is possible when filled with 2 M sucrose. Here, the combination of a CW and a TP laser beam, both operating at 800 nm, permits for super-position of the trapping center with the TPE-volume. Hence, trapping and FCS can be combined, permitting to study processes in real-time. A conceivable application arising from the combination of both laser beams is to study retention times of liposomal tethering which may be analyzed in terms of adsorption isotherms. Furthermore, fusion to a single LUV can be monitored on a min timescale.

## Chapter 2

# Introduction

### 2.1 Presynaptic Processes

Exocytosis of synaptic vesicle cargo into the synaptic cleft succeeds in signal transduction from one nerve cell to the other [49]. As a result of an incoming action potential signal transducers like e.g. glutamate are released upon  $\text{Ca}^{2+}$  stimulation. The synaptic vesicle proteins as well as the proteins located on the plasma membrane site that maintain exocytosis have been investigated extensively [112, 21, 101]. Wherein the SNARE proteins, consisting of syntaxin 1, synaptobrevin and SNAP 25, were identified as the core fusion machinery [49]. The role of other proteins - like synaptotagmin-1 - is not entirely clear yet. Synaptotagmin-1 is thought of as being capable of priming and triggering the actual assembly of the fusion machinery [49]. However, the underlying mechanism of how  $\text{Ca}^{2+}$  influx primes and triggers exocytosis of synaptic vesicle cargo still remains unclear [49]. Within the past years a multitude of conflicting results concerning the role of synaptotagmin-1 and other proteins have been reported. A hierarchy of the sequential arrangement of protein action and interaction ranging from vesicle priming towards  $\text{Ca}^{2+}$  triggered exocytosis is still missing [49]. A major challenge of assigning the particular role of proteins like synaptotagmin-1 within synaptic vesicle exocytosis is the speed of the  $\text{Ca}^{2+}$  response. Priming, triggering and fusion take place on a millisecond timescale [49, 29]. Moreover, it has been shown that the synapse adheres distinct pools of exocytotic vesicles [93, 25]. Here, the rise in action potential determines whether a synaptic vesicle species is released or not [93, 25]. Profound knowledge of the sequence of events is currently emerging. So far, two potential pathways for synaptic vesicle priming and triggering have been proposed [49] which are explained in further detail in subsection 2.2.2.

### 2.2 SNARE proteins: The fusion machinery

SNARE proteins are members of a highly conserved protein family among animals [49, 102, 103]. The SNARE motif consists of an extended coiled-coil stretch that is formed by syntaxin-1, synaptobrevin and SNAP25. There are four subtypes of this SNARE motif called: Qa, Qb, Qc and R-SNARE

[54, 49]. In most cases this motif is connected to a C-terminal transmembrane domain (TMD) via a flexible linker [1, 49]. In case of SNAP25 its Qb and Qc motifs are not connected via a trans membrane domain. Instead, they are connected via a linker carrying a palmitoylation [49]. Syntaxin-1 contains an antiparallel three-helix-bundle, the Habc domain and at its N-terminus the N-peptide [15, 49]. While SNAP25 and syntaxin-1 are located on the presynaptic plasma membrane, synaptobrevin is embedded in synaptic vesicles [49, 112]. In fact, synaptobrevin represents the most abundant synaptic vesicle protein [112]. SNARE assembly, which is accomplished by forming a bundle of four parallel  $\alpha$ -helices, is a prerequisite for synaptic vesicle exocytosis [109, 49]. This molecular zipper is formed from the N-terminal (*trans*) to the C-terminal (*cis*) end which reduces the intermembrane distance [49, 76]. This docked intermediate is also known as the *trans*-complex, because the C-terminal trans membrane domains of the proteins are in separate membranes. Thus, bringing the membranes tightly together [49, 76]. Consecutively the trans membrane domains of syntaxin-1 and synaptobrevin come together, merging the two membranes by forming the *cis*-complex [49, 52]. Disassembly of the zippered state requires a specialized protein called *N*-Ethylmaleimide-sensitive factor (NSF) and its cofactor, the soluble NSF attachment protein (SNAP) [49, 133].

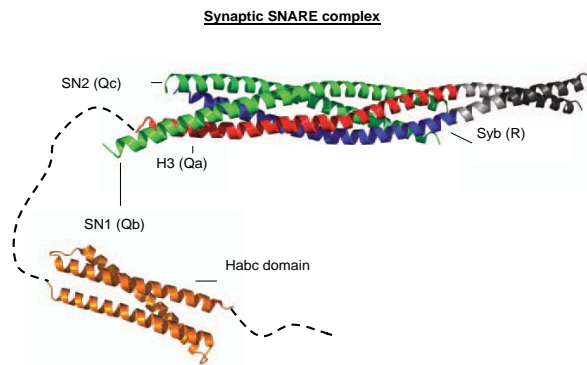


Figure 2.1: Structure of SNARE complex. Synaptobrevin (blue), syntaxin with its H3 (red) and Habc (orange) domain and SNAP25 (green) with its Qb and Qc motif form the SNARE motif [109]

### 2.2.1 Synaptotagmin-1: triggering exocytosis

Synaptotagmins belong to a rather large protein family which play a pivotal role in all kinds of cellular exocytotic processes [49]. Neuronal exocytosis is controlled by synaptotagmin-1. The protein senses a rise in synaptic  $\text{Ca}^{2+}$  concentration upon stimulus which results in fast exocytosis. Calcium ions are bound via its two  $\text{C}_2$  domains,  $\text{C}_2\text{A}$  and  $\text{C}_2\text{B}$ , which coordinate three and two  $\text{Ca}^{2+}$ , respectively. In case of bound  $\text{Ca}^{2+}$ , the  $\text{C}_2$  domains can bind to anionic lipids like phosphatidylserine (PS), therefore completing the coordination of  $\text{Ca}^{2+}$  [44].

In addition, the C<sub>2</sub>B domain possesses a basic poly-lysine patch, called KKKK-patch. This poly-lysine patch in particular binds to phosphatidylinositol-(4,5)-bisphosphate (PiP<sub>2</sub>), but can also bind to other anionic lipids as PS. [6, 49]. Binding to PiP<sub>2</sub> increases the affinity of synaptotagmin-1 for Ca<sup>2+</sup> in a co-operative manner [118]. Besides all this, synaptotagmin-1 can bind to either free or SNARE complexed syntaxin [17, 49, 91]. Moreover, synaptotagmin-1 is anchored to the synaptic vesicle membrane by a transmembrane domain [49]. The crystal structure of the C<sub>2</sub> domains reveal two rigid, oval shaped  $\beta$ -sandwiches. Unfortunately, the whole crystal structure of synaptotagmin-1, including the transmembrane domain and the linker region, has not yet been resolved.

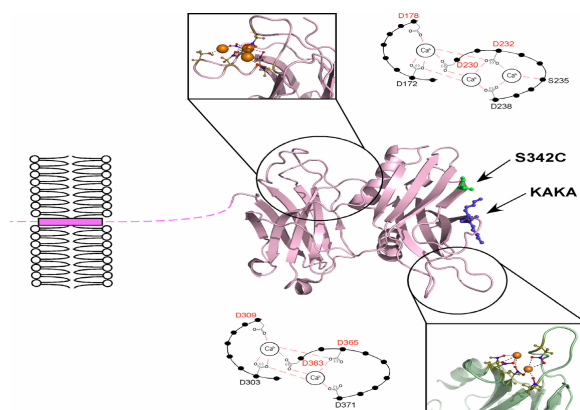


Figure 2.2: Structure of synaptotagmin-1 [87]. The Ca<sup>2+</sup> (orange) binding domains, C<sub>2</sub>A (pink) and C<sub>2</sub>B (green) as well as the poly-lysine patch (KAKA) are highlighted.

Recently it has been shown that synaptotagmin-1 can also bind in *cis* to its own host membrane and that *cis*-binding is actually favoured over *trans*-binding in liposomes, demonstrating that membrane binding is primarily electrostatically controlled [121]. Compounds like adenosine triphosphate (ATP) have been proposed to account for electrostatic screening of synaptotagmin-1 and hence increased synaptic vesicle fusion [83]. Here, ATP is thought to chelate Ca<sup>2+</sup> and thus compete with Ca<sup>2+</sup>-dependent membrane binding of synaptotagmin-1 by shielding the coordination site of acidic phospholipids [83]. So far it is still not clear at which step of priming, triggering and fusion ATP contributes to increased fusion rates. Furthermore, synaptotagmin-1 has been suggested to serve as a distance regulator acting upstream of SNARE nucleation [119]. However,

this study was performed under non-physiological conditions in order to resolve potentially hidden electrostatic interactions. Therefore, it still remains unclear whether or not this behaviour has to be taken into account in case of cellular exocytosis at all.

### 2.2.2 Two models explain the role of calcium in exocytosis

As mentioned beforehand, two models have been employed in order to describe synaptotagmin-1 based priming and triggering of vesicle fusion [49]. This is because a multitude of studies have revealed conflicting observations concerning the role of synaptotagmin in vesicle exocytosis [49]. Each of these two models aims to address and combine these previous findings, though [49]. In the first pathway the synaptic vesicle arrests in a docked state via partially zippered SNARE proteins. Here, complexin ensures the proper complex formation. Upon an action potential the  $\text{Ca}^{2+}$  concentration increases and complexin and probably also Munc18 dissociate from this complex [49]. Upon  $\text{Ca}^{2+}$  influx, synaptotagmin tethers to the plasma membrane which finally leads to fusion and release of the synaptic vesicle cargo into the synaptic cleft [49]. The basis for this model is e.g. given by the observation that different SNARE mutations exhibit an effect on fusion kinetics [49, 105, 128, 130]. Nevertheless, the model disregards the effects of synaptotagmin and/or complexin which have been shown to influence SNARE assembly *in vitro* [14, 27, 49]. Additionally, other studies state that vesicles can even undergo fusion in the absence of calcium with only one SNARE complex included in the fusion reaction [49, 117]. In contrast, the second model describes a synaptic vesicle being docked to the plasma membrane through synaptotagmin [49]. Here, synaptotagmin can either bind to  $\text{PiP}_2$  clusters that colocalize with syntaxin or directly to the SNARE proteins in a calcium independent manner [49]. This model is supported by the high cooperativity of synaptotagmin towards  $\text{Ca}^{2+}$  when bound to  $\text{PiP}_2$  [49, 118]. Upon calcium influx, synaptotagmin-1 brings both membranes closer together, thereby permitting for full SNARE assembly. Munc18 is released and substituted by complexin, resulting in fusion [49].

Both models take into account that in any case full zippering seems to be prevented either due to an energy barrier or by an interfering protein with the most promising prime candidates being complexin or synaptotagmin [49]. For synaptotagmin there are in total five potential priming modes discussed [49]:

1. The fusion clamp model: Synaptotagmin loosens from the zippered SNARE complex [19].
2. Synaptotagmin binds to the zippered SNARE complex and replaces the inhibitory complexin [132].
3. Synaptotagmin binds directly to the plasma membrane which positions synaptobrevin in close proximity to the SNAREs. The lipid bilayer is then destabilized at the fusion site [106, 64, 131].

4. Synaptotagmin binds directly to the plasma membrane and increases curvature stress. It displaces lipids in the plasma membrane [72, 45].
5. Synaptotagmin binds directly to the plasma membrane. Due to its positively charged C<sub>2</sub> domains it reduces the intermembrane distance, allowing for SNARE complex formation [2].

### **Two Models describing the action of synaptic vesicle fusion**

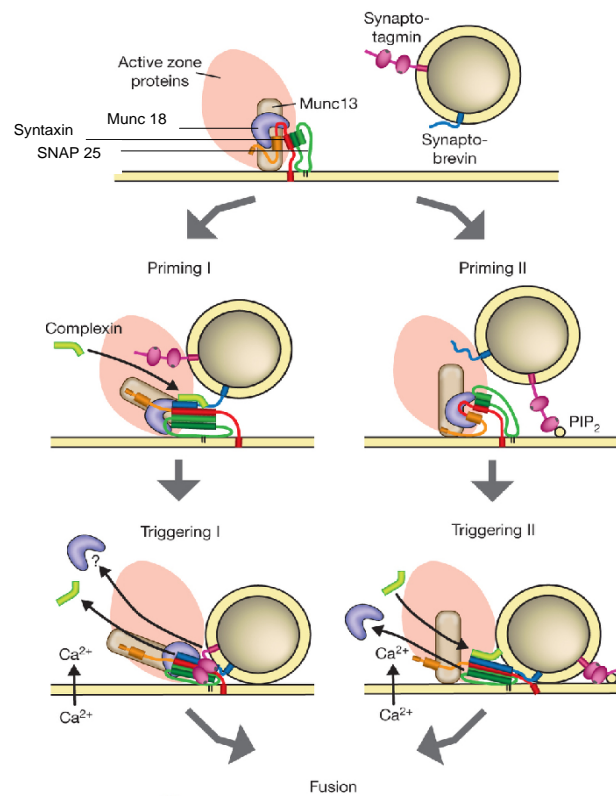


Figure 2.3: Currently there are two alternative models describing the process of priming, triggering and final fusion of a neuronal vesicle with the plasma membrane. Priming I includes the formation of a partially zippered SNARE complex. Upon Ca<sup>2+</sup> influx synaptotagmin assembles with the SNARE complex resulting in fusion via displacement of complexin. Priming II suggests a preliminary docking of synaptotagmin to PIP<sub>2</sub>, followed by distance reduction of vesicle and plasma membrane and, as a consequence of Ca<sup>2+</sup> influx, SNARE assembly and exocytosis [49].

## 2.3 Methods in optical spectroscopy

### 2.3.1 The basic principle of fluorescence

A prerequisite for fluorescence is the excitation of an electron of a molecule from a lower electronic state ( $S_0$ ) to a higher electronic state ( $S_1$ ). This excitation process follows the Franck-Condon-principle [5]. Within this higher electronic state the molecule encounters internal vibrational relaxation processes (VR) through its surrounding environment. This continues until the molecule finds itself in the vibrational ground state ( $v_0$ ) of the first excited electronic state ( $S_1$ ). Now the molecule can either fall back into the electronic ground state via radiationless transfer of its energy to the surrounding media, or it releases this excess amount of energy by emitting a photon. Radiative emission from molecules is often either called fluorescence or phosphorescence. While fluorescence describes the emission of light from the ( $S_1$ ) to the ( $S_0$ ) state, phosphorescence includes a third electronic state - the so called triplet state ( $T_1$ ).  $T_1$  is populated from the ( $S_1$ ) state via intersystem crossing (ISC). The  $T_1$  lifetime can be several  $\mu$ seconds or even seconds and thus phosphorescence can persist on longer time scales after excitation. In contrast to phosphorescence, fluorescence usually takes place within the order of  $10^{-9}$  seconds [5, 63].

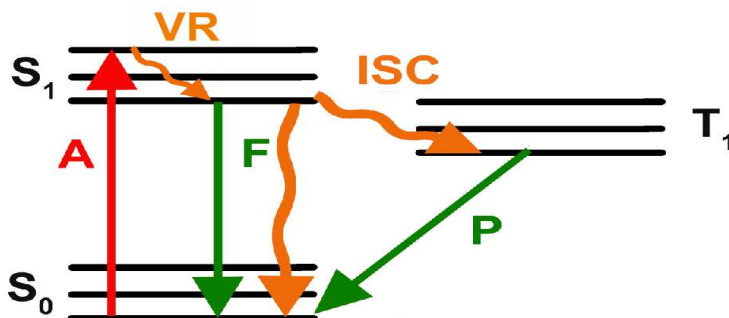


Figure 2.4: The Jablonski diagram depicts all relevant processes in fluorescence spectroscopy. When a photon is absorbed (A) an electron in a molecule is elevated from the ground state ( $S_0$ ) to an electronic excited state ( $S_1$ ). The molecule can reduce its excess energy via vibrational relaxation (VR). After reaching the vibrational ground state of  $S_1$  the molecule can then emit a photon and relax to the ground state  $S_0$ . This process is called fluorescence. Molecules can also undergo intersystem crossing (ISC) into the triplet state ( $T_1$ ). The following emission of a photon is then called phosphorescence (P).

Figure 2.4 shows a scheme of the emergence of fluorescence and phosphorescence including all important adjacent processes mentioned beforehand. The

typical time scale between absorption and emission of a photon is an important characteristic of a molecule. A quantitative description is provided by the fluorescence lifetime of a molecule. Figure 2.5 shows a histogram of photons collected after a laser pulse has excited identical molecules. The decay of intensity over time can be described by a monoexponential curve of the form

$$y = A \cdot e^{-k\tau_{life}} \quad (2.1)$$

Fitting the monoexponential decay function the recorded histogram yields the fluorescence lifetime  $\tau_{life}$  of this species.

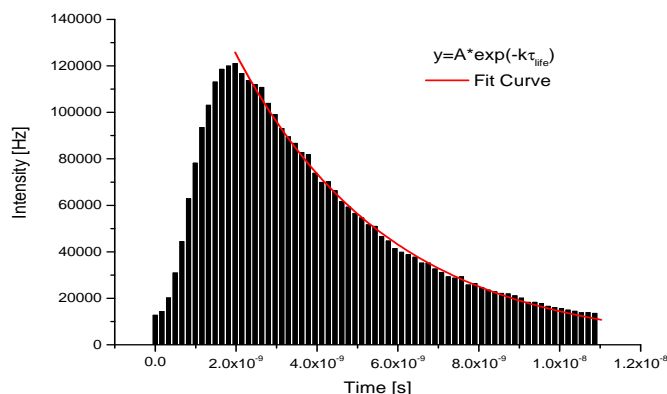


Figure 2.5: Histogram of photons collected after a laser pulse has excited identical molecules in solution. The monoexponential decay gives the fluorescence lifetime  $\tau_{life}$

The fluorescence lifetime, although it is characteristic for a fluorescent molecule, can be significantly reduced by Förster-resonance-energy-transfer (FRET) to an acceptor molecule in close proximity. In the following subsection Förster-resonance-energy-transfer is described in more detail.

### 2.3.2 Förster-resonance-energy-transfer (FRET)

Förster-resonance-energy-transfer requires a dipole-dipole interaction between a donor and an acceptor. The strength of this interaction depends on the distance of both molecules and on the orientation of the dipole moments [63]. The dipole-dipole interaction can be described by classical laws of physics [5]:

$$V_{dipole} = \frac{\kappa}{4\pi\epsilon_0} \frac{\mu_D \mu_A}{r^3} \quad (2.2)$$

Here,  $\epsilon_0$  is the permittivity of the vacuum,  $\mu_D$  and  $\mu_A$  are the transition dipole moments of the two interacting molecules,  $r$  the distance between both of them and  $\kappa$  is an orientation factor.  $\kappa$  is a measure of the average orientation of the dipole moments of the donor and acceptor molecule. It can adopt values from 0 to 4, where 0 reflects the orthogonal orientation of donor and acceptor dipole moment, 1 the parallel orientation and the 4 colinearity of both. For free rotating particles in solution  $\kappa^2$  is on average  $\frac{2}{3}$  [22, 63].

Since energy can only be transferred in quanta, the energy provided by the donor has to be exactly isoenergetic to the difference in the energy levels  $S_0$  and  $S_1$  of the acceptor.

The transfer rate  $k_{ET}$  of this process has been shown to follow the expression below [34, 35]:

$$k_{ET} = \frac{1}{\tau_D} \left( \frac{R_0}{r} \right)^6 \quad (2.3)$$

Here,  $\tau_D$  is the fluorescence lifetime of the donor in the absence of an acceptor and  $R_0$  is the so called Förster distance. The Förster distance is defined by the distance at which 50% of the energy of the donor is transferred to the acceptor.

The Förster distance itself depends on the intrinsic properties of the molecules, namely the orientation factor  $\kappa$ , the quantum yield of the donor  $Q_D$  and the spectral overlap of the emission spectrum of the donor and the absorption spectrum of the acceptor  $J(\lambda)$ , as well as of the refractive index  $n$  of the media [63].

$$R_0^6 = \frac{9000 \cdot \ln(10) \cdot \kappa^2 \cdot Q_D}{128 \cdot \pi^5 \cdot N_A \cdot n^4} \cdot J(\lambda) \quad (2.4)$$

$N_A$  is the avogadro constant. Likewise the overlap integral can be calculated as follows [86]:

$$J(\lambda) = \int_0^\infty F_D(\lambda) \cdot \epsilon_A(\lambda) \cdot \lambda^4 \cdot d(\lambda) \quad (2.5)$$

Figure 2.6 depicts the normalized absorption and emission spectra of Oregon green (green) and Texas red (red). The excited donor molecule induces an oscillation in the acceptor molecule which subsequently elevates the electron of the acceptor into the  $S_1$  state. The acceptor can now relax via the two distinct pathways described above in subsection 2.3.1.

As a consequence of FRET the intensity of the initially excited donor molecule as well as its fluorescence lifetime decrease. Equation 2.6 and 2.7 describe the relationship between the efficiency of FRET and the resulting fluorescence lifetime  $\tau_{DA}$  of the donor molecule, being in close proximity to the acceptor molecule [126].

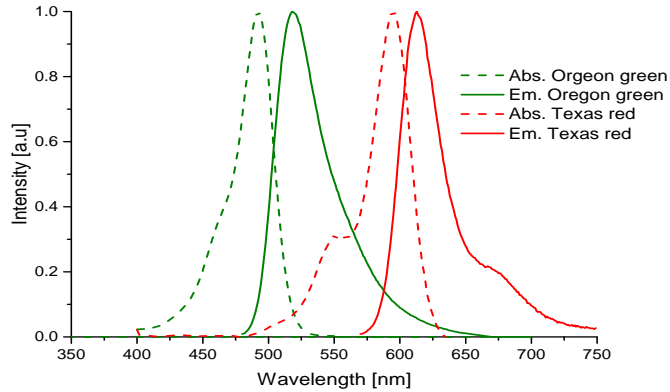


Figure 2.6: Absorption and emission spectra of Oregon green (green) and Texas red (red).

$$E = 1 - \frac{\tau_{DA}}{\tau_D} \quad (2.6)$$

or

$$E = \frac{k_{ET}}{\tau_D^{-1} + k_{ET}} = \frac{R_0^6}{r^6 + R_0^6} \quad (2.7)$$

### 2.3.3 Fluorescence-correlation-spectroscopy

#### Auto-correlation-function

In Fluorescence-Correlation-Spectroscopy (FCS) fluorescence fluctuations originating from fluorescing particles diffusing in and out of a small volume are analyzed [126]. These fluctuations are caused by differently sized particles leading to a distinct profile of fluctuating fluorescence intensities [126, 97]. The concentration range for proper FCS analysis is in the nM-range. An auto-correlation of such fluctuations compares the self-similarity of signals at time points  $t$  with signals recorded at other times  $t + \tau$  [32, 71, 41]. Figure 2.7 depicts a time trace of a fluorescence signal. The purple bar indicates the time point  $t$ . If the time trace is shifted by  $t + \tau$  the intensity ( $I$ ) below the purple bar changes.

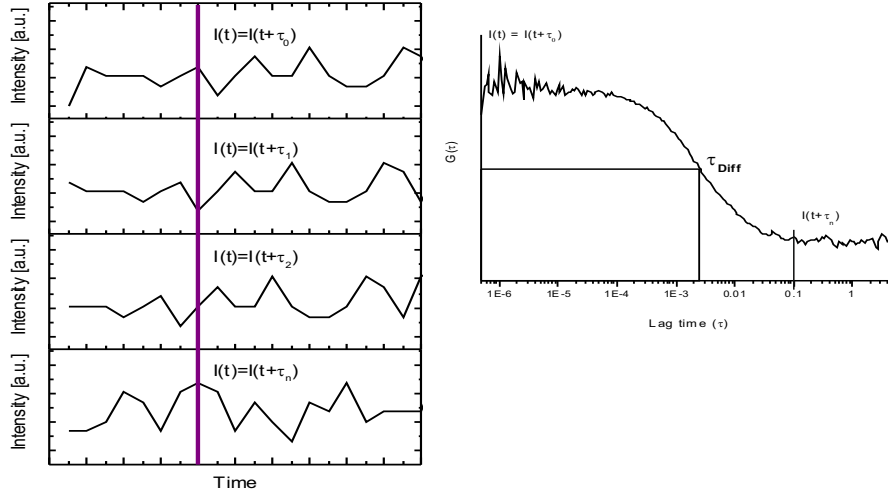


Figure 2.7: The stacked graphs (left) represent the same time traces shifted by means of  $\tau$ . This results in an autocorrelation (right) of the observed species. The amplitude of the curve yields the inverse particle number  $N$  while the inflection point corresponds to the diffusion time  $\tau_{Diff}$ .

In an auto-correlation analysis the mean of  $I(t) \cdot I(t + \tau)$  and the square of the average intensity  $\langle I(t) \rangle^2$  are determined and the quotient is calculated [86, 126]:

$$G(\tau) = \frac{\langle I(t) \cdot I(t + \tau) \rangle}{\langle I(t) \rangle^2} - 1 = \frac{\delta \langle I(t) \cdot \delta I(t + \tau) \rangle}{\langle I(t) \rangle^2} \quad (2.8)$$

The recorded intensity  $I(t)$  depends on the fluorescence originating from infinitesimal small volume elements  $dV$  of the focal volume [86, 97, 126]. For uncorrelated signals the quotient of  $I(t) \cdot I(t + \tau)$  and the square of the average intensity measured over the entire recording time  $I(t)$  lead to 1. For fluorescing particles the intensity  $I(t)$  depends on the concentration  $C(r, t)$  of the particles at a given space and time, the molecular brightness  $\eta$  of the fluorophore - which is connected to its quantum yield, the detection efficiency and the cross-section of absorption and finally on the detection volume of the experimental setup which can be described by the probability distribution  $W(r)$  [97]:

$$W(r) = \exp\left(-2\frac{x^2 + y^2}{r_0^2}\right) \cdot \exp\left(-2\frac{z^2}{z_0^2}\right) \quad (2.9)$$

Here,  $r_0$  and  $z_0$  are the  $\frac{1}{e^2}$ -width of the focal volume in lateral and axial direction, which can also be expressed as

$$r_0 = \frac{FWHM_{xy}}{\sqrt{2\ln 2}} \quad (2.10)$$

and

$$z_0 = \frac{FWHM_z}{\sqrt{2\ln 2}}, \quad (2.11)$$

respectively. In fact, a 3D Gaussian is only an approximation, but serves as a common simplification. Furthermore both values are connected via the structural parameter  $w = \frac{r_0^2}{z_0^2}$ . It describes the geometry of the focal volume. The value of  $w = \frac{r_0^2}{z_0^2}$  for the water immersion objective used in this study (UPlanSApo 60x/1.2w, Olympus) is 0.25 [86]. Here,  $FWHM$  is the full width at half maximum of the corresponding Gaussian distribution of the detected fluorescence signal. This finally leads to an equation describing all determining factors in terms of  $I(t)$  [86]:

$$I(t) = \int W(r) \cdot \eta \cdot C(r, t) \, dV \quad (2.12)$$

Insertion of equation 2.12 in equation 2.8 leads to [86, 126]:

$$G(\tau) = \frac{\int \int W(r)W(r') \langle \delta C(r, t) \delta C(r', t + \tau) \rangle dV dV'}{(\int W(r) \langle \delta C(r, t) \rangle dV)^2} \quad (2.13)$$

Here,  $r$  and  $r'$  are the coordinates for the integration in space  $dV$  and  $dV'$ , at the two different times  $t$  and  $t + \tau$ , respectively. It follows that [86, 126]:

$$G_{3D}(\tau) = \frac{1}{\langle C \rangle \cdot \pi^{(2/3)} \cdot r_0^2 \cdot z_0} \cdot \left(1 + \frac{4D\tau}{r_0^2}\right)^{-1} \cdot \left(1 + \frac{4D\tau}{z_0^2}\right)^{-0.5} \quad (2.14)$$

where  $D$  is the diffusion coefficient of the free diffusing particle and  $\pi^{3/2}w_0^2z_0 = V_{eff}$ . The diffusion time  $\tau_D$  and the diffusion coefficient are related as follows [33]:

$$\tau_{Diff,xy} = \frac{r_0^2}{4D} \quad (2.15)$$

and

$$\tau_{Diff,z} = \frac{z_0^2}{4D} \quad (2.16)$$

Combining equation 2.15 for the lateral diffusion and equation 2.14 yields [86, 126]:

$$G_{3D}(\tau) = \frac{1}{N} \cdot \left(1 + \frac{\tau}{\tau_D}\right)^{-1} \cdot \left(1 + \frac{\tau}{\tau_D} \cdot \frac{r_0^2}{z_0^2}\right)^{-0.5} \quad (2.17)$$

For the sake of simplicity the time dependent part of equation 2.17 is abbreviated with  $\Psi$ .

$$\Psi = \left(1 + \frac{\tau}{\tau_D}\right)^{-1} \cdot \left(1 + \frac{\tau}{\tau_D} \cdot w^2\right)^{-0.5} \quad (2.18)$$

For spherical particles the diffusion coefficient can also be characterized in terms of the Stokes-Einstein equation [33]:

$$D = \frac{kT}{6\pi R\eta} \quad (2.19)$$

With an auto-correlation it is difficult to characterize more than one species of particles, when their diffusion coefficients do not differ by at least a factor of 2. For studying interaction between two differently labelled objects one can then perform cross-correlation analysis.

### Cross-correlation-function

Within a cross-correlation two fluorescence signals originating from two distinct fluorophores are analyzed using the following function [55, 23]:

$$G_{ij}(\tau) = \frac{\delta\langle I_i(t) \cdot \delta I_j(t + \tau) \rangle}{\langle I_i(t) \cdot I_j(t) \rangle} \quad (2.20)$$

Only those particles that carry both fluorophores  $i$  and  $j$  contribute to the correlation amplitude. Referring to the above introduced auto-correlation-function  $G_{ij}(\tau)$  can analogously be expressed as [55]:

$$G_{ij}(\tau) = \frac{\langle C_{ij} \rangle \cdot \Psi_{ij}}{V_{eff}(\langle C_i \rangle + \langle C_{ij} \rangle)(\langle C_j \rangle + \langle C_{ij} \rangle)} = G_{ij}(0) \cdot \Psi_{ij} \quad (2.21)$$

It should be noted here that two emitters being in close proximity might exhibit altered characteristics in their emission. However, for an immediate treatment of FCCS as presented in this subsection this aspect is not considered. Of course, the detection volume for both species has to be exactly the same. This can easily be achieved by applying two-photon-excitation (TPE) and will be further explained in section 2.4.

At  $\tau = 0$ ,  $G_{ij}(\tau)$  can be simplified as [90]:

$$G_{ij}(0) = \frac{N_{ij}}{(N_i + N_{ij}) \cdot (N_j + N_{ij})} \quad (2.22)$$

Here,  $N_{ij}$  is the number of interacting particles emitting fluorescence on both channels. Consequently,  $N_i$  and  $N_j$  are the single labeled particles, not interacting with one another. These two numbers can be calculated from the autocorrelation of the respective channel [122]:

$$N_i + N_{ij} = N_i(0) = \frac{1}{G_i(0)} \quad (2.23)$$

and

$$N_j + N_{ij} = N_j(0) = \frac{1}{G_j(0)} \quad (2.24)$$

Insertion of the apparent conditions listed in equation 2.23 and 2.24 into equation 2.22 permits to specify the dependency of cross-correlation and particle numbers in an even simple manner [122]:

$$N_{ij} = G_{ij}(0) \cdot N_i(0) \cdot N_j(0) \quad (2.25)$$

### 2.3.4 Optical trapping

The first description of a so-called single beam gradient force trap was made in 1986 by Ashkin [3, 4]. It was used to capture dielectric particles that follow the Rayleigh approximation. One can distinguish two different modes of trapping. One describes trapping in the Rayleigh regime, where the radius  $r$  of a particle is small compared to the wavelength  $\lambda$  of photons and the ray optics regime, which specifies the capture of a particle that is large compared to the wavelength of the applied photons [66]. In this study large unilamellar vesicles (LUVs) are used. These particles are about 110 nm in diameter. Since the wavelength used here is 800 nm, the Rayleigh approximation can be applied. In the Rayleigh regime particles can be thought of as a collection of dipoles interacting with the laser light according to Lorentz' law [42]:

$$\vec{F} = q(\vec{E} + \vec{v} \times \vec{B}) \quad (2.26)$$

Here  $\vec{F}$  is the Lorentz force,  $q$  is the charge of the particle,  $\vec{E}$  the electric field strength,  $\vec{v}$  the speed of the particle and  $\vec{B}$  the magnetic flux density.

Generally, a force that acts on an object can also be described as [4, 111]:

$$F = \frac{Qn_{media}P}{c} \quad (2.27)$$

with  $Q$  being a dimensionless coefficient reflecting the fraction of force applied to the object in comparison to the total amount of power  $P$  of the laser.  $n_{media}$  and  $c$  are, of course, the refractive index of the media - in case of water 1.33 - and the speed of light. In the Rayleigh regime optical trapping is achieved by the interplay of two distinct forces: the gradient force and the scattering force. The gradient force is a direct result of the Lorentz force as depicted in equation 2.26 and can be thought of as dipoles interacting with the electromagnetic field of the laser light. It pulls the object towards the direction of highest laser intensity [116, 4]:

$$\vec{F}_{grad} = -\frac{n_{media}}{2} \cdot \alpha \nabla E^2 = -\frac{n_{media}^3 r^3}{2} \cdot \left(\frac{m^2 - 1}{m^2 + 2}\right) \cdot \nabla E^2 \quad (2.28)$$

Here,  $\alpha$  is the polarizability of the object and  $m = \frac{n_{object}}{n_{media}}$ .

Refraction itself follows Snell's law [42]:

$$\frac{\sin \theta_{water}}{\sin \theta_{object}} = \frac{n_{object}}{n_{water}} = m \quad (2.29)$$

where  $\theta$  is half the angle of the laser beam leaving the objective. The scattering force for an object fulfilling the Rayleigh approximation  $r \ll \lambda$  can be characterized as follows [53, 116]:

$$\vec{F}_{scat} = \frac{I_0}{c} \cdot \frac{128\pi^5 r^6}{3\lambda^4} \left(\frac{m^2 - 1}{m^2 + 2}\right)^2 n_{media} \quad (2.30)$$

The scattering force acts towards the direction of the incident laser beam with intensity  $I_0$  due to the applied radiation pressure. Here, two impulses impact the particle, one along the beam propagation of the incident light beam and one opposite to the direction of the emitted photon [116]. A net force is directed along the propagation of light. However, in a highly focussed laser beam the Poynting vector  $S$  of the gradient force possesses an additional component to the one acting perpendicular to it. This component acts against the scattering force. The resulting net force restores the position of the particle in all three dimensions with respect to the trapping center [116]. Hence, scattering and gradient force together determine the final trapping position of the object with radius  $r$ . It becomes obvious from equation 2.28 and equation 2.30 that besides the laser intensity and the radius of the object the difference in the refractive index of the media and the object is important. In fact, the greater  $m$  the better an object is trapped. As a matter of course, a  $r = 55$  nm sized LUV

is not orders of magnitude smaller than the applied wavelength of 800 nm. However, an exact description of  $r \approx \lambda$  has to be given by Lorentz-Mie theory which would be beyond the scope of this work.

## 2.4 Lasers

In this study two different light sources are used: a continuous wave (CW) laser (Mira 900 laser system, Coherent (California, USA)) and a pulsed laser (Chameleon Ti:Sa laser system, Coherent (California, USA)) permitting for two photon excitation (TPE). Both lasers are titanium sapphire lasers which are based on an  $\text{Al}_2\text{O}_3$  crystal endowed with  $\text{Ti}^{3+}$  ions. The  $\text{Ti}^{3+}$  ions enable the crystal to emit fluorescence photons from 670 to 1070 nm with a maximum at 800 nm. Titanium sapphire lasers are 4 level system:

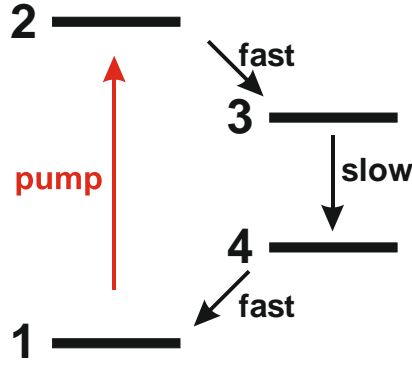


Figure 2.8: In a 4 level laser where the relaxation from level 3 to level 4 occurs slowly compared to all other processes, population inversion between level 3 and 4 can be achieved by pumping the transition  $1 \rightarrow 2$ .

For a pulsed operation using  $\text{Al}_2\text{O}_3:\text{Ti}^{3+}$  crystals, the Kerr lens effect is used. The Kerr lens effect describes intensity dependent variations of the refractive index [110]:

$$n = n_0 + n_2 I, \quad (2.31)$$

Moreover it permits for passive mode coupling [110]. Here,  $n_0$  is the static refractive index of the material,  $n_2$  is the nonlinear part of the refractive index and  $I$  is the pulse intensity inside the crystal. Due to the Kerr lens effect, a Gaussian-shaped beam that passes through the crystal experiences a greater refractive index at the center than at the edges. Thereby, it acts as a self

focusing lens which slightly focuses the beam within the crystal [42, 110]. Mode coupling is achieved by an overlap of the laser mode with that of the pump laser. Pulsed laser light exhibits a higher power than CW laser light. Thus, the pulsed laser light is focussed compared to the CW light. Together with a slit one can generate an intensity dependent loss of photons, yielding in a preferred generation of pulsed laser light [110].

The benefit of a continuous laser beam is the capability of providing a light source for optical trapping as described in subsection 2.3.4, while only with a pulsed laser it is possible to record fluorescence lifetimes (compare subsection 2.3.1) or to perform gentle two-photon excitation of biological samples. Figure 2.9 illustrates the process of two photon excitation (TPE). Of course, multi photon excitation is also possible with three photons or with two photons of unequal energy [126] as long as the total photon energies equal the  $S_0 \rightarrow S_1$  transition energy.

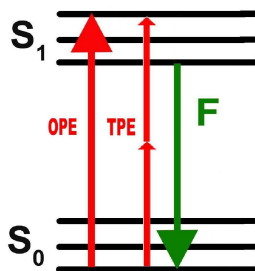


Figure 2.9: Excitation of a molecule via TPE requires two photons whose sum of energy resembles that of one photon required for OPE. The resulting fluorescence (F) is not altered.

While in OPE the likelihood of excitation depends directly on the laser intensity, the likelihood of two-photon excitation varies with the square of the laser intensity. As a consequence, also the effective excitation volume in two-photon excitation is altered [86, 126]:

$$OPE : V_{eff} = \pi^{3/2} \cdot r_0^2 \cdot z_0 \quad TPE : V_{eff} = \left(\frac{\pi}{2}\right)^{3/2} \cdot r_0^2 \cdot z_0 \quad (2.32)$$

and therefore also the diffusion time  $\tau_{Diff}$  changes to (compare equation 2.15 and 2.16)

$$TPE : \tau_{Diff,xy} = \frac{r_0^2}{8D} \quad \tau_{Diff,z} = \frac{z_0^2}{8D} \quad (2.33)$$

The benefits of using TPE instead of OPE are:

1. Less photobleaching
2. No pinhole required, since excitation only takes place within a very tiny volume
3. Greater penetration into tissue due to the larger wavelength used
4. Simultaneous excitation of green and red fluorophores within exactly the same volume possible

Wherein benefit No. 4 is the most important for this study.

## 2.5 Physical Chemistry

### 2.5.1 1<sup>st</sup> order kinetics

In the optical trapping experiments performed in this study the surface of a LUV (d= 110nm) is roughly 13 times greater than that of a SUV (d= 30nm). Thus, one can estimate the binding sites on the LUV surface to be constant in a first approach. Therefore the reaction observed in an optical trap resembles a unimolecular reaction where the concentration of the SUV determines its kinetics. The tethering and fusion of a protein containing SUV [A] can consequently be described by first order kinetics [5].

$$\frac{d[A]}{dt} = -k[A] \quad (2.34)$$

With the corresponding integral being:

$$- \int_{[A]_0}^{[A]} \frac{d[A]}{[A]} = \int_0^t k dt \quad (2.35)$$

Solving the integral then leads to:

$$\ln \frac{[A]}{[A]_0} = -kt \quad (2.36)$$

or

$$[A] = [A]_0 \cdot e^{-kt} \quad (2.37)$$

### 2.5.2 Hill equation

The Hill equation is commonly used to characterize cooperative effects as published in [118]. Very often proteins require a ligand as some sort of external trigger in order to bind their target molecule. It describes the fraction of protein binding as a function of the ligand concentration [65]:

$$y = V_{max} \frac{x^n}{K_D^n + x^n} \quad (2.38)$$

or

$$y = Start + (End - Start) \frac{x^n}{K_D^n + x^n} \quad (2.39)$$

Wherein  $V_{max}$  resembles the maximum reaction speed which can, of course, be replaced by the rise of the corresponding graph in terms of  $Start + (End - Start)$ .  $K_D$  is the dissociation constant and  $n$  the Hill-coefficient. The dissociation constant specifies the ligand concentration occupying half of the binding sites of the protein. A Hill coefficient of  $n > 1$  indicates positive,  $n = 1$  no and  $n < 1$  negative cooperativity. In case of  $n = 1$  one assumes binding properties of a molecule that can also be described by Langmuir adsorption isotherms. The physical parameters of Langmuir adsorption and two of its variants are described in the next subsection.

### 2.5.3 Adsorption isotherms

The simplest form of adsorption can be described by Langmuir adsorption isotherms. Here, the following assumptions are made beforehand [5]:

1. Adsorption can not proceed beyond monolayer coverage.
2. All binding sites are equivalent and the surface is uniform. This means the surface has to be perfectly flat on a microscopic scale.
3. The ability of a molecule to adsorb at a given site is independent of the occupation of neighbouring sites. This means no interaction between adsorbed molecules takes place.

Therefore the equilibrium constant  $K$  for a molecule  $A$  binding to a surface site  $S$  can be written as [5]:

$$K = \frac{[SA]}{[A][S]} \quad (2.40)$$

The so called fractional coverage is then defined as [5]:

$$\Theta = \frac{\text{number of adsorped molecules}}{\text{maximum number of molecules at adsorped}} = \frac{N}{N_\infty} \quad (2.41)$$

As a matter of course,  $\Theta$  depends on the rate of adsorption and desorption. At equilibrium there is no net change and thus equation 2.41 changes to [5]:

$$\Theta = \frac{Kx}{1 + Kx} \quad (2.42)$$

Here,  $x$  describes a variable parameter such as partial pressure of a molecule  $A$  over the surface or its concentration in solution. Of course, Langmuir isotherms depict an idealized model of adsorption. Other models like Freundlich or Gunary account for surface roughness and adsorbate-adsorbate interaction. The Freundlich isotherms can be expressed as [5]:

$$\Theta = K \cdot x^n \quad (2.43)$$

Here  $K$  is the Freundlich coefficient and  $n$  the Freundlich potency.

The Gunary isotherms imply that the first adsorbate molecule is adsorbed most, while the second adsorbate is adsorbed less and so on. Hence, the Gunary isotherms can be described as follows [40]:

$$\Theta = K_1 + K_2x + K_3\sqrt{x} \quad (2.44)$$

Generally, it may become difficult to decide which model fits best to the data. While models like Gunary do not directly permit further discrimination, the Langmuir isotherms predict that a straight line is obtained when  $\frac{x}{N}$  is plotted against  $x$  [5]. Whereas, in case of a Freundlich adsorption, a straight line is obtained when plotting  $\log \Theta = \log K + n \cdot \log x$  [5].

# Chapter 3

## Material and Methods

### 3.1 Material

#### 3.1.1 Chemicals

All standard chemicals used in this study are purchased from the following companies: Sigma (Deisenhofen, Germany), Sigma-Aldrich (St. Louis, USA), AppliChem (Darmstadt, Germany), Merck (Darmstadt, Germany), Roth (Karlsruhe, Germany), Biorad (Richmond, USA), Serva (Heidelberg, Germany), Boehringer (Ingelheim, Germany), Fluka (Switzerland) and Anatrace (USA). Sephadex G50, used for gel filtration, is purchased from GE Healthcare (Freiburg, Germany). The molecular weight protein standard (SM0671) is purchased from MBI Fermentas (St. Leon- Rot, Germany).

#### 3.1.2 Proteins

All the protein constructs used in this study are from *Rattus norvegicus*. The proteins are cloned in the pET28a (Novagen) vector and expressed in *Escherichia coli* strain BL21 (DE3) except the  $\Delta N$  complex, in which syntaxin 1A (Sx1A) (183-288) and synaptobrevin 2 (49-96) are cloned in pET Duet-1 (Novagen), and SNAP 25A is cloned in pET28a. The expression constructs of the full-length synaptotagmin-1 (1-421) has been described elsewhere [106]. Also the following point mutants of the full-length synaptotagmin-1 aB (D178, 230, 232A), Ab (D309, 363, 365A), ab (D178, 230, 232, 309, 363, 365A), and KAKA mutant (K326, 327A) have been described earlier [106].

All proteins are expressed in *Escherichia coli* strain BL21 (DE3) (Novagen) and purified using Ni<sup>2+</sup>-nitrilotriacetic acid beads (Ni-NTA, GE Healthcare) followed by ion exchange chromatography (IEXC) on the Aekta system (GE Healthcare) as described in the literature [85, 106]. The synaptotagmin-1 purification protocol is followed as described in [121]. Expression and purification of the synaptotagmin-1 wt protein is performed by Dr. W. Vennekate. The  $\Delta N$  complex is co-expressed with pET Duet-1 and pET28a vectors and purified by IEXC with 50 mM n-octyl-b-D-glucoside [85]. The mutants of the full-length synaptotagmin-1 and synaptobrevin are provided by Dr. Angel Perez and Dr. Geert van den Bogaart [106, 118, 119]. The sequences of all the proteins are given in Table 3.1.

Table 3.1: Summary of all proteins used in this study.

Abbreviation	Protein	Sequence
syt-1	synaptotagmin-1	1-421 [114]
aB	synaptotagmin-1 aB	1-421, D178, 230, 232A [106, 118, 119]
Ab	synaptotagmin-1 Ab	1-421, D309, 363, 365A
ab	synaptotagmin-1 ab	1-421, D178, 230, 232, 309, 363, 365A
KAKA	synaptotagmin-1 KAKA	1-421, K326, 327A
Sb <sup>1-96</sup>	synaptobrevin 2 1-96	1-96 [35]
$\Delta N$ complex	Sx1A	183-288
	SNAP25A	1-206, C84, 85, 90, 92S [85]
	Sb2 49-96	49-96

### 3.1.3 Antibodies

All antibodies used in this study are listed below in table 3.2

Table 3.2: Summary of all antibodies used in this study.

Abbreviation	Antibody	Company
1 <sup>st</sup> anti syt-1	synaptotagmin-1, cytoplasmic tail, mouse monoclonal, purified IgG, unlabeled (105011)	SynapticSystems

Abbreviation	Antibody	Company
1 <sup>st</sup> anti sb 2	synaptobrevin 2, mouse monoclonal, purified IgG, unlabeled (104211)	SynapticSystems
2 <sup>nd</sup> anti mouse	IRDye 680LT Donkey anti-Mouse IgG (H + L)	LicorBioScience

### 3.1.4 Phospholipids and cholesterol

All the phospholipids used in this study are purchased from Avanti Polar Lipids Inc. (Alabama, USA), except Texas red phosphatidylethanolamine and Oregon green phosphatidylethanolamine, which are purchased from Invitrogen Molecular Probes 3.3

Table 3.3: Summary of all lipids and cholesterol used in this study.

Abbreviation	Lipid/Cholesterol	Company
PC	L-a-Phosphatidylcholine	Avanti Polar Lipids Inc.
PE	L-a-Phosphatidylethanolamine	Avanti Polar Lipids Inc.
PS	L-a-Phosphatidylserine	Avanti Polar Lipids Inc.
PiP <sub>2</sub>	Phosphatidylinositol-4,5- biphosphate	Avanti Polar Lipids Inc.
Cholesterol	Cholesterol	Avanti Polar Lipids Inc.
TRPE	Texas red-PE Invitrogen	Molecular Probes
OGPE	Oregon green-PE Invitrogen	Molecular Probes

### 3.1.5 Further fluorescence dyes and components

All fluorophores additionally used in this study are listed below in table 3.4

Table 3.4: Summary of all additionally used dyes/fluorescent components in this study.

Dye	Company
Fluo5N	Invitrogen
Fura2	Invitrogen
FluoSpheres 20 nm	Invitrogen
FluoSpheres 40 nm	Invitrogen
FluoSpheres 1.0 $\mu$ m	Invitrogen

### 3.1.6 Buffers

All buffers used in this study are listed below in table 3.1.6:

Table 3.5: Summary of all buffers used in this study.

Buffer	Concentration	Components
Chloroform/MeOH	2/3 (v/v)	Chloroform
	1/3 (v/v)	MeOH
DTT stock solution	1 mM	DTT in ddH <sub>2</sub> O (Milli-Q)
	20 mM	HEPES, pH 7.4
	150 mM	KCl
HPCholate	2 mM	DTT
	20 mM	HEPES, pH 7.4
	150 mM	KCl
ATP buffer	2 mM	DTT
	5% (w/v)	Sodium Cholate
	20 mM	HEPES, pH 7.4
	120 mM	potassium glutamate
	20 mM	potassium acetate
	3 mM	ATP

Buffer	Concentration	Components
MOPS buffer	50 mM	3-(N-Morpholino)- propanesulfonic acid, pH 7.7
	50 mM	Tris-Base
	0.1%	Sodiumdodecylsulfate
	1 mM	EDTA
sucrose buffer	20 mM	HEPES, pH 7.4
	150 mM	KCl
	2 mM	DTT
	2M	sucrose

### 3.1.7 Software

The software products used for data analysis are MATLAB 2009b (The Math- Works, Inc.), Origin 8.0G (MicroCal Inc.), Microsoft Office Suite 2010 (Microsoft Corp.) and Excel (Microsoft Corp.).

### 3.1.8 Instruments

All instruments used in this study are listed below in table 3.1.8:

Table 3.6: Summary of all instruments used in this study.

Instrument	Supplier
<b>Biochemical Instrumentation</b>	
Electrophoresis chamber	Biorad (Richmond, USA)
Mini-Protean II Power Pac 300	Biorad (Richmond, USA)
Rotating Evaporator R-124	Büchi
Sonifier 450	Branson
Extrusion cassette	Avanti Polar Lipids Inc.
Syringe #1725	Hamilton

Instrument	Supplier
<b>Columns</b>	
Sephacryl S-1000 Superfine HR Econo-column, 0.5cm x 10cm Econo-column, 2.5cm x 10cm	GE Healthcare (Germany) Biorad, (Richmond, USA) Biorad, (Richmond, USA)
<b>Fluorescence spectrometer/ reader</b>	
FluoroMax-2 Typhoon Trio Imager	Horiba Scientific GE Healthcare
<b>Components for FCS measurements</b>	
Chameleon Ti:Sa laser system Solid State Thermoelectric Thermal Control Unit T225P IX71 inverted microscope UPlanSApo 60x/1.2w water immersion objective Avalanche photodiode (APD, SPCM-AQR-13) PRT 400, 4-channel router TimeHarp200, TCSPC card 715 DSCPXR dichroic mirror 590 DCXR dichroic mirror	Coherent (California, USA) Coherent (California, USA)  Olympus (Germany) Olympus (Germany)  Perkin-Elmer (Canada) Perkin-Elmer (Canada) PicoQuant GmbH (Germany) PicoQuant GmbH (Germany) AHF (Germany) AHF (Germany)
<b>Components for FCS measurements</b>	
E700SP2 short pass filter Ultra-broadband dielectric mirror, 650-1130 nm HQ 645/75 bandpass filter HQ 535/50 bandpass filter Coverslip 18 x 18 mm	AHF (Germany) Newport (USA) Newport (USA) AHF (Germany) AHF (Germany) Menzel-Gläser (Germany)
<b>Components for optical trapping</b>	
Mira 900 laser system Polcube, PBS202 Variable ND filter, NDC-100C-2 Polarisation filter $\frac{\lambda}{2}$ , 10RP52-2 wide field camera U-TV1X-2 Refractometer AR2 Stage, Clean Damper, D4Cl-50 Picomotor LMR05/M Syringe M750	Coherent (California, USA) Thorlabs (New Jersey, USA) Thorlabs (New Jersey, USA) Newport (USA) Olympus (Tokyo) Krüss Vexta Thorlabs (New Jersey, USA) Hamilton

## 3.2 Methods

### 3.2.1 Determination of calcium concentration

The calcium concentrations are calculated with the help of MaxChelator [73, 74]. Using Fluo5N and Fura2 the actual calcium concentration is determined once for all HP150 based buffers. For the buffers containing 3 mM ATP the calcium buffers are always prepared freshly and consequently the actual calcium concentration is determined for every preparation.

### 3.2.2 SDS PAGE and Western Blot

The reconstitution of synaptotagmin-1 and synaptobrevin 2 is analyzed with SDS-PAGE (Sodium dodecyl sulfate polyacrylamide gel electrophoresis) [62]. The tricine gels are bought from Invitrogen (NP0341BOX). The protein samples are mixed with 5x sample buffer and heated to 90°C for 10 min. Different amounts of protein are loaded into the gel pockets. The gel tank is filled with MOPS buffer. Starting with 10 mA and later increasing the amperage to 25 mA per gel, the sample is run through the gel. The proteins caught in the gel matrix are blotted onto a cellulose membrane (PerkinElmer, Whatman Protan, Pure nitrocellulose transfer an immobilization membrane, pore size 0.2  $\mu\text{m}$ ). Western-Blot is complete after 1 h. The membrane is then washed 3 times for 10 min with milk solution (frema, Reform, Istant Milchpulver). For staining, the membrane is incubated with a mixture of the first antibodies against synaptotagmin-1 (1:1,000, see 3.2) and synaptobrevin 2 (1:10,000, see 3.2). After 1 h incubation the membrane is washed again 4 times (2 x 20 min, 2 x 5 min) with milk solution to remove unbound antibody. Afterwards the membrane is incubated for at least 1 h with the secondary antibody (see 3.2). Again, the membrane is washed 4 times (2 x 20 min, 2 x 5 min) with milk solution to remove unbound antibodies. Finally, a picture is taken with a fluorescence reader (see 3.1.8), exciting the secondary antibody at 633 nm and recording the emission at 655-685 with a band pass filter BP670/30. Quantification of the fluorescence signal is performed with ImageJ [50, 88].

### 3.2.3 Reconstitution of proteins into SUVs

Proteins are reconstituted into SUVs using size exclusion chromatography as described in earlier publications [98, 117] with the following modifications. All the lipid components are solved in a chloroform/methanol solution (see 3.3) and mixed according to their composition for the liposome. The lipid

Table 3.7: Summary of SUV composition

Lipid/Cholesterol	Concentration
<b>Vesicle 1 (no PS, no PiP<sub>2</sub>)</b>	
PC	69
PE	20
PS	0
PiP <sub>2</sub>	0
Cholesterol	10
<b>Vesicle 2 (PS, no PiP<sub>2</sub>)</b>	
PC	49/54
PE	20
PS	20/15
PiP <sub>2</sub>	0
Cholesterol	10
<b>Vesicle 3 (PS, 1% PiP<sub>2</sub>)</b>	
PC	48/53
PE	20
PS	20/15
PiP <sub>2</sub>	1
Cholesterol	10

solution is dried to a lipid film with nitrogen gas. The proteins are added to the lipid mixture at a protein:lipid ratio of 1:1,000 for synaptotagmin-1, 1:250 for synaptobrevin 2 and 1:1,000 for syntaxin 1A. HP150 is used to dilute the lipid protein mixture to a final cholate concentration of 2.5% (v/v). The liposomes are formed by detergent removal using a Sephadex G50 econo column (GE Healthcare, Biorad). The running buffer for the column is HP150. About 250  $\mu$ L of vesicles solution is collected. All lipid compositions used in this study are listed in table 3.7. Either 1.5% Oregon green or 1% Texas red are added accordingly.

### 3.2.4 Reconstitution of $\Delta$ N-complex into LUVs

LUV mixtures are prepared according to subsection 3.2.3. A rotary evaporator is used to dry out the lipid film. Preparation of LUVs is carried out according to [43] by reverse phase evaporation and extrusion through polycarbonate membranes with a pore size of 100 nm. The  $\Delta$ N complex is inserted into

the preformed LUVs at a protein:lipid ratio of 1:500 using detergent n-octyl- $\beta$ -D-glucoside followed by an overnight dialysis [24, 43].

### 3.2.5 General FCCS experiments

For the FCCS experiments presented in section 4.1 the liposomes are diluted about 1:20. Subsequently the particle number is determined via FCS. Oregon green and Texas red labeled liposomes are mixed in a 1:1 ratio and incubated for 30 min at RT. The power of the TPE laser beam is kept constant at 20 mW. As a control a protein free Texas red labeled liposome is mixed with an Oregon green labeled one. The corresponding cross-correlation is determined owing to crosstalk from photons emitted by Oregon green and detected on the red channel. Subsequently, this false contribution to the cross-correlation amplitude is subtracted from the cross-correlation amplitude obtained within the actual measurement including reconstituted synaptotagmin-1. Of course the Oregon green fluorescence lifetimes slightly vary over different OG-DHPE batches and thus are normalized to the initially measured lifetime of 4.05 ns.

### 3.2.6 Optical trapping experiments

For the optical trapping experiments presented in section 4.2 the liposomes are diluted in HP150 buffer containing varying  $\text{Ca}^{2+}$  concentrations. Subsequently the particle number is determined via FCS. LUVs and SUVs are mixed in a 1:10 ratio with the particle number of the LUVs being 0.2 in the focal volume. Incubation takes 30 min at RT. A sample volume of at least 100  $\mu\text{L}$  is pipetted on top of the coverslip. Time traces of each sample are recorded for up to 30 min.

Having identified a trapping event, the corresponding time frame is subdivided into periods of several seconds. The SUV diffusion time and the Oregon green fluorescence lifetime, are determined via self-written Matlab codes as can be deduced from section 7.2. Periods revealing diffusion times in the high millisecond or even second range reflect aggregated particles and are thus not taken into account for further data analysis. The mean of the remaining auto-correlation curves is calculated and subsequently fitted to the auto-correlation function depicted in equation 2.17. The fluorescence lifetime is analyzed accordingly. The power of the TPE laser beam is kept constant at 20 mW, while the CW power is kept at 100 mW for all optical trapping experiments.

### 3.2.7 TPE confocal fluorescence microscopy setup

To simultaneously excite two different populations of liposomes within an identical volume - one labelled with Oregon green the another labelled with Texas red, TPE is applied. This is achieved by using 20 mW of the output power of a 87 MHz Chameleon titanium-sapphire laser (Coherent, USA) that pulses in the fs-range. As previously described [121, 24] a wavelength of 800 nm is used for TPE. A lens system expands and collimates the laser beam and couples it into an IX71 inverted microscope (Olympus, Germany). The beam is then reflected towards the objective of the microscope by a dichroic mirror DC1 (715 DSCPXR, AHF, Germany) and finally focussed by an UPlanSApo 60x/1.2w water immersion objective (Olympus, Germany).

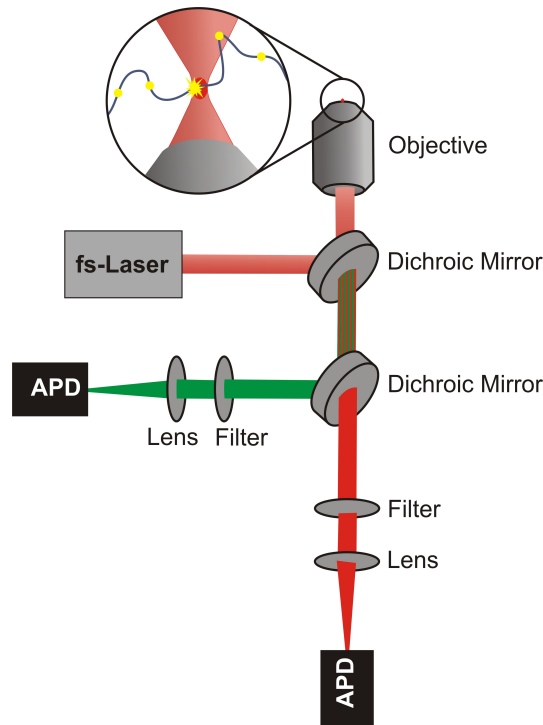


Figure 3.1: Two-photon fluorescence microscopy setup. An fs-laser is coupled into the objective to excite fluorophores within a given sample. The fluorescence is then collected by the objective and directed back into the microscope. A dichroic mirror splits up the green and the red fluorescence photons, which are consequently recorded with the help of two avalanche photodiodes (APDs).

The fluorescence photons again pass through the objective and the dichroic mirror DC1. Scattered light from the excitation beam is blocked by a two-photon rejection filter 2P-SP (E700SP2, AHF, Germany). The fluorescence light is collimated using a second lens system and reflected into the detection side of the setup by an ultra broad band dielectric mirror M (650-1130 nm, Newport, USA). Leaving the actual microscope the emitted photons are fur-

thermore chromatically separated by a second dichroic mirror DC2 (590 DCXR, AHF, Germany), splitting up the green and red part of the fluorescence in a perpendicular manner. Before being focussed with a lens (either L1 or L2, respectively) and detected by the avalanche photo diodes (APD1 or APD2, respectively; SPCM-AQR-13, Perkin-Elmer, Canada) the fluorescence photons are additionally filtered by two bandpass filters BP1/BP2 (HQ 645/75 and HQ 535/50; AHF, Germany). The TTL (transistor-transistor-logic) signals from the APD are analyzed using a 4-channel router (PRT 400, PicoQuant GmbH, Germany) and a TCSPC (time-correlated single photon counting) card (Time-Harp200, PicoQuant GmbH, Germany) and saved in PicoQuant's TTTR (time-tagged time-resolved) format. The correlation is processed using a home-made program (written by Matthias Grunwald). The effective volume of TPE in this study is about 0.8 fl. Figure 3.1 displays the basic setup used in this study.

# Chapter 4

## Results

### 4.1 Synaptotagmin-1 is a distance regulator

Recently it has been shown that synaptotagmin-1 may be a distance regulator acting upstream of SNARE nucleation in a  $\text{Ca}^{2+}$  and  $\text{PiP}_2$  dependent manner [119]. This assumption is based on FRET experiments of Texas red and Oregon green labeled liposomes performed under low ionic strength conditions at 5 mM KCl, which is much lower than the actual physiological concentration of 150 mM KCl and thus, permits to investigate the contribution of electrostatic interactions of synaptotagmin-1 based tethering. Furthermore, this suggestion was based on the observation of an increased FRET in steady state measurements performed in bulk solution. However, quantitative assessments of the transmembrane FRET efficiency as a function of e.g.  $\text{Ca}^{2+}$  or the  $\text{PiP}_2$  concentration are not possible in a bulk assay. Therefore, final evidence for this hypothesis is still missing. Furthermore, previous studies show that ATP enhances liposome fusion [83]. The authors hypothesize that this is due to ATP preventing *cis*-binding of synaptotagmin-1 to its own host membrane although *cis*-binding is generally favoured over *trans*-binding [121]. The first two studies were not capable of discriminating docking from fusion though. In FCCS one analyzes fluorescence fluctuations caused by diffusion of single particles through the focal volume (in case of TPE about 1 fL) [24]. With FCCS it is not only possible to differentiate between docked and fused state, but also to calculate absolute tethering amounts [24, 121]. The first part of this chapter provides a link between the above listed findings. Thereby, the focus lies on the potential distance regulation function of synaptotagmin-1 and how it may be altered. It first describes the influence of electrostatic effects that might hinder/facilitate synaptotagmin-1 *cis/trans*-binding and subsequent intermembrane distance shortening. Moreover, the concentration of PS and  $\text{PiP}_2$  in the liposome membrane and the concentration of ATP in solution are addressed in particular. Additionally, the influence of synaptobrevin 2 and syntaxin 1A are analyzed. The role of the functional domains ( $\text{C}_2\text{A}$ ,  $\text{C}_2\text{B}$ , KKKK) of synaptotagmin-1 is characterized as well with regard to their particular functionality in distance regulation.

### 4.1.1 Synaptotagmin-1 binding depends on ionic strength conditions and liposome concentration

The first experiments indicating that synaptotagmin-1 may be a distance regulator were published in 2010 [119]. The authors of this publication furthermore address the capability of synaptotagmin-1 to induce liposomal clustering. Since high salt concentrations may screen potentially important electrostatic interactions [113, 119] the measurements shown in this publication were performed under low ionic strength buffer conditions (5 mM KCl), which is significantly below the physiological condition (150 mM KCl). Moreover, the experiments illustrating the capability of synaptotagmin-1 to act as a distance regulator were performed in bulk solution [119]. Since this study aims to further characterize this potential distance regulation function of course, the corresponding experiments have to be reproduced under low and physiological ionic strength conditions in terms of single molecule FCCS measurements.

The sample preparation is performed equivalently to the one described in [119]. The liposomes contain 15% PS each. Again, 1% PiP<sub>2</sub> is present in the target membrane of one of the two liposome combinations. The FCCS experiment presented in figure 4.1 is furthermore performed under low ionic strength conditions. The cross-correlation which reflects the amount of tethered liposomes, and the fluorescence lifetime which, in this case, is a measure for the actual liposome distance are analyzed as a function of the apparent calcium ion concentration.

Interestingly, no tethering or lifetime alterations at all are recorded for the solely PS containing liposome (figure 4.1(A)). In contrast to this, with 1% PiP<sub>2</sub> in the target membrane, tethering becomes apparent with a  $K_D$  value at around 100  $\mu\text{M}$  (figure 4.1(B)). However, determination of an exact dissociation constant is rather critical since the overall increase in tethering is very small. The recorded lifetime changes are rather minor. Therefore, the  $K_D$  value here should not be over-interpreted. Hence, the figures 4.1(A) and (B) demonstrate that under non-physiological conditions FCCS does not reveal any significant alterations neither in tethering nor in the recorded fluorescence lifetime.

The most obvious difference between the two experiments described above and those published elsewhere [119] is the concentration of liposomes used within the measurement. Since FCCS operates in the nM-range, the liposomes are mixed in the nM-range and incubated for 30 min prior to measuring. Whereas in the bulk study described above [119] concentrations in the  $\mu\text{M}$ -range have been used. Therefore, the next set of experiments is performed by mixing the two distinct liposome populations at  $\mu\text{M}$ -concentrations. Buffer is then added afterwards, right before measuring, in order to dilute the sample to FCCS-applicable concentrations.

Figure 4.2 displays the amount of tethered liposomes under varying KCl concentrations either in the presence or absence of Ca<sup>2+</sup> as determined for a sample mixture pre-incubated in the  $\mu\text{M}$ -range. Under physiological buffer conditions tethering is increased in the presence of calcium ions.

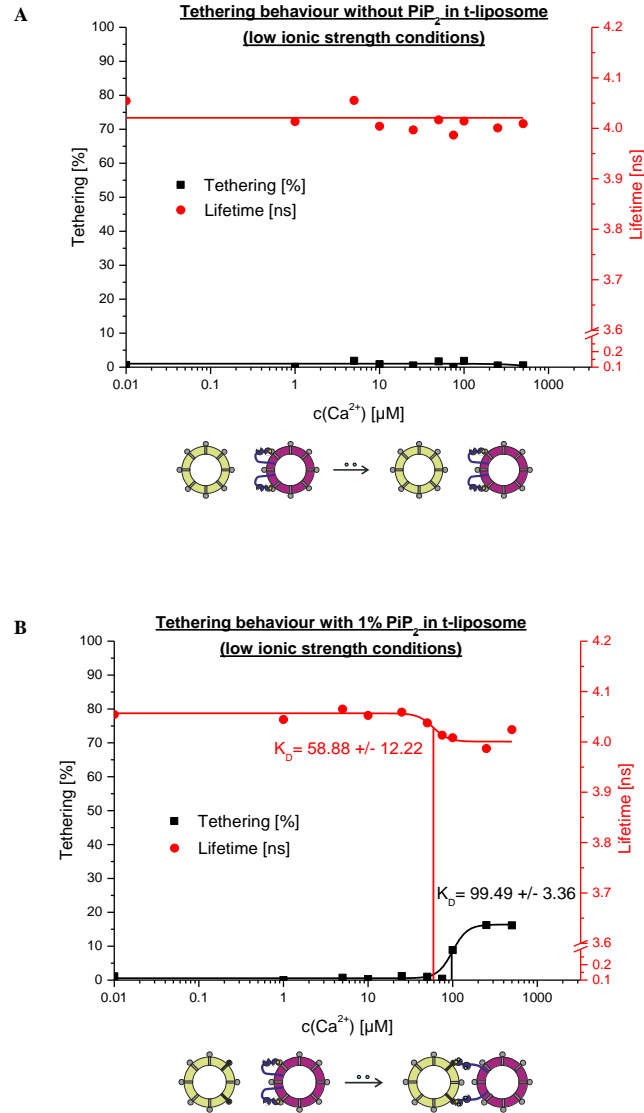


Figure 4.1: Synaptotagmin-1 tethering (black) and fluorescence lifetime (red) response towards increasing calcium concentrations. Target liposomes contain 15% PS and (if indicated) 1%  $\text{PiP}_2$ . Host liposomes contain 15% PS and reconstituted full-length synaptotagmin-1. In the control no synaptotagmin-1 is present in the Texas red liposome. Error bars are left out for the sake of clarity. Hill fits are applied to the data points with the resulting dissociation constant ( $K_D$ ) indicated (black and red strokes). Tethering and fluorescence lifetimes are determined under non-physiological buffer conditions for (A) the  $\text{PiP}_2$ -less and the (B) 1%  $\text{PiP}_2$  containing liposome.

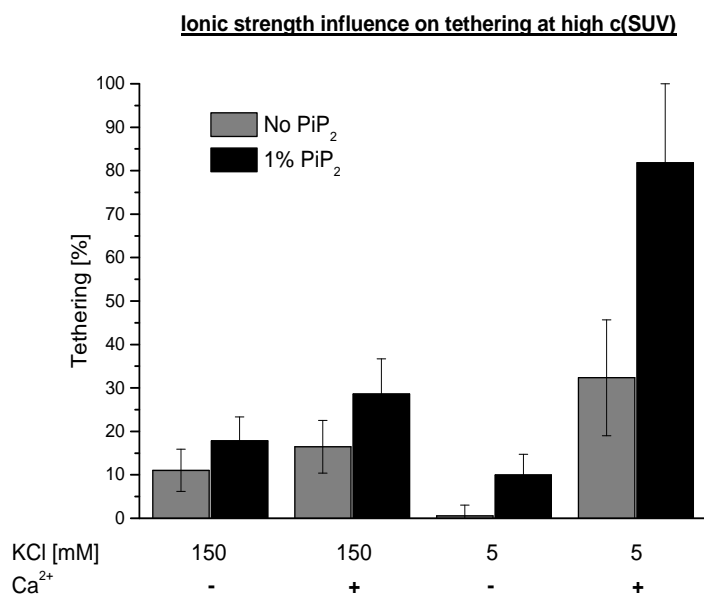


Figure 4.2: Reconstituted synaptotagmin-1 tethering to a solely 15% PS containing liposome (gray) and a liposome that additionally hosts 1% PiP<sub>2</sub> (black). Synaptotagmin-1 host liposomes also contain 15% PS. Liposomes are mixed and incubated in the  $\mu$ M-range. Buffer conditions and calcium concentrations are shown on the x-axis. In the control no synaptotagmin-1 is present in the Texas red liposome. Error bars represent the standard deviation of several measurements.

Moreover, PiP<sub>2</sub> additionally increases the amount of tethered liposomes. Under non-physiological buffer conditions tethering is almost completely abolished in the absence of calcium. Even with 1% PiP<sub>2</sub> in the target liposome the amount of tethering does not exceed 10%. A completely different picture is drawn in the presence of calcium. Here, even without PiP<sub>2</sub> the amount of tethered liposomes is already around 35%. With PiP<sub>2</sub> being incorporated into the target membrane, tethering increases up to 85%.

Figure 4.2 demonstrates that the differences in synaptotagmin-1 induced tethering are quite dramatic, depending on the ionic strength of the surrounding media. Moreover, the influence of calcium becomes more dominant under non-physiological buffer conditions. The data presented in figure 4.2 is in line with the previously mentioned study [119] showing that synaptotagmin-1 induces liposome clustering and that clustering is PiP<sub>2</sub> and calcium dependent. Comparing the findings above with those presented in figure 4.1 it becomes obvious that the applied liposome concentration has a tremendous effect on the outcome of an experiment.

As a matter of course, it becomes reasonable to also take a closer look at the fluorescence lifetime recorded under  $\mu$ M-range conditions. Figure 4.3

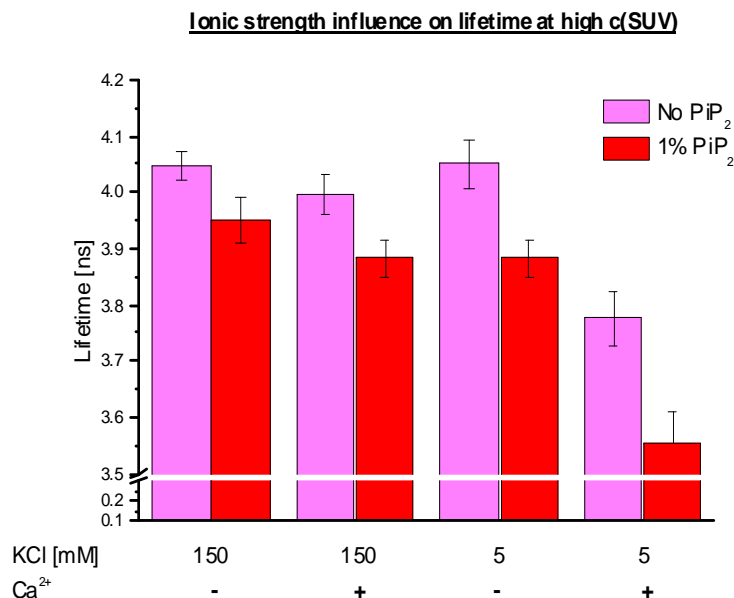


Figure 4.3: Fluorescence lifetime of Oregon green in a synaptotagmin-1 carrying SUV as a result of tethering to a solely 15% PS containing liposome (magenta) and a liposome that additionally hosts 1% PiP<sub>2</sub> (red). Liposomes are mixed and incubated in the  $\mu$ M-range. Buffer conditions and calcium concentrations are shown on the x-axis. Synaptotagmin-1 host liposomes also contain 15% PS. In the control no synaptotagmin-1 is present in the Texas red liposome. Error bars represent the standard deviation of several measurements

demonstrates the influence of KCl and Ca<sup>2+</sup> on the Oregon green lifetime in the target liposomes. Under physiological conditions the lifetime of the solely 15% PS carrying Oregon green liposome is neither affected in the presence nor in the absence of calcium ions. Here, the lifetime is about 4.05 ns which represents the lifetime of the corresponding Oregon green liposome measured in the absence of any synaptotagmin-1 carrying Texas red liposome. However, the lifetime of the 1% PiP<sub>2</sub> containing Oregon green liposome is indeed decreased. Moreover, the lifetime shift is larger in the presence of calcium, indicating a potential calcium and PiP<sub>2</sub> dependent shortening of the distance between both liposome membranes.

Under non-physiological buffer conditions in the absence of calcium, the lifetime shows a very similar behaviour to what has been described above for the measurements performed under physiological salt concentrations. The lifetime for the solely 15% PS carrying Oregon green liposome is not affected, while the one carrying 1% PiP<sub>2</sub> already displays a significantly shorter fluorescence lifetime. Here, the lifetime even seems to be further shortened compared to the calcium free measurement under physiological buffer conditions. The last

column represents the measurement performed under non-physiological buffer conditions and in the presence of calcium. Surprisingly, here both liposome combinations reveal a decrease in fluorescence lifetime. Nevertheless, again the lifetime for the 1% PiP<sub>2</sub> carrying liposome is significantly shorter than the one for the solely 15% PS containing one. This is in line with the findings shown in figure 4.2 and [119]. Not only clustering but also a potential membrane distance shortening under low ionic strength conditions is heavily dependent on the concentration of calcium and PiP<sub>2</sub>. In order to quantitatively compare the normalized fluorescence lifetime changes (*NFLC*) achieved under physiological and low ionic strength conditions, the relative alteration in fluorescence lifetime is normalized by the fraction of tethering in the different samples as presented in figure 4.4:

$$NFLC = (\Delta Lifetime / \Delta Tethering) \quad (4.1)$$

The error bars are calculated via error analysis as can be deduced from chapter 7. Here the standard deviations presented in figure 4.2 and figure 4.3 are taken into account.

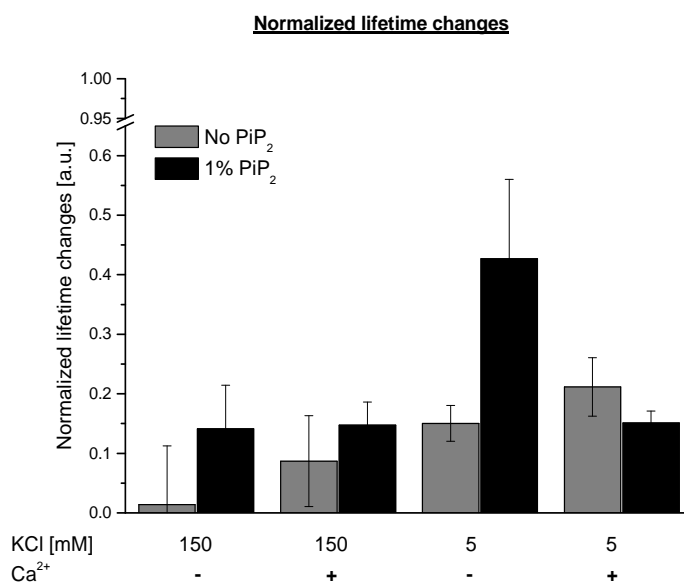


Figure 4.4: Normalized fluorescence lifetime changes of the data presented above in figure 4.2 and 4.3. Reconstituted synaptotagmin-1 tethers to a solely 15% PS containing liposome (gray) and a liposome that additionally hosts 1% PiP<sub>2</sub> (black). Buffer conditions and calcium concentrations are shown on the x-axis. Synaptotagmin-1 host liposomes also contain 15% PS. In the control no synaptotagmin-1 is present in the Texas red liposome. The tethering based normalized fluorescence lifetime changes are calculated according to their relative changes in lifetime and tethering. Error bars are calculated via error analysis.

Figure 4.4 shows that a normalized fluorescence lifetime change of  $0.01 \pm 0.09$  is determined in the absence of both,  $\text{PiP}_2$  and  $\text{Ca}^{2+}$  (first gray bar) under physiological ionic strength conditions. In the presence of  $\text{PiP}_2$  the normalized fluorescence lifetime change increases to  $0.14 \pm 0.07$  (first black bar). Addition of calcium ions yields to normalized fluorescence lifetime change of  $0.09 \pm 0.07$  and  $0.15 \pm 0.04$ , respectively (second group of bars of figure 4.4). Interestingly, in the presence of  $\text{PiP}_2$ , calcium ions do not enhance the normalized fluorescence lifetime change any further.

Under non-physiological conditions the most prominent normalized fluorescence lifetime change is calculated in the presence of  $\text{PiP}_2$ , but in the absence of calcium (third black bar). Again, in the absence of  $\text{PiP}_2$  calcium ions increase the normalized fluorescence lifetime changes (third and fourth gray bars). Strikingly, under non-physiological conditions the normalized fluorescence lifetime change is smaller in the presence of  $\text{PiP}_2$  and  $\text{Ca}^{2+}$ , then in the absence of  $\text{Ca}^{2+}$ , which should not be over-interpreted. The corresponding normalized fluorescence lifetime changes are calculated as follows (from left to right):  $0.15 \pm 0.08$ ,  $0.43 \pm 0.13$ ,  $0.22 \pm 0.05$  and  $0.15 \pm 0.02$ .

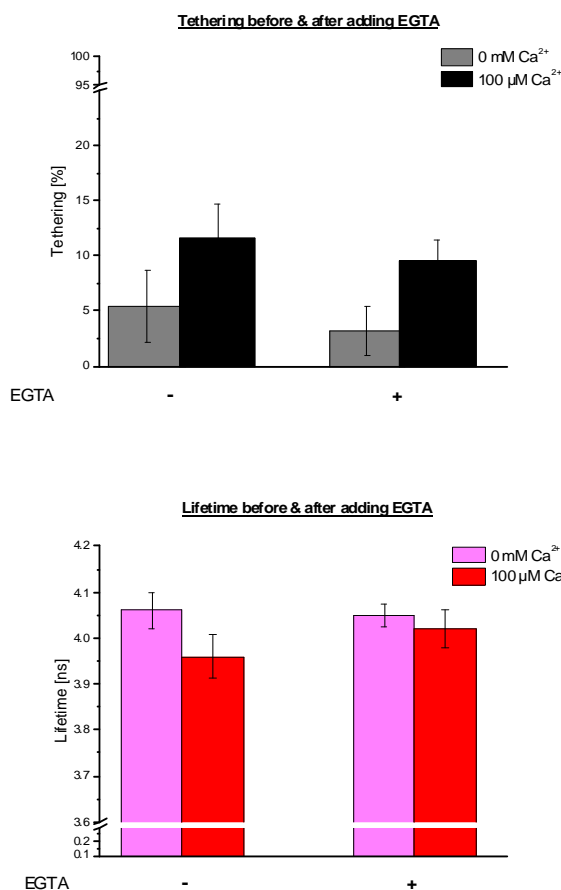


Figure 4.5: Tethering and fluorescence lifetime of Oregon green before (left bars) and after (right bars) the addition of excess amounts of EGTA. Liposomes are mixed and incubated for 30 min and are subsequently measured. Addition of EGTA is followed by an additional incubation of 30 min. Colour codes indicate the original  $\text{Ca}^{2+}$  concentrations the samples are incubated in.

As a control for distance based FRET and to exclude fusion, the above meas-

ured 15% PS liposome combinations including 1% PiP<sub>2</sub> in the target liposome are incubated at nM concentrations under physiological ionic strength conditions and measured again (left bars). There is no apparent difference to what has been reported above in figure 4.2 and 4.3 in terms of tethering and fluorescence lifetime. Samples are then incubated with additional excess amounts of EGTA (20 mM) and measured for once more. EGTA complexes Ca<sup>2+</sup> ions, thus removing calcium ions even from the sample combination previously measured in the presence of 100  $\mu$ M Ca<sup>2+</sup>. Incubation before and after the addition of EGTA takes 30 min.

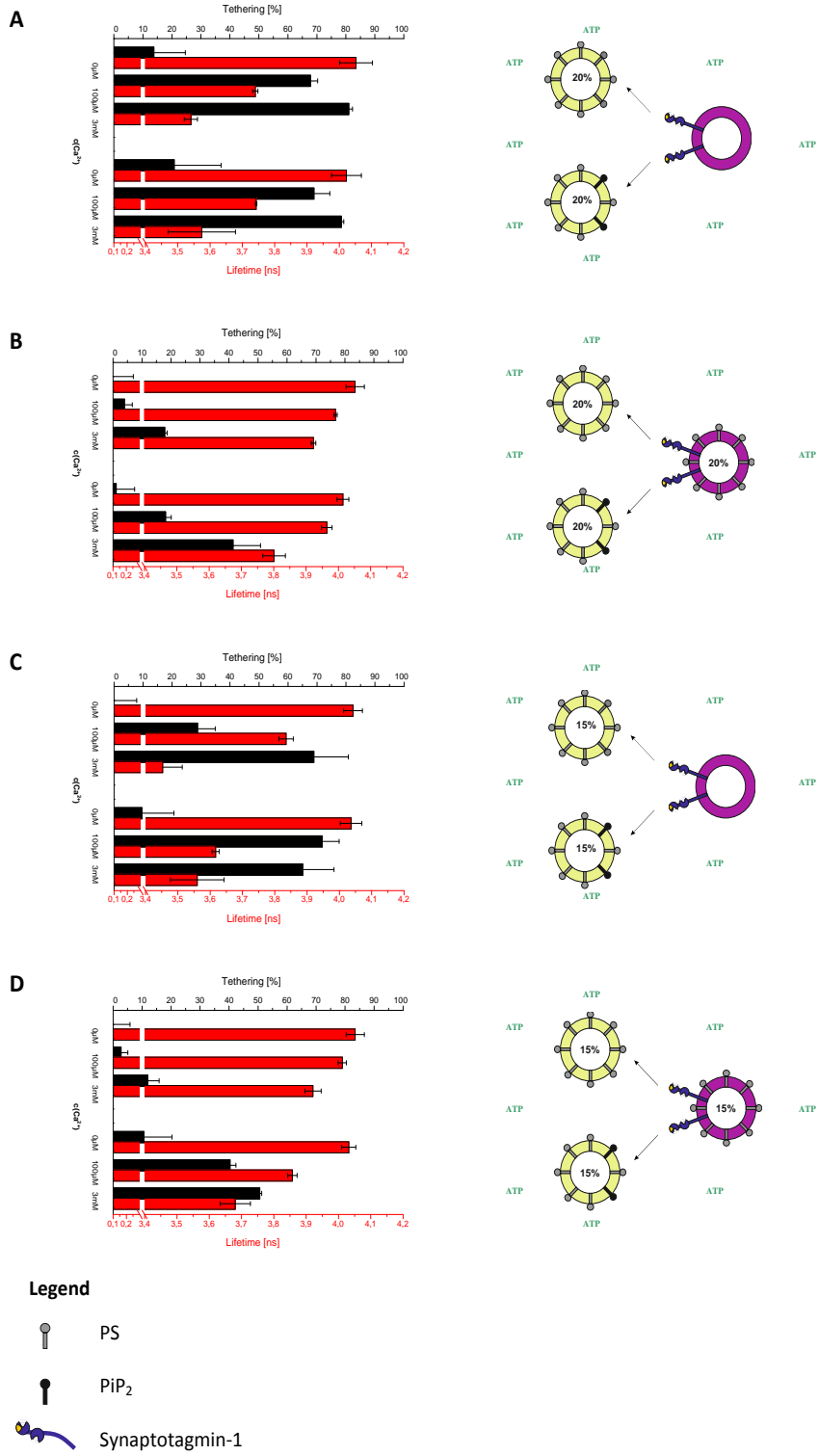
As can be deduced from Figure 4.5 (upper left) tethering is still greater for the sample combination formerly including calcium. Figure 4.5 furthermore demonstrates that although the liposomes stay tethered after the addition of EGTA, the lifetime returns to almost its original value. Hence, fusion of the sample can be excluded. The observed FRET effect is caused by minimizing the distance between two liposomes upon increasing calcium concentrations.

### 4.1.2 ATP can enhance liposome tethering

As previously mentioned, earlier studies investigated the capability of synaptotagmin-1 to act either in *cis* or *trans* [121]. Within this study small unilamellar liposomes (SUVs) containing either no or 20% anionic lipids were used in order to describe the influence of different mutations on the overall tethering percentage of synaptotagmin-1. Here, *trans*-binding was completely abolished when carrying 20% PS in the host (h) and target (t) membrane. Other studies show that with PS concentrations below 20% fusion can be enhanced by addition of 3 mM ATP [83]. Here, the authors state that ATP induces an electrostatic screening effect which in turn may prevent *cis*-binding as described in subsection 2.2.1. Nevertheless, further evidence is required for this hypothesis, e.g. it still remains unclear whether ATP can also enhance tethering prior to fusion. If so, then ATP may enable synaptotagmin-1 to overcome the electrostatic barrier induced by the presence of PS in host and target liposomes.

Hence, two distinct liposome populations are prepared as described in [121]. These populations either contain no, 20 % or 15% PS. A second set of liposomes additionally contains 1% PiP<sub>2</sub>. The two distinct liposome populations are mixed in a 1:1 ratio and incubated for 30 min at RT in ATP buffer or HP150 buffer prior to measuring. The following experiments are performed under ionic strength conditions similar to the physiological state. Synaptotagmin-1 is reconstituted into liposomes that are labeled with Texas red-DHPE, whereas the protein-free target liposomes are labeled by using Oregon green-DHPE. In order to correspond to the findings quoted above [83], the measurements are performed with either no, 100  $\mu$ M or excess amounts (3 mM) of Ca<sup>2+</sup>. Of course, at such high concentrations spontaneous fusion can not be fully excluded.

Figure 4.6 shows the overall tethering amount and the fluorescence lifetime changes upon mixing the synaptotagmin-1 carrying liposomes. Here, Figure 4.6(A) and (B) represent the same set of experiments as published in [121], ex-



cept that here, 3 mM ATP are present. By comparing the present results with the previously published ones [83, 121] it becomes clear that ATP does not alter binding of liposomes containing 20% PS. While there is almost full tethering in the absence of PS in the host membrane 4.6(A), tethering is still below 20% at 100  $\mu\text{M}$  calcium ions when PS is incorporated into the host liposome 4.6(B). Here, the presence of  $\text{PiP}_2$  in the target liposome seems to enhance tethering. Accordingly, the fluorescence lifetime is not altered significantly either, unless excess amounts of  $\text{Ca}^{2+}$  are added. On the other hand, figure 4.6(A) indeed illustrates an alteration in fluorescence lifetime depending on the concentration of calcium ions. Since there are no anionic lipids present in the host membrane, the calcium dependency can not be explained by simple reduction of the electrostatic barrier induced by the presence of calcium ions. Thus, already anticipating a potential distance regulation function of synaptotagmin-1 that is triggered by  $\text{Ca}^{2+}$ .

A slightly different picture can be drawn from figure 4.6(C). Here, 15% PS are present in the target liposomes. Again, as tethering increases upon increasing  $\text{Ca}^{2+}$  concentrations, the lifetime decreases. Interestingly this effect is more prominent for the  $\text{PiP}_2$  containing measurement. In line with this are the observations represented in figure 4.6(D). Here also the host liposome contains 15% PS. The alterations in tethering and lifetime are smaller compared to figure 4.6(C), because of the electrostatic barrier created by the presence of PS. Nevertheless, the  $\text{PiP}_2$  containing liposome shows a more pronounced response in tethering and fluorescence lifetime towards increasing  $\text{Ca}^{2+}$  concentrations. Comparing the results depicted in figure 4.6(D) which are measured in the presence of ATP with those measured in the absence of ATP (figure 4.7(A) and (B)), it becomes obvious that indeed ATP seems to enhance tethering. However, a more elaborate analysis is given in subsection 4.1.3.

In summary, 3 mM ATP do not seem to help to overcome *cis*-binding to 20% PS and therefore support *trans*-binding, which is in line with earlier fusion studies [83]. The effect of 3mM ATP on 15% PS containing liposomes shows that indeed tethering is enhanced. Moreover, the data depicted in figure 4.6 shows that the fluorescence lifetime is reduced. To shed light on this issue, a more detailed picture of the influence of ATP is drawn in subsection 4.1.3. Measurements in a range from 0 to 3 mM  $\text{Ca}^{2+}$  are performed in order to further characterize the tethering and fluorescence lifetime modifications.

---

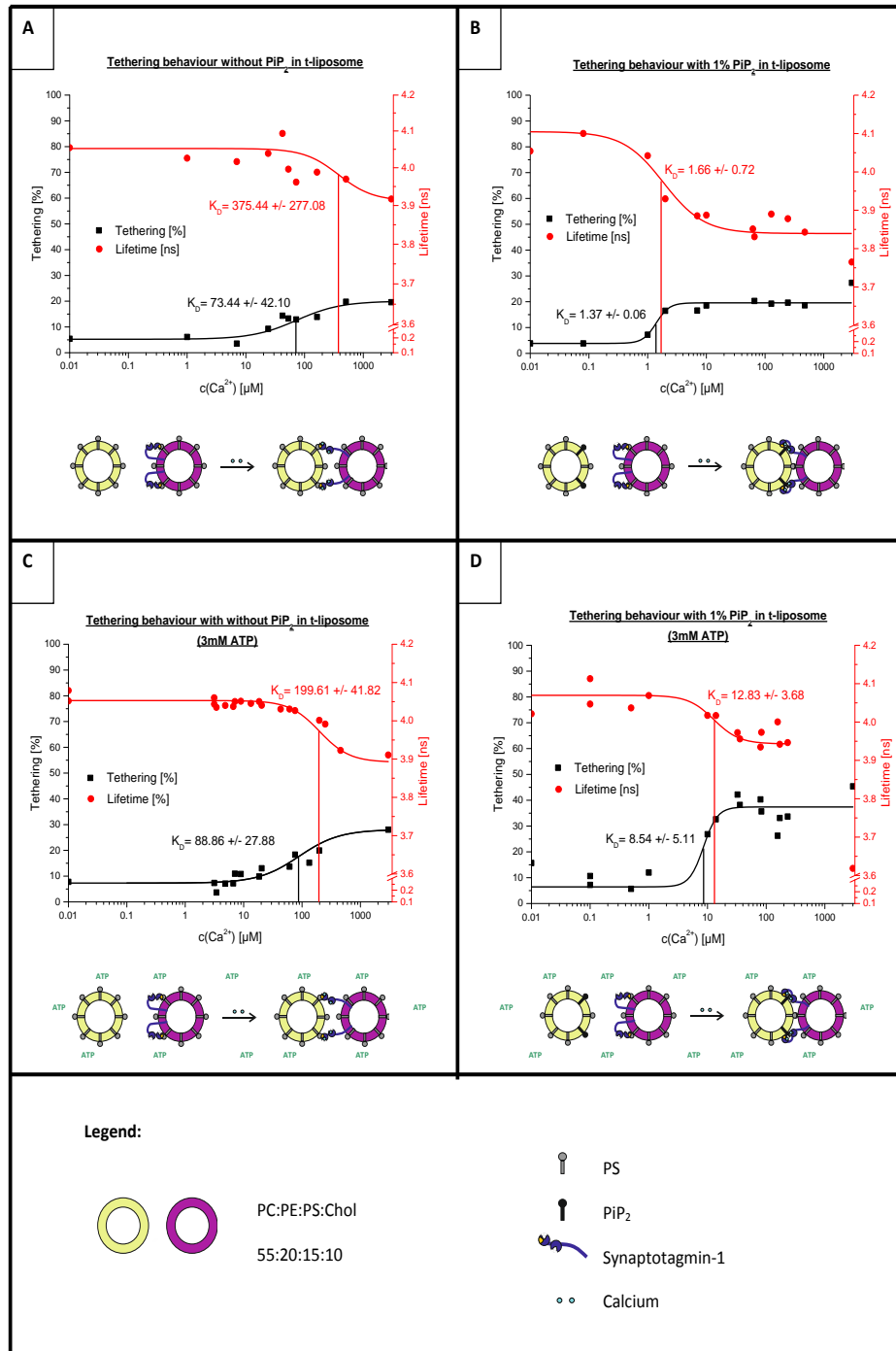
Figure 4.6 (*preceding page*): Synaptotagmin-1 tethering (black) and fluorescence lifetime (red) response towards increasing calcium concentrations. Target liposomes contain either 20% or 15% PS and (if indicated) 1%  $\text{PiP}_2$ . Host liposomes contain no (A) and (C), 20% (B), or 15% (D) PS and reconstituted full-length synaptotagmin-1. In the control no synaptotagmin-1 is present in the Texas red liposome. 3 mM ATP is present in all measurements.

### 4.1.3 Synaptotagmin-1 acts as a distance regulator when bound to PiP<sub>2</sub> and is affected by electrostatic screening through ATP

If synaptotagmin-1 really acts as a distance regulator when bound to PiP<sub>2</sub>, the amount of tethering should increase while the corresponding fluorescence lifetime for Oregon green should simultaneously with increasing calcium concentrations. In other words, the dissociation constant ( $K_D$ ) of the corresponding Hill fits should be equal. The following measurements are performed under physiological buffer conditions with up to three biological replicates. Again, a target liposome with having no synaptotagmin-1 reconstituted is measured as a control. The liposome measurements without ATP are performed in HP150 buffer, those containing 3 mM ATP are carried out in ATP buffer, exhibiting a virtually equal ionic strength. The samples are moreover treated as described in subsection 4.1.2.

The graphs shown in this section display representative measurements of one day. The fit is set free to converge without any constraints. All parameters deduced from the shown Hill fits are in good agreement with others originating from the above mentioned biological replicates. Indeed, a preference for synaptotagmin-1 to bind to PiP<sub>2</sub> is shown in figure 4.7(A) and (B). Not only is the overall tethering amount at high calcium concentrations about  $\frac{1}{3}$  higher than in the absence of PiP<sub>2</sub> in the target liposome, but the dissociation constant is additionally shifted to the low  $\mu\text{M}$ -range. The simultaneously recorded lifetime development does not show any significant decrease in figure 4.7(A) unless reaching excess ( $> 400 \mu\text{M}$ ) concentrations of Ca<sup>2+</sup>. Therefore, the illustrated  $K_D$  of  $374.44 \pm 277.08 \mu\text{M}$  should not be over-interpreted. In contrast to this, with 1% PiP<sub>2</sub> in the target liposome, the alterations for both - tethering and fluorescence lifetime - are quite distinct. Moreover, the dissociation constants for tethering and lifetime are exactly the same. This indicates that distance regulation of synaptotagmin-1 is not only dependent on Ca<sup>2+</sup>, but also on binding to PiP<sub>2</sub>.

In order to further investigate the influence of 3 mM ATP on tethering and distance regulation the same set of experiments are performed in the presence of ATP as depicted in figure 4.7(C) and (D). Both tethering curves in figure 4.7(C) and (D) show an increase in the overall tethering amount when compared to figure 4.7(A) and (B). The amount of tethered liposomes adds up to almost 40% compared to 20% for the PiP<sub>2</sub> liposome combination measured in the absence of ATP. Additionally, the dissociation constant for tethering is shifted to higher calcium concentrations. While the  $K_D$  value for the liposome carrying 1% PiP<sub>2</sub>, measured in the presence of ATP, is still in the lower  $\mu\text{M}$ -range, for the solely PS containing target liposome it is in a moderate  $\mu\text{M}$ -range. Both liposome mixtures excluding PiP<sub>2</sub> (figure 4.7(C) and (A)) reveal  $K_D$  values for the fluorescence lifetime in the high  $\mu\text{M}$ -range of Ca<sup>2+</sup>. When comparing 4.7(B) and (D) it becomes obvious that the overall lifetime decrease is less with 3 mM ATP than without. An increased electrostatic environment can most likely account for this, which is in line with the observations made in subsection 4.1.1.



For both PiP<sub>2</sub> containing sample combinations tethering and fluorescence lifetime alter simultaneously. Since the potency  $n$  heavily depends on the goodness of the fit, it is not considered for further interpretation of the data. Especially, because the alterations in tethering and fluorescence lifetime are rather small. Table 4.1.3 summarizes all fit values achieved. The R<sup>2</sup> values presented in table 4.1.3 are all in a reasonable range. Only (A) shows a poor coefficient of determination owing to the small overall changes.

Table 4.1: Summary of Hill fit values determined for synaptotagmin-1 wt presented in figure 4.7.

parameter	A	B	C	D
<b>Tethering</b>				
Start [%]	5.23 ± 0.92	3.86 ± 0.20	7.31 ± 2.42	6.44 ± 0.5
End [%]	20.03 ± 3.10	19.23 ± 0.53	28.08 ± 3.92	37.40 ± 1.73
K <sub>D</sub> [μM]	73.44 ± 42.10	1.37 ± 0.06	88.86 ± 27.88	8.45 ± 5.11
n	1.15 ± 0.61	4.02 ± 0.41	1.24 ± 0.54	3.65 ± 5.73
R <sup>2</sup>	0.87	0.99	0.90	0.96
<b>Lifetime</b>				
Start [ns]	4.05 ± 0.02	4.10 ± 0.01	4.05 ± 0.00	4.07 ± 0.00
End [ns]	3.91 ± 0.05	3.85 ± 0.03	3.89 ± 0.02	3.94 ± 0.01
K <sub>D</sub> [μM]	375.44 ± 277.01	1.66 ± 0.72	199.61 ± 41.82	12.89 ± 3.79
n	1.48 ± 2.05	1.39 ± 0.68	1.69 ± 0.27	2.02 ± 0.91
R <sup>2</sup>	0.64	0.98	0.99	0.99

As a control for fluorescence lifetime stability, which may have been affected by varying calcium ion concentrations and to exclude unspecific binding, a titration experiment as depicted above in figure 4.7 is performed with empty liposomes with no protein being reconstituted in either of the two membranes. Figure 4.8 demonstrates that tethering as well as the fluorescence lifetime are

---

Figure 4.7 (*preceding page*): Synaptotagmin-1 tethering (black) and fluorescence lifetime (red) response towards increasing calcium concentrations. Target liposomes contain 15% PS and (if indicated) 1% PiP<sub>2</sub>. Host liposomes contain 15% PS and reconstituted full-length synaptotagmin-1. In the control no synaptotagmin-1 is present in the Texas red liposome. Error bars are left out for the sake of clarity. Hill fits are applied to the data points with the resulting dissociation constant (K<sub>D</sub>) being indicated (black and red strokes). (A) and (B) Tethering and fluorescence lifetime development under physiological buffer conditions. (C) and (D) Tethering and fluorescence lifetime development under physiological buffer conditions with 3 mM ATP being added.

not altered upon rising Ca<sup>2+</sup> concentrations. A straight line with slope  $m = 0$  is applied to the data. Hence, the increase in tethering and the decrease in fluorescence lifetime depicted in figure 4.7 are due to specific binding of synaptotagmin-1 to anionic lipids and its capability to reduce the intermembrane distance.

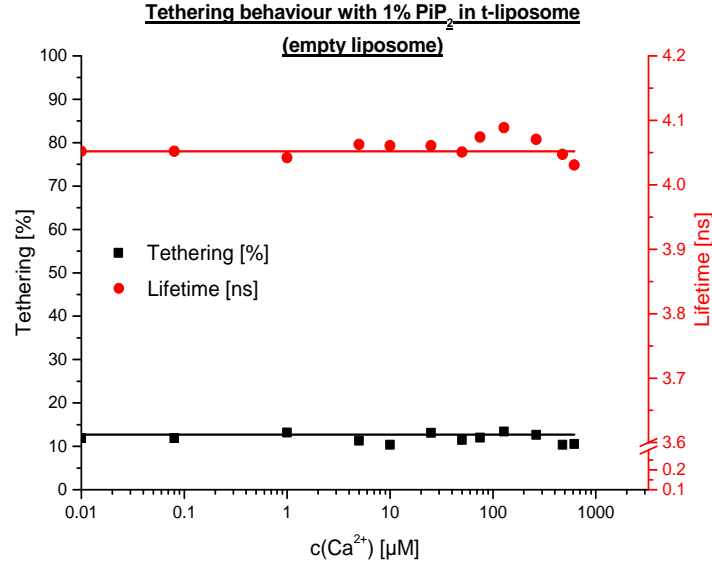


Figure 4.8: Tethering (black) and fluorescence lifetime (red) response of empty liposomes towards increasing calcium concentrations. Target liposomes contain 15% PS and 1% PiP<sub>2</sub>. Host liposomes contain 15% PS. Error bars are left out for the sake of clarity.

Although the data depicted in figure 4.7 show a distinct difference in tethering and fluorescence lifetime depending on the presence of calcium and PiP<sub>2</sub>, the overall alterations are rather small. In order to proof the existence of a distance regulation function of synaptotagmin-1 a variety of evaluations of the underlying data is necessary. Hence four different approaches of data processing are presented in the following paragraphs.

#### Amount of tethered liposomes: $f_{bound}$

Since the amount of tethered  $f_{bound}$  and freely diffusing liposomes  $f_{unbound}$  are known from the Hill fit, it is moreover possible to calculate the quenched fluorescence lifetime  $\tau_{bound}$  of the bound liposome fraction  $f_{bound}$  with the help of the unaffected Oregon green lifetime  $\tau_{unbound}$  according to:

$$\tau_{measured} = f_{bound} \cdot \tau_{bound} + f_{unbound} \cdot \tau_{unbound} \quad (4.2)$$

which leads to

$$\tau_{bound} = \frac{(\tau_{measured} - f_{unbound} \cdot \tau_{unbound})}{f_{bound}} \quad (4.3)$$

This calculation provides a 1<sup>st</sup> measure for the fluorescence lifetime of the bound liposome fraction. For calculations, the fluorescence lifetime and tethering after reaching the saturation plateau are taken. Here, the unaffected fluorescence lifetime is set to the start value obtained from the Hill fit. The errors of tethering and fluorescence lifetime resulting from the applied Hill fits are furthermore taken for error analysis as can be deduced from chapter 7. Hence, the fluorescence lifetime of the tethered liposomes can be calculated for all four different conditions as follows: Under the conditions presented in figure 4.7(A) a  $\tau_{bound}$  of  $3.35 \pm 1.37$  ns is determined, under (B) the quenched fluorescence lifetime is  $2.79 \pm 0.26$  ns, under (C) the lifetime decreases to  $3.48 \pm 1.31$  ns and finally for the measurement conditions presented in figure 4.7(D) including both - ATP and PiP<sub>2</sub> - a fluorescence lifetime of  $3.73 \pm 0.38$  ns is calculated. Consequently the sample combination in figure 4.7(B) including PiP<sub>2</sub>, but excluding ATP shows the most prominent decrease in fluorescence lifetime. This again demonstrates that in the presence of ATP the intermembrane distance between both liposomes is enhanced.

### Linear Regression

To further emphasize on the distance regulation function of synaptotagmin-1 it is necessary to plot the actually measured lifetime against the amount of tethered liposomes. Although it has been shown that synaptotagmin-1 tethering to PiP<sub>2</sub> enhances its sensitivity for calcium ions in a cooperative manner [118], all synaptotagmin-1 wt samples investigated in this study showed a linear behaviour of the fluorescence lifetime development depending on increasing amounts in tethering. The more efficient synaptotagmin-1 accomplishes the shortening of liposome distance, the steeper the decrease in fluorescence lifetime. Figure 4.9 depicts the decrease in fluorescence lifetime depending on increasing amounts of tethering for all sample combinations presented in figure 4.7.

The samples solely including PS do not show any significant alterations in fluorescence lifetime unless reaching about 20% of tethering. Moreover, the sample combination neither including PiP<sub>2</sub> nor ATP shows the least changes. Therefore, making it impossible to apply a reasonable fit. A significant and continuous fluorescence lifetime shift is only detected for those sample combinations including 1% PiP<sub>2</sub>. Here, the sample excluding ATP shows the steeper slope. The R<sup>2</sup> value of the linear fits applied are 0.98 for the one excluding ATP and 0.96 for the sample combination including 3 mM ATP. Consequently the linear regression permits for calculating the fluorescence lifetime for complete tethering  $\tau_{bound}$ . The results of the fit shown in figure 4.9 as well as the calculated  $\tau_{bound}$  are presented in the table 4.2 below .

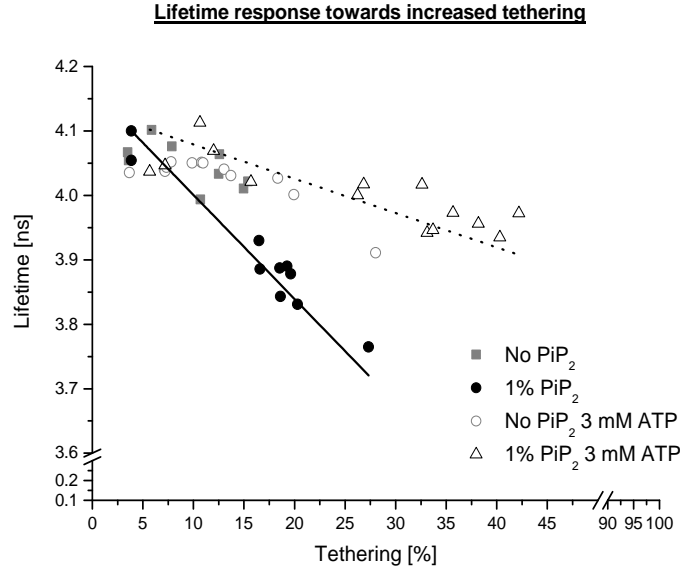


Figure 4.9: The fluorescence lifetime is plotted against tethering for reconstituted synaptotagmin-1 liposome combinations either containing no (gray symbols) or 1%  $\text{PiP}_2$  (black symbols) and no (filled symbols) or 3 mM ATP (empty symbols), respectively. For those samples containing  $\text{PiP}_2$  a linear fit is applied (black lines). For the samples solely including PS no linear regression can be obtained. Error bars are not shown for the sake of clarity.

Table 4.2: Summary of linear regression fit values determined for synaptotagmin-1 wt presented in figure 4.9. The slope is presented in  $\frac{\text{ns}}{\%}$ . Intercept and  $\tau_{bound}$  are given in ns.

parameter	A	B	C	D
slope	—	$-1.6 \cdot 10^{-2} \pm 6.33 \cdot 10^{-4}$	—	$-5.3 \cdot 10^{-3} \pm 3.16 \cdot 10^{-4}$
intercept	—	$4.16 \pm 2.66 \cdot 10^{-3}$	—	$4.13 \pm 5.16 \cdot 10^{-3}$
$\tau_{bound}$	—	$2.56 \pm 0.01$	—	$3.6 \pm 0.01$
$R^2$	—	0.98	—	0.96

The Linear Regression Model, for once more, points towards a more pronounced fluorescence lifetime decrease in the absence of ATP.

### Biexponential fitting

A third way to determine the fluorescence lifetime for full tethering  $\tau_{bound}$  is given by fitting the measured fluorescence lifetime histograms to a biexponential function in the form of:

$$y = A_1 \cdot e^{\left(\frac{-x}{\tau_{unbound}}\right)} + A_2 \cdot e^{\left(\frac{-x}{\tau_{bound}}\right)} + y_0 \quad (4.4)$$

Here,  $A_1$  and  $A_2$  represent the relative amount of tethered and untethered liposomes,  $\tau_{unbound}$  is the unaffected Oregon green fluorescence lifetime and  $y_0$  represents the recorded background signal. First, the instrument response function (IRF) is measured using free Oregon green. The IRF and the fluorescence lifetime histogram are standardized and subsequently the IRF is subtracted from the histogram. Afterwards the remaining histogram is fitted to the equation 4.4 above. The resulting fluorescence lifetimes for the bound liposomes as depicted in figure 4.7(A) to (D) are the following: For the sample mixture neither including PiP<sub>2</sub> nor ATP  $\tau_{bound}$  is determined to be  $3.28 \pm 0.30$  ns, whereas for the sample mixture including 1% PiP<sub>2</sub> it is  $3.10 \pm 0.17$  ns. The corresponding lifetimes for the Oregon green liposomes measured in the presence of ATP are  $3.61 \pm 0.17$  ns and  $3.39 \pm 0.09$  ns. All  $R^2$  values obtained are 0.99. Again, this demonstrates that in the presence of PiP<sub>2</sub> the intermembrane distance is indeed reduced. The presence of ATP in turn enhances the liposomal distance.

### Burst analysis

To further test whether ATP prevents too close contact of both liposome membranes the sample combinations measured and represented in figure 4.7(B) and (D) are diluted to concentrations around 0.1 particles in focus. Time traces are recorded for 360 s each. A single burst analysis as described in [24] is performed. Figure 4.10(A) demonstrates how a single burst is chosen. Here, the Oregon green and the Texas red fluorescence intensity rise simultaneously. Of course, it can not be excluded that the simultaneous rise is not due to multibinding since several copies of synaptotagmin-1 are reconstituted into one SUV. Nonetheless, aggregated particles would yield a more pronounced peak and thus the underlying docking of the highlighted peak should be a result of a specific binding mode. The fluorescence lifetime histogram of Oregon green originating from this particular time frame is then calculated. In order to get meaningful fitting results a whole series of measurements are carried out and their histograms are summed up. A monoexponential fit is applied to the tail of the histogram, revealing indeed a shorter lifetime for Oregon green in the absence of ATP and a longer fluorescence lifetime in the presence of 3 mM ATP. Figure 4.10(B) exemplarily shows a resulting histogram from one sample preparation measured in the presence of 100  $\mu$ M Ca<sup>2+</sup>. All sample preparations lead to similar results. Here, the fitted fluorescence lifetime of Oregon green for the sample combination measured in the absence of ATP is  $3.39 \pm 0.16$  ns, while

the one determined for the sample combination measured in the presence of ATP is  $3.88 \pm 0.18$  ns.

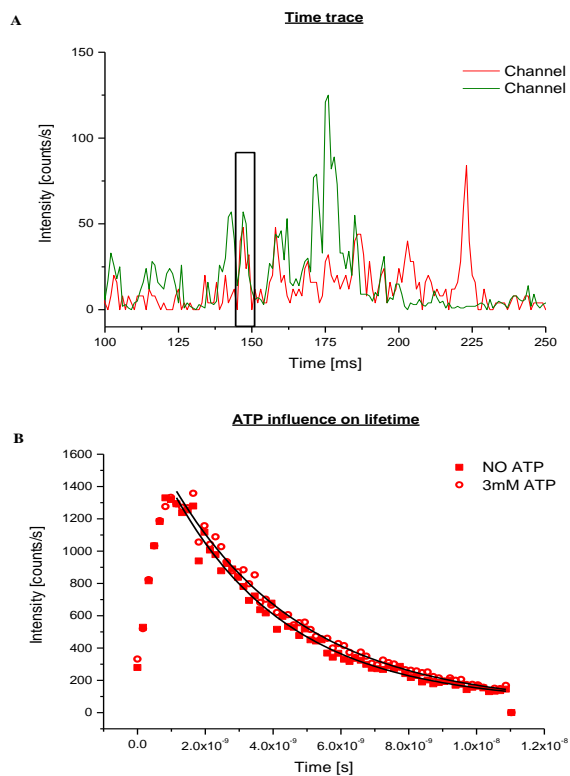


Figure 4.10: (A) Time trace of two distinctly labeled liposome populations. Channel 1 records in the red, channel 2 in the green visible spectra. (B) Liposome combination from figure 4.7 (B) and (D) are used for fluorescence lifetime histogram analysis. The resulting histograms show a shorter fluorescence lifetime in the absence of ATP. 100  $\mu\text{M}$  calcium ions are present in both measurements.

In summary, all four evaluation methods demonstrate that indeed the presence of  $\text{PiP}_2$  reduces the distance between liposomal membranes. Moreover,  $\text{Ca}^{2+}$  is absolutely required to trigger  $\text{PiP}_2$  dependent distance regulation. ATP, which has been shown to increase the overall amount of fusion [83] and tethering (figure 4.7), however, prevents too close contact of the liposome membranes.

All fluorescence lifetimes obtained by individual approaches are summarized in table 4.3. Here, the previously introduced normalized fluorescence lifetime change is calculated as well. The results are in line with the previous observations. Of course, the determined fluorescence lifetimes in table 4.3 vary among the distinct analysis methods. First, the fluorescence lifetimes presented in the titration curves are normalized to 4.05 ns for better comparability. However, the raw data obtained from individual measurements used for biexponential fitting or monoexponential fitting in burst analysis represent the original inherent Oregon green fluorescence lifetime of the individual fluorescence dye batches. Thus, the fluorescence lifetimes depicted in table 4.3 and in all following tables should be interpreted in terms of identifying consistent trends within the data pool.

The present subsection demonstrates that ATP may enhance tethering but

at the same time also enhances the distance between both liposome membranes. Additionally, ATP and shifts the dissociation constant for tethering and fluorescence lifetime to higher calcium concentration. Nevertheless, it still remains elusive whether ATP enables synaptotagmin-1 to overcome *cis*-binding and promote fusion [83].

Table 4.3: Summary of Oregon green fluorescence lifetimes. Fluorescence lifetimes of the bound liposome population are obtained by individual approaches. The fluorescence lifetimes are given in [ns]. The normalized fluorescence lifetime changes are shown as well.

parameter	A	B	C	D
$f_{bound}$	$3.35 \pm 1.37$	$2.78 \pm 0.26$	$3.48 \pm 1.31$	$3.73 \pm 0.38$
Linear regression	–	$2.56 \pm 0.00$	–	$3.60 \pm 0.01$
Biexponential fit	$3.28 \pm 0.30$	$3.10 \pm 0.17$	$3.61 \pm 0.17$	$3.39 \pm 0.09$
Burst analysis	–	$3.39 \pm 0.16$	–	$3.88 \pm 0.18$
NFLC	$0.17 \pm 0.06$	$0.32 \pm 0.06$	$0.14 \pm 0.02$	$0.08 \pm 0.01$

It has been described that for SUVs having only synaptotagmin-1 reconstituted the effect of increased fusion in either the absence or presence of ATP can be neglected [83]. Rather an additional protein density as in native synaptic vesicle (SVs) and chromaffin granules (CGs) is required to observe a dramatic effect of ATP. Moreover, the distinct role of  $\text{PiP}_2$  needs to be characterized further. In fact,  $\text{PiP}_2$  clusters are thought to provide a platform for liposome fusion in the synapse [120, 44]. Hence, the following subsections address this lack of understanding.

#### 4.1.4 Synaptotagmin-1 induced distance regulation is affected by synaptobrevin 2

It has been shown that the presence of additional proteins, as in synaptic vesicles and chromaffin granules, tremendously alters the ATP dependent fusion reaction [83]. Since fluorescently labeled native liposomes from *Rattus norvegicus* brain with a suitable dye for FCCS are not available, SUVs containing synaptotagmin-1 and synaptobrevin 2 in a 1:4 ratio are prepared. Synaptobrevin 2 is the most abundant protein in synaptic vesicles and known to interact with synaptotagmin-1 [112]. Moreover, it has been shown that the N-terminal domain of Vam3p - a member of the synaptobrevin family - coordinates priming and docking in yeast vacuole fusion [61]. Although this 1:4 ratio resembles the native protein ratio this is already the maximum amount of protein which can be incorporated into SUVs. Figure 4.11 shows a Western Blot obtained with antibodies either against synaptotagmin-1 or against synaptobrevin 2 and

a fluorescent secondary antibody against mouse. Analysis of protein ratio is performed with ImageJ demonstrating that indeed incorporation of both proteins works properly and constantly reveals a ratio of about 1:4.

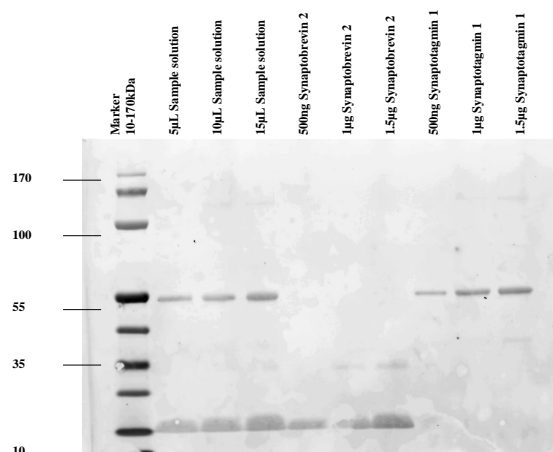
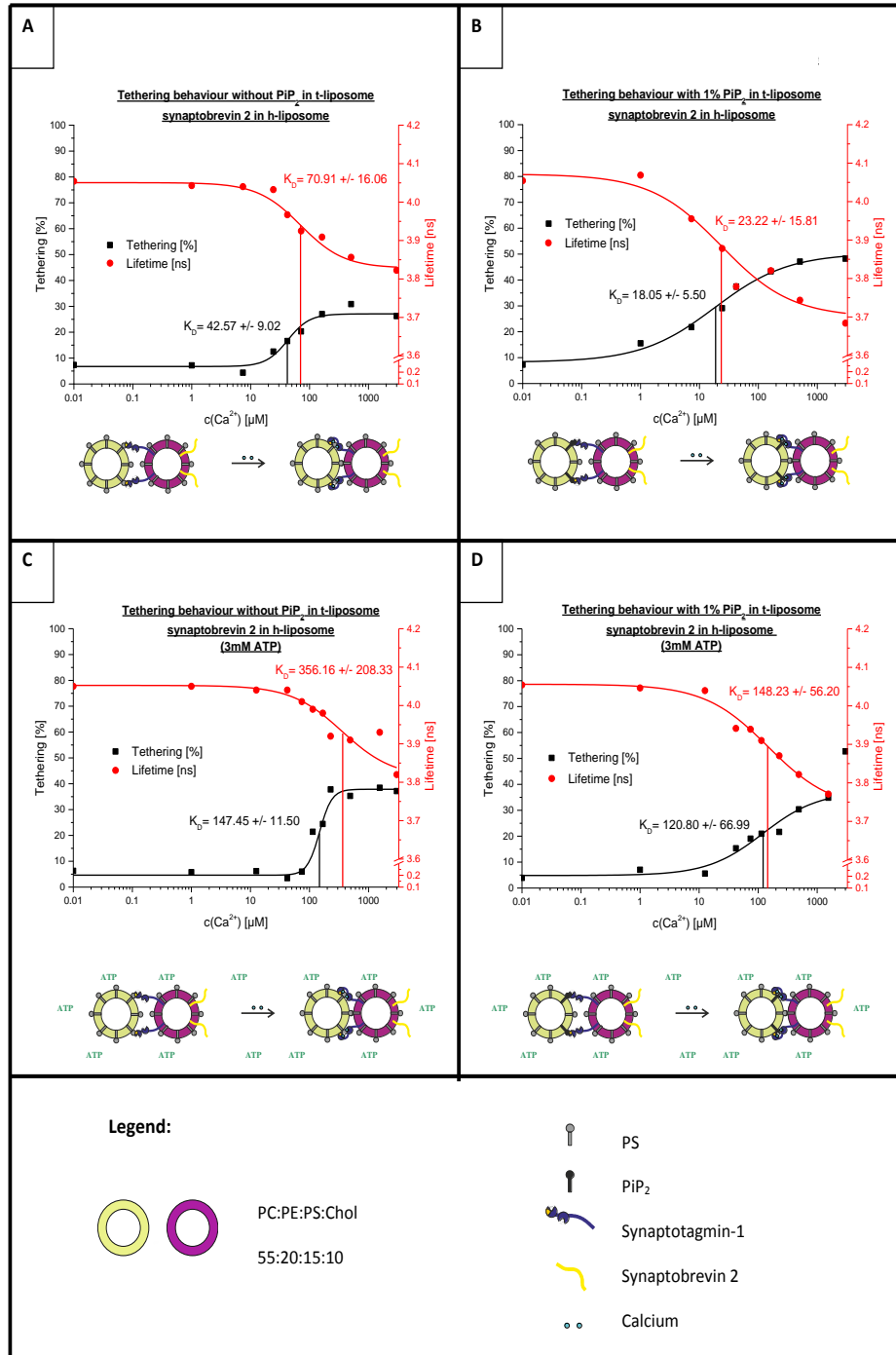


Figure 4.11: Western Blot detecting synaptotagmin-1 and synaptobrevin 2. Lane 1 shows the 170 kD ladder. In lane 2 to 4 different amounts of liposome preparation are loaded. Lane 5 to 7 and 8 to 10 show precise amounts of synaptobrevin 2 and synaptotagmin-1, respectively.

Next, the same set of FCCS experiments is carried out with this type of liposomes as described above in subsection 4.1.3. The overall tethering amount for the solely PS containing liposomes shown in figure 4.12(A) and (C) are increased compared to figure 4.7(A) and (C). Either with (figure 4.12(C)) or without ATP (figure 4.12(A)) the fluorescence lifetime decreases to almost 3.8 ns. Again, the PiP<sub>2</sub> containing liposome mixtures - figure 4.12(B) and (D) - reveal a simultaneous change in tethering and lifetime. The total amount of tethered liposomes is also increased compared to figure 4.7(B) and (D). Additionally, the fluorescence lifetime is significantly lower than in 4.7(B) and (D). The lifetime decrease is more prominent in the presence of PiP<sub>2</sub> (figure 4.12(B)) than in the absence of PiP<sub>2</sub> (figure 4.12(A)). In general, the dissociation constants in tethering are shifted towards higher Ca<sup>2+</sup> concentrations for any liposome mixture.

Interestingly, the quenched fluorescence lifetimes do not differ as dramatically as depicted in and calculated for figure 4.7. Again, all fit parameters determined are listed in the table 4.4 below.

According to equation 4.3 it is now possible to calculate the fluorescence lifetime of the bound liposome fraction. While in figure 4.12(A) the corresponding fluorescence lifetime of the tethered liposomes is  $3.22 \pm 0.44$  ns, the one for the analogous measurement having PiP<sub>2</sub> incorporated into the target membrane (figure 4.12(B)) adds up to  $3.35 \pm 0.49$  ns. The corresponding measurements performed in the presence of ATP reveal quenched fluorescence lifetimes of 3.67



$\pm 0.52$  ns and  $3.19 \pm 1.26$  ns. The errors of these calculations are determined via error analysis as can be seen in chapter 7. The error of tethering and fluorescence lifetime resulting from the applied Hill fits are taken for error analysis.

Table 4.4: Summary of Hill fit values determined for synaptotagmin-1 wt and synaptobrevin 2 presented in figure in 4.12.

parameter	A	B	C	D
<b>Tethering</b>				
Start [%]	$6.76 \pm 0.76$	$8.23 \pm 2.25$	$4.61 \pm 0.81$	$4.84 \pm 1.07$
End [%]	$27.09 \pm 1.38$	$50.34 \pm 2.66$	$37.86 \pm 2.30$	$37.29 \pm 5.91$
$K_D$ [ $\mu$ M]	$42.57 \pm 9.20$	$18.05 \pm 5.50$	$147.45 \pm 11.50$	$120.80 \pm 66.99$
n	$2.36 \pm 1.00$	$0.69 \pm 0.15$	$4.17 \pm 1.33$	$0.92 \pm 0.35$
$R^2$	0.96	0.98	0.96	0.95
<b>Lifetime</b>				
Start [ns]	$4.05 \pm 0.01$	$4.07 \pm 0.03$	$4.05 \pm 0.01$	$4.07 \pm 0.01$
End [ns]	$3.83 \pm 0.02$	$3.70 \pm 0.05$	$3.91 \pm 0.02$	$3.73 \pm 0.04$
$K_D$ [ $\mu$ M]	$70.91 \pm 16.06$	$23.22 \pm 15.81$	$356.16 \pm 208.33$	$148.23 \pm 56.20$
n	$1.18 \pm 0.32$	$0.72 \pm 0.33$	$1.98 \pm 0.69$	$0.80 \pm 0.19$
$R^2$	0.97	0.94	0.92	0.98

Moreover, the obtained values for the fluorescence lifetime are plotted against the amount of tethered liposomes as depicted in figure 4.9. A linear regression can be applied even to the  $\text{PiP}_2$ -less sample combinations, yielding a linear equation of  $-8.49 \cdot 10^{-3}x + 4.10$  with an  $R^2$  of 0.90 for the data presented in figure 4.12(A). For the measurement depicted in figure 4.12(B) an equation of

---

Figure 4.12 (*preceding page*): Synaptotagmin-1 tethering (black) and fluorescence lifetime (red) response towards increasing calcium concentrations. Target liposomes contain 15% PS and (if indicated) 1%  $\text{PiP}_2$ . Host liposomes contain 15% PS, reconstituted full-length synaptotagmin-1 and synaptobrevin 2. In the control no synaptotagmin-1 is present in the Texas red liposome. Error bars are left out for the sake of clarity. Hill fits are applied to the data points with the resulting dissociation constant ( $K_D$ ) being indicated (black and red strokes). (A) Tethering and fluorescence lifetime development without  $\text{PiP}_2$  in the target liposome and without ATP in the buffer. (B) Tethering and fluorescence lifetime development with 1%  $\text{PiP}_2$  in the target liposome and without ATP in the buffer. (C) Tethering and fluorescence lifetime development without  $\text{PiP}_2$  in the target liposome and 3 mM ATP in the buffer. (D) Tethering and fluorescence lifetime development with 1%  $\text{PiP}_2$  in the target liposome and 3 mM ATP in the buffer.

$-8.78 \cdot 10^{-3}x + 4.15$  with an  $R^2$  of 0.94 is determined. Furthermore plotting the fluorescence lifetime data presented in figure 4.12(C) and (D) against the amount of tethered liposomes results in a linear equation in the form of  $-3.60 \cdot 10^{-3}x + 4.06$  with an  $R^2$  of 0.92 and  $-9.75 \cdot 10^{-3}x + 4.10$  with an  $R^2$  of 0.98, respectively. It is noteworthy, that although the linear regressions are not presented in detail here, the  $R^2$ s reveal sophisticated fit results. Hence the Oregon green fluorescence lifetimes of the bound fraction can be calculated as  $3.25 \pm 0.18$  ns,  $3.27 \pm 0.12$  ns,  $3.70 \pm 0.06$  ns and  $3.13 \pm 0.10$  ns, respectively.

Biexponential fitting of the Oregon green fluorescence lifetime histograms reveals the following fluorescence lifetime for the bound liposome fraction:  $2.58 \pm 0.09$  ns for the sample combinations presented in figure 4.12(A),  $2.76 \pm 0.06$  ns for figure 4.12(B),  $2.38 \pm 0.10$  ns for figure 4.12(C) and  $2.32 \pm 0.06$  ns for figure 4.7(D). All  $R^2$  values obtained for the biexponential fits are 0.99. Table 4.5 lists all fluorescence lifetimes determined as well as the normalized fluorescence lifetime changes. Here, the presence of ATP reveals a smaller fluorescence lifetime of the bound liposome fraction. The normalized fluorescence lifetime change is the same for all sample combinations except for (C). Here, the normalized fluorescence lifetime change is reduced by  $\frac{1}{2}$  compared to the others.

Table 4.5: Summary of Oregon green fluorescence lifetimes in case of synaptobrevin 2 additionally reconstituted into the host liposome. Fluorescence lifetimes of the bound liposome population are obtained by individual approaches. The fluorescence lifetimes are given in [ns]. The normalized fluorescence lifetime changes are shown as well.

parameter	A	B	C	D
$f_{bound}$	$3.23 \pm 0.44$	$3.33 \pm 0.49$	$3.68 \pm 0.52$	$3.18 \pm 1.26$
Linear regression	$3.25 \pm 0.18$	$3.27 \pm 0.12$	$3.70 \pm 0.06$	$3.13 \pm 0.10$
Biexponential fit	$2.58 \pm 0.09$	$2.76 \pm 0.06$	$2.38 \pm 0.10$	$2.32 \pm 0.06$
NFLC	$0.20 \pm 0.02$	$0.18 \pm 0.02$	$0.09 \pm 0.01$	$0.22 \pm 0.30$

Comparison of the calculated values for the fluorescence lifetime of the bound liposome population does not reveal any further trends within the data. Contradictorily, the normalized fluorescence lifetime changes, the linear regression and the  $f_{bound}$  method point towards the least  $\tau_{bound}$  determined for (C), while biexponential fitting here reveals the second lowest fluorescence lifetime. Hence, the only valid conclusion one can draw from these experiments is that synaptobrevin 2 influences synaptotagmin-1 based distance regulation by shifting the dissociation constant to higher  $Ca^{2+}$  concentrations. Furthermore, the amount of tethering is enhanced in the presence of synaptobrevin 2.

As mentioned beforehand, the role of  $PiP_2$  clusters remains to be characterized. The following subsection 4.1.5 finally addresses this issue.

### 4.1.5 The concentration of PiP<sub>2</sub> and Ca<sup>2+</sup> determine the amount of tethered liposomes

Having demonstrated the influence of PiP<sub>2</sub> on the dissociation constant of synaptotagmin-1 tethering, the question arises whether increasing amounts of PiP<sub>2</sub> in the target membrane may have an influence on the overall tethering amount of tethered liposomes, especially because there is evidence that syntaxin 1A, which interacts with synaptotagmin-1, colocalizes with PiP<sub>2</sub> clusters in the plasma membrane [44]. A support of the concentration of PiP<sub>2</sub> on synaptotagmin-1 binding to the plasma membrane, where syntaxin 1A is already colocalized, might describe a new driving force for synaptotagmin-1 induced liposome fusion.

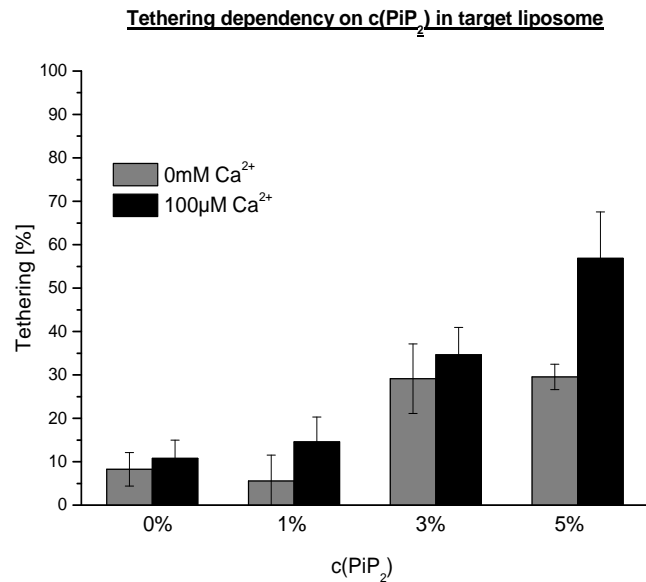


Figure 4.13: Total amount of synaptotagmin-1 tethering at 0 mM and 100 µM Ca<sup>2+</sup> for varying PiP<sub>2</sub> concentrations in the target membrane.

To further prove this finding, liposomes with varying concentrations of PiP<sub>2</sub> are prepared, ranging from 0 to 5% PiP<sub>2</sub> in the target membrane. The total change in tethering and lifetime after 30 min of incubation is determined.

Figure 4.13 shows the influence of increasing amounts of PiP<sub>2</sub> in the target membrane. At first glance it becomes obvious that increasing amounts of PiP<sub>2</sub> also increase the amount of tethered liposomes disregarding the absence or presence of calcium ions. Tethering is already above 30% with 3% PiP<sub>2</sub> in the target membrane even in the absence of any calcium ions. In fact, tethering is even further enhanced in the presence of Ca<sup>2+</sup>, therefore supporting a model in which PiP<sub>2</sub> rafts provide a platform for increased synaptic vesicle docking [44]. The concentration of PiP<sub>2</sub> in these clusters is indeed estimated to be around 3% [44].

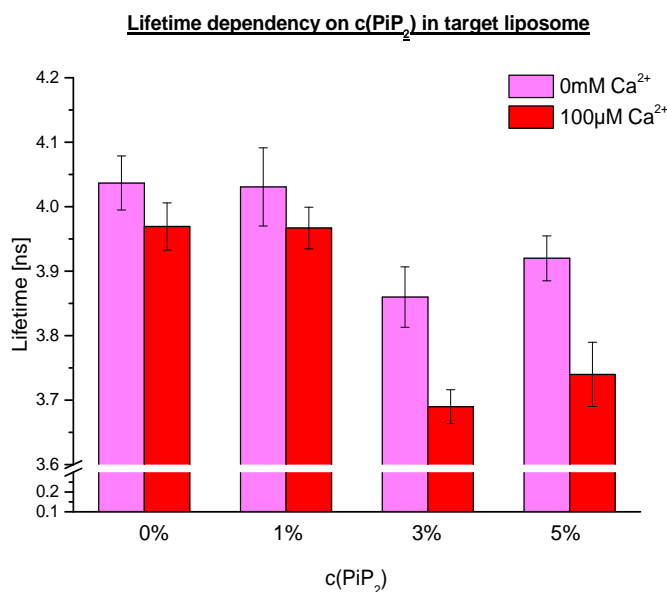


Figure 4.14: Total amount of Oregon green lifetime in the corresponding synaptotagmin-1 tethering experiment presented in figure 4.13 at 0 mM and 100  $\mu\text{M}$   $\text{Ca}^{2+}$ .

The simultaneously recorded fluorescence lifetime as presented in figure 4.14 does not reveal any dramatic alterations in the absence of  $\text{Ca}^{2+}$ . The fluorescence lifetime reduction for the sample combinations containing 3% and 5%  $\text{PIP}_2$  are rather small when compared to the total amount of tethered liposomes. In contrast, in the presence of  $\text{Ca}^{2+}$  the fluorescence lifetime shows a clear trend. Upon increasing  $\text{PIP}_2$  concentrations in the target membrane, the fluorescence lifetime is decreased significantly. Again, to rule out whether distance regulation is furthermore affected by the concentration of  $\text{PIP}_2$  in the target liposome and not only a result of enhanced tethering, further analysis is required.

Once more, the fluorescence lifetime of the bound liposome fraction  $\tau_{bound}$  is calculated. In the absence of calcium ions the following fluorescence lifetimes are calculated:  $4.05 \pm 3.83$  ns,  $4.05 \pm 8.73$  ns,  $3.39 \pm 2.21$  ns and  $3.60 \pm 0.87$  ns. Whereas in the presence of calcium ions the fluorescence lifetimes are given by:  $2.53 \pm 2.99$  ns,  $3.41 \pm 3.19$  ns,  $3.00 \pm 1.37$  ns and  $3.50 \pm 1.51$  ns. Here, the error bars obtained via error analysis are very large, and thus do not permit for further interpretation. The fluorescence lifetimes obtained via biexponential fitting reveal the following results for the samples excluding  $\text{Ca}^{2+}$ :  $2.53 \pm 0.42$  ns,  $2.68 \pm 0.52$  ns,  $3.69 \pm 0.13$  ns,  $3.79 \pm 0.16$  ns, and including  $\text{Ca}^{2+}$ :  $2.45 \pm 0.29$  ns,  $2.64 \pm 0.26$  ns,  $3.43 \pm 0.13$  ns,  $3.62 \pm 0.09$  ns. All  $R^2$  values obtained for the biexponential fit are 0.99.

Again, to pinpoint the role of  $\text{PIP}_2$  in distance regulation the actual FRET has to be normalized according to the observed rise in tethering by calculating  $NFLC = \frac{\Delta Lifetime}{\Delta Tethering}$ . Here, the relative alterations in fluorescence lifetime and

tethering are taken into account. Comparing the fluorescence lifetimes listed in table 4.6 the conclusion arises that increasing amounts of PiP<sub>2</sub> indeed increase tethering, but do not facilitate further membrane distance shortening per se. According to figure 4.7 PiP<sub>2</sub> binding of synaptotagmin-1 instead increases the sensitivity for Ca<sup>2+</sup> dependent distance regulation.

Table 4.6: Summary of Oregon green fluorescence lifetimes in case of different PiP<sub>2</sub> concentrations in the target liposome. Fluorescence lifetimes of the bound liposome population are obtained by individual approaches. The fluorescence lifetimes are given in [ns]. The normalized fluorescence lifetime changes are shown as well.

		c(PiP <sub>2</sub> )			
		0%	1%	3%	5%
<i>f<sub>bound</sub></i>	-	4.05 ± 3.83	4.05 ± 8.73	3.39 ± 2.21	3.60 ± 0.87
	+	2.53 ± 2.99	3.41 ± 3.19	3.00 ± 1.37	3.50 ± 1.51
Biexp. fit	-	2.53 ± 0.42	2.68 ± 0.52	3.69 ± 0.13	3.79 ± 0.16
	+	2.45 ± 0.29	2.64 ± 0.26	3.43 ± 0.13	3.62 ± 0.09
NFLC	-	0.24 ± 0.06	0.39 ± 0.20	0.20 ± 0.01	0.15 ± 0.00
	+	0.47 ± 0.04	0.23 ± 0.03	0.29 ± 0.01	0.15 ± 0.00

#### 4.1.6 Syntaxin 1A circumvents synaptotagmin-1 dependent distance regulation

As depicted above in subsection 4.1.5, the concentration of PiP<sub>2</sub> determines the amount of tethered liposomes as well as the liposomal distance. Since recent studies were able to show that syntaxin 1A colocalizes with PiP<sub>2</sub> clusters [44], the question whether syntaxin 1A has an effect on synaptotagmin-1 induced distance regulation arises. Therefore syntaxin-1A is incorporated into 3% PiP<sub>2</sub> carrying target liposomes. The following measuring procedure is carried out as described earlier in subsection 4.1.2.

Figure 4.15 shows the tethering and lifetime response of synaptotagmin-1 carrying liposomes in the absence and presence of calcium. Again, at high PiP<sub>2</sub> concentrations tethering seems to become almost independent of calcium.

Having syntaxin 1A reconstituted into the target liposome or not, does not affect the total amount of tethering significantly. Hence, the presence of syntaxin 1A does not have any influence on tethering. However, with syntaxin 1A in the target liposome a fluorescence lifetime shift can be detected even in the absence of calcium. Furthermore, with syntaxin-1A in the target membrane

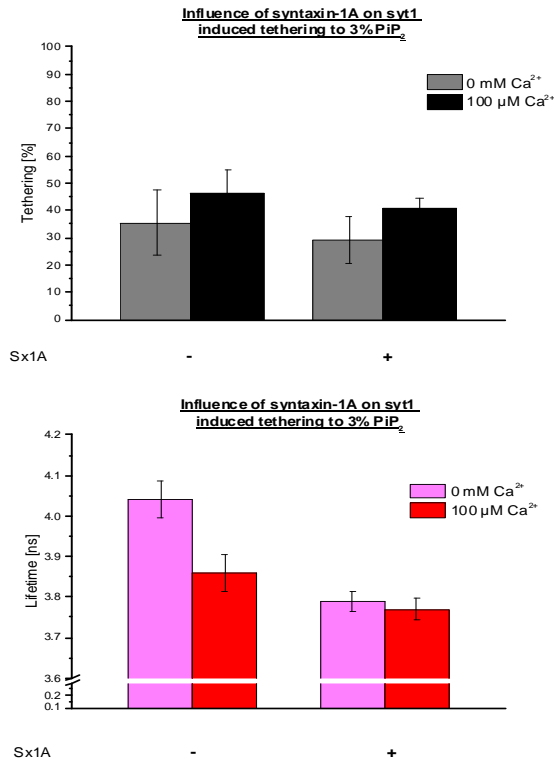


Figure 4.15: Synaptotagmin-1 tethering (black/gray) and lifetime (red/magenta) response towards increasing calcium concentrations. Target liposomes contained 15% PS, 3% PiP<sub>2</sub> and reconstituted syntaxin 1A. Host liposomes contain 15% PS and reconstituted full-length synaptotagmin-1. In the control no synaptotagmin-1 is present in the Texas red liposome. Error bars indicate the corresponding standard deviation.

there is no significant difference in the lifetime decrease upon varying calcium concentrations. Syntaxin 1A seems to permit synaptotagmin-1 to bring both liposomes closer together even without any external trigger like calcium.

Here, the fluorescence lifetimes of the bound liposomes  $\tau_{bound}$  can be calculated to be  $4.01 \pm 2.87$  ns and  $3.63 \pm 1.72$  ns for the naked Oregon green liposome, whereas the syntaxin 1A carrying ones display lifetimes of  $3.15 \pm 2.17$  ns and  $3.35 \pm 0.75$  ns. Biexponential fitting results in fluorescence lifetimes of  $4.05 \pm 0.25$  ns and  $3.88 \pm 0.10$  ns for the naked Oregon green liposomes and  $3.65 \pm 0.19$  ns and  $3.66 \pm 0.17$  ns for the liposomes carrying syntaxin 1A. All R<sup>2</sup> values obtained for the biexponential fit are 0.99.

Table 4.7 demonstrates that, indeed, syntaxin 1A is capable of circumventing synaptotagmin-1 dependent distance regulation. Nevertheless having demonstrated beforehand that indeed synaptotagmin-1 may be a distance regulator, it is remarkable that such a striking mechanism can be overcome so easily. The functional role of this apparent circumvention remains to be addressed in chapter 5.

Although the influence of  $\text{PiP}_2$ , calcium ions and other proteins on synaptotagmin-1 based distance regulation have been investigated, the role of the three distinct functional domains of synaptotagmin-1 still remains unclear. Hence, the following subsection focusses on addressing this issue.

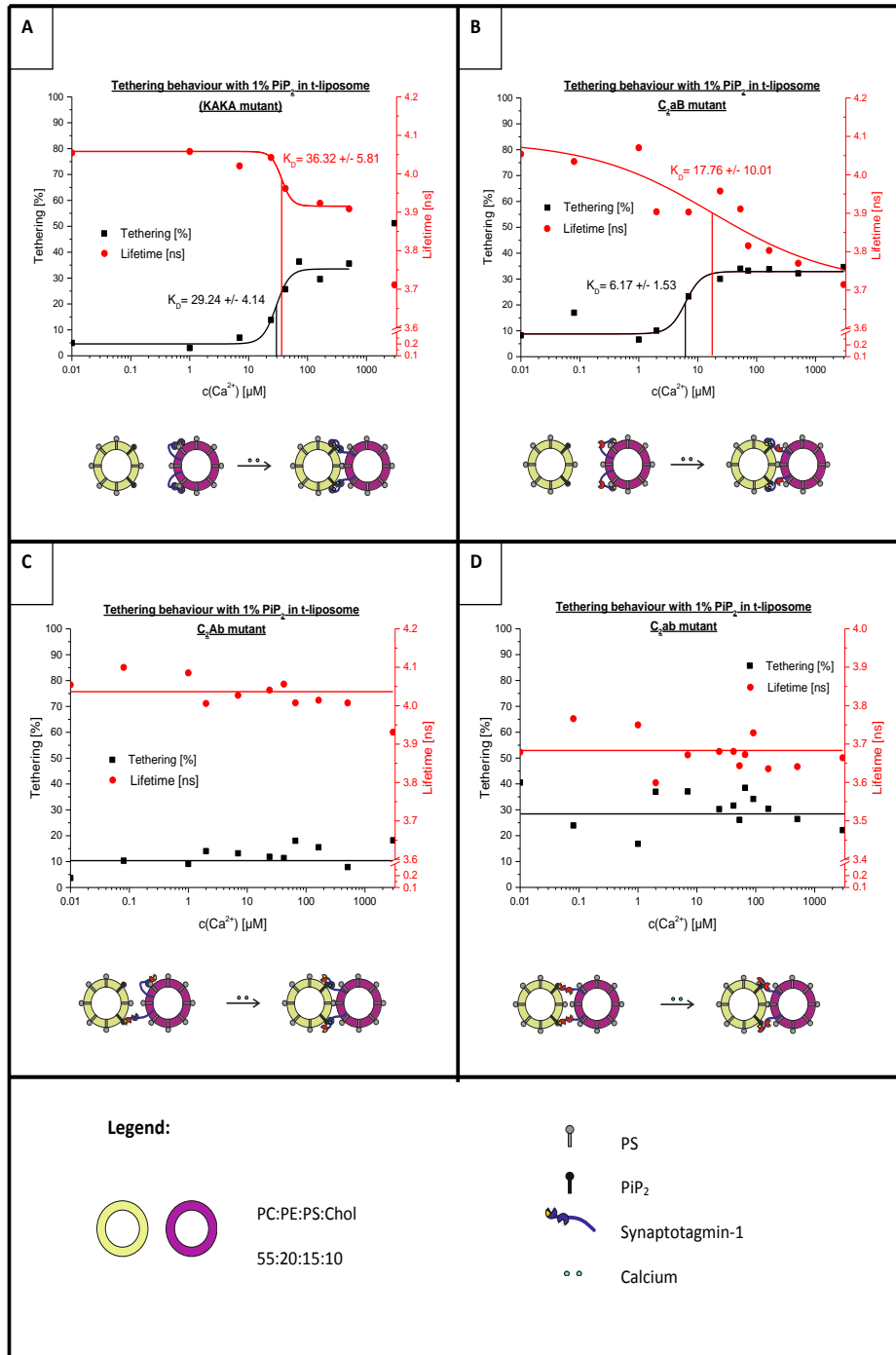
Table 4.7: Summary of Oregon green fluorescence lifetimes in case of 3%  $\text{PiP}_2$  and syntaxin 1A being reconstituted into the target liposome. Fluorescence lifetimes of the bound liposome population are obtained by individual approaches. The fluorescence lifetimes are given in [ns]. The normalized fluorescence lifetime changes are shown as well.

		Syntaxin 1A	
		-	+
$f_{bound}$	-	$4.01 \pm 2.87$	$3.15 \pm 2.17$
	+	$3.63 \pm 1.72$	$3.35 \pm 0.75$
Biexponential fit	-	$4.05 \pm 0.25$	$3.65 \pm 0.19$
	+	$3.88 \pm 0.10$	$3.66 \pm 0.17$
NFLC	-	$0.01 \pm 0.01$	$0.22 \pm 0.01$
	+	$0.10 \pm 0.01$	$0.17 \pm 0.01$

#### 4.1.7 Both $C_2$ domains of synaptotagmin-1 are required to maintain proper distance regulation

The following titration experiments are performed under the same conditions as described earlier in subsection 4.1.3. The target liposome contains 1%  $\text{PiP}_2$  and is labeled with Oregon green. Here, four mutants of synaptotagmin-1 are reconstituted into the host liposome labeled with Texas red and measured in order to investigate their contribution to tethering and distance regulation. A mutation in either one or both  $C_2$  domains leads to a disruption of  $\text{Ca}^{2+}$  binding and thus a disruption of anionic lipid binding. Upon mutating two lysines in the poly-lysine patch, its capability to bind to either PS or  $\text{PiP}_2$  is destroyed. Again, the liposomes are mixed in equimolar ratio at nM concentrations and incubated for 30 min at RT prior to measuring.

Mutating the poly-lysine patch and thus reducing its cationic charge density shifts the dissociation constants for tethering and lifetime to higher  $\text{Ca}^{2+}$  concentrations. Nevertheless, both dissociation constants still alter simultaneously around 30  $\mu\text{M}$ . Hence, the  $\text{PiP}_2$  affinity is significantly reduced but synchronization of tethering and distance regulation is maintained. Although the total amount of tethered liposomes is increased, the fluorescence lifetime decrease is less than reported for synaptotagmin-1 wt (figure 4.7(A)), which is in line with the hypothesis that the poly-lysine patch interacts with  $\text{PiP}_2$  and consequently contributes to a reduction in the intermembrane distance [6, 119].



The fluorescence lifetime analysis of the C<sub>2</sub>aB mutant shows a very disperse distribution of data points. Hence, the C<sub>2</sub>A domain is required for proper distance regulation, while it has no effect on tethering in *trans*. Both dissociation constants roughly are still in the same regime around 10  $\mu$ M. Again, the amount of tethered liposomes is increased compared to figure 4.7(A), most likely because the C<sub>2</sub>A domain can bind in *cis* even in the absence of calcium ions [7]. If *cis*-binding is prevented then *trans*-binding may be indirectly promoted. The total decrease in fluorescence lifetime is not altered compared to figure 4.7(A).

Table 4.8: Summary of Hill fit values determined for synaptotagmin-1 mutants presented in figure in 4.16. In case of no sigmoidal curve present, a linear fit with a slope  $m=0$  is applied.

parameter	KAKA	C <sub>2</sub> aB	C <sub>2</sub> Ab	C <sub>2</sub> ab
<b>Tethering</b>				
Start [%]	$4.59 \pm 0.90$	$8.79 \pm 1.42$	$10.34 \pm 1.55$	$28.12 \pm 1.97$
End [%]	$33.53 \pm 2.46$	$32.90 \pm 2.65$	$10.34 \pm 1.55$	$28.12 \pm 1.97$
$K_D$ [ $\mu$ M]	$29.24 \pm 4.14$	$6.17 \pm 1.53$	—	—
n	$3.82 \pm 2.28$	$3.21 \pm 4.33$	—	—
R <sup>2</sup>	0.96	0.88	—	—
<b>Lifetime</b>				
Start [ns]	$4.06 \pm 0.00$	$4.09 \pm 0.00$	$4.04 \pm 0.01$	$3.68 \pm 0.01$
End [ns]	$3.92 \pm 0.02$	$3.71 \pm 0.00$	$4.04 \pm 0.01$	$3.68 \pm 0.01$
$K_D$ [ $\mu$ M]	$36.32 \pm 5.81$	$17.76 \pm 10.01$	—	—
n	$5.01 \pm 2.18$	$0.41 \pm 0.10$	—	—
R <sup>2</sup>	0.89	0.84	—	—

The most striking feature is observed when mutating the C<sub>2</sub>B domain. Here, the C<sub>2</sub>Ab titration curve shown in figure 4.16(C) depicts an amount of tethered liposomes which is unaffected by rising Ca<sup>2+</sup> concentrations. The amount of tethered liposomes remains at 10% for all calcium concentrations measured, which is most likely a result of unspecific interaction. Thus, the C<sub>2</sub>B domain is

---

Figure 4.16 (*preceding page*): Synaptotagmin-1 mutant tethering (black) and fluorescence lifetime (red) response towards increasing calcium concentrations. Target liposomes contained 15% PS and (if indicated) 1% PiP<sub>2</sub>. Host liposomes contain 15% PS and reconstituted full-length synaptotagmin-1. In the control no synaptotagmin-1 is present in the Texas red liposome. Error bars are left out for the sake of clarity. Hill fits are applied to the data points with the resulting dissociation constant ( $K_D$ ) being indicated (black and red strokes). (A) KAKA mutant, (B) C<sub>2</sub>aB mutant, (C) C<sub>2</sub>Ab mutant, (D) C<sub>2</sub>ab mutant.

identified as the only domain that can bind notably in *trans* with rising calcium concentrations.

A similar picture is drawn from the measurement performed with the double mutant C<sub>2</sub>ab. Here, tethering is insensitive towards increasing calcium concentrations. The amount of tethered liposomes remains constant at 28 %, thus again supporting the hypothesis of the C<sub>2</sub>B domain being the only functional domain to conduct *trans*-binding as a function of Ca<sup>2+</sup> concentration. Since calcium binding is completely abolished, *trans*-binding has to be accomplished by the poly-lysine patch and hence, shows a greater affinity for PiP<sub>2</sub> than for PS. The fluorescence lifetime does not show any alterations upon rising Ca<sup>2+</sup> concentrations. It is noteworthy that the fluorescence lifetime for the double mutant already demonstrates a FRET effect in the absence of calcium ions. Thus, the y-axis is modified in order to illustrate all data points measured. Moreover, the observed FRET is quite tremendous reaching lifetimes around 3.68 ns.

According to equation 4.3 the fluorescence lifetimes of the bound liposomes are calculated. Here, (A) reveals a fluorescence lifetime of  $3.64 \pm 0.62$  ns, which is somewhat larger than  $\tau_{bound}$  for (B) with  $3.02 \pm 0.57$  ns. As previously mentioned, mutating either the C<sub>2</sub>B domain alone or both C<sub>2</sub> domains does not result in any alterations of the fluorescence lifetime upon rising Ca<sup>2+</sup> concentrations. The fluorescence lifetime of the C<sub>2</sub>B mutant does not change at all. For calculation  $\tau_{bound}$  of the double mutant an unaffected lifetime of 4.05 ns is considered. Here, the double mutant reveals the lowest Oregon green fluorescence lifetime.

Again, the obtained values for fluorescence lifetime are plotted against the amount of tethered liposomes as demonstrated in subsection 4.1.3. A linear regression is applied yielding a linear equation of  $-4.59 \cdot 10^{-3}x + 4.08$  with an R<sup>2</sup> of 0.79 for 4.7(A). For 4.7(B) an equation of  $-8.78 \cdot 10^{-3}x + 4.12$  with an R<sup>2</sup> of 0.59 is determined. Here, the R<sup>2</sup> values obtained for fitting the mutant data are by far not as stringent as for the wild type measurements either in the presence or the absence of synaptobrevin 2. Thus, pointing towards a linear distance regulation upon tethering for which all three functional domains are required. Of course, plotting 4.7(C) and (D) is redundant.

Biexponential fitting of the Oregon green fluorescence lifetime histograms reveals the following fluorescence lifetimes for the bound liposome fraction:  $2.96 \pm 0.11$  ns for 4.16(A),  $2.88 \pm 0.12$  ns for 4.16(B),  $3.16 \pm 0.10$  ns for 4.16(C) and  $2.38 \pm 0.06$  ns for 4.16(D). Here, biexponential fitting of the fluorescence lifetimes presented in 4.16(C) and (D) is performed with the measurement obtained at 3 mM Ca<sup>2+</sup> ion concentration. All R<sup>2</sup> values obtained for the biexponential fit are 0.99.

Table 4.1.7 lists all fluorescence lifetimes determined as well as the normalized fluorescence lifetime changes. As can be deduced from table 4.1.7, the normalized fluorescence lifetime change is the greatest upon mutating both C<sub>2</sub> domains. Nonetheless, the normalized fluorescence lifetime change is still in the same range as demonstrated for the wild type. Interestingly, mutating the poly-

lysine patch only reveals a minor effect on the normalized fluorescence lifetime change and thus shows the largest deviation towards the wild type normalized fluorescence lifetime change of  $0.32 \pm 0.06$ .

Table 4.9: Summary of Oregon green fluorescence lifetimes of all four synaptotagmin-1 mutants. Fluorescence lifetimes of the bound liposome population are obtained by individual experiments. The fluorescence lifetimes are given in [ns].

parameter	KAKA	C <sub>2</sub> aB	C <sub>2</sub> Ab	C <sub>2</sub> ab
$f_{bound}$	$3.64 \pm 0.62$	$3.02 \pm 0.57$	—	$2.72 \pm 0.52$
Linear regression	$3.63 \pm 0.13$	$3.24 \pm 0.11$	—	—
Biexponential fit	$2.96 \pm 0.11$	$2.88 \pm 0.12$	$3.16 \pm 0.10$	$2.38 \pm 0.06$
NFLC	$0.10 \pm 0.02$	$0.28 \pm 0.00$	—	$0.33 \pm 0.01$

## 4.2 Optical trapping

The diffusion based FCCS-FRET assay described in the previous section 4.1 possesses some striking advantages. First, it permits to discriminate between docked and fused state. Second, it allows for fluorescence lifetime analysis. Third, it circumvents potential artefacts introduced by surface tension as e.g. it may be the case for other single liposome-liposome content and lipid mixing systems based on immobilized target liposomes [60]. Nevertheless, independently diffusing SUVs can obviously not be observed for longer than a few ms, as it is the case for surface supported or linked membranes. Therefore, individual processes related to fusion of liposomes can not be observed. Thus, a new approach is presented in this section making use of optically trapped large unilamellar liposomes (LUVs) with a diameter of about 110 nm, thereby trying to combine the advantages arising from both previously published approaches [24, 121, 60]. Here, the first part of this section focuses on the physical properties and requirements of optically trapping a LUV. The second part then continues with a description of potential applications of optically trapped LUVs. Since the optically trapped LUVs provide a surface for interaction, the employment of adsorption isotherms in terms of synaptotagmin-1 tethering and de-tethering is tested. Having identified and characterized the distance regulation function of synaptotagmin-1 in the previous section 4.1, the corresponding application of such measurements in terms of optical trapping remains to be shown. Furthermore, fusion of SUVs to trapped LUVs has to be investigated as well. For studying the employment of the above listed applications the fluorescence dyes have to be exchanged by one another. Now, full length synaptotagmin-1 is reconstituted into an Oregon green labeled SUV, while the LUV, serving as the plasma membrane substitute, is labeled with Texas red.

### 4.2.1 Characterization of the setup

First, a CW laser for trapping the liposomes is combined with the TPE laser beam used in the previous section 4.1. The beams are directed towards a polarizing beam splitting cube. The cube is hit in parallel by the TPE beam and perpendicular by the CW beam, thus combining both beams. A wave plate is put in between the CW laser and the polarizing beam splitting cube, hence permitting for power regulation. Furthermore a neutral density filter is put in between the TPE laser and the cube in order to also regulate the excitation power. Both laser beams are coupled into the microscope as described in chapter 3. Furthermore, both lasers operate at 800 nm hence, allowing for simultaneous refraction in z-direction. In fact, simultaneous refraction is a prerequisite for the combination of FCS and fluorescence lifetime analysis in the context of optical trapping. Both foci are super-imposed in x- and y-direction with the help of a wide field camera. Accordingly, the fluorescence is collected as described earlier in chapter 3. The APDs are aligned towards the point of highest intensity originating from the TPE focus by blocking the CW beam. An additional ND filter is put in front of the APD recording the red fluorescence photons.

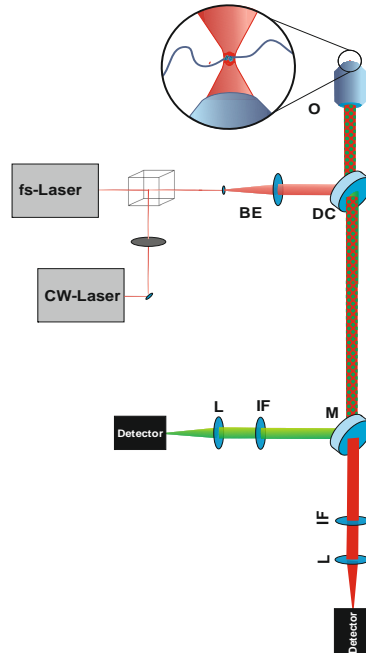


Figure 4.17: Extended setup for combining optical trapping and TP-FCS. The basic setup is the same as described in chapter 3. Additionally a CW-laser beam is combined with the fs-laser beams used for TPE through a polarizing beam splitting cube. The intensity of the CW beam is further controlled by a  $\frac{\lambda}{2}$  wave plate.

## 4.2.2 Characterization of the effective focal volume

In order to characterize the effective focal volume under trapping conditions, z-scans are performed with either one beam blocked or both beams propagating through the objective. A dilute sample of 1  $\mu\text{m}$  fluorescent beads is put on a cover slip and dried out. The coverslip is put in a self-built frame that fits into a stage, thus permitting to keep the sample in a distinct z-position while the objective is moved in vertical direction. Single fluorescent beads are identified and positioned in x,y-direction with the stage to fit the excitation laser beam (figure 4.18(A)). The z-position is altered until the beads are in focus of the camera. Beads are excited either with the trapping laser operating in pulsed mode, 20 mW TPE or a combination of 100 mW CW and 20 mW TP excitation. The intensity originating from exciting the beads is recorded. Afterwards the z-position is changed in 1  $\mu\text{m}$  steps towards positions below and above the original plane. After each step the fluorescence intensity is recorded again. The same procedure is repeated under the three above listed excitation conditions. The

z-position of highest fluorescence intensity does not change over the different excitation modes measured. Thus, demonstrating that CW- and TP-excitation beam are focussed within the same plane.

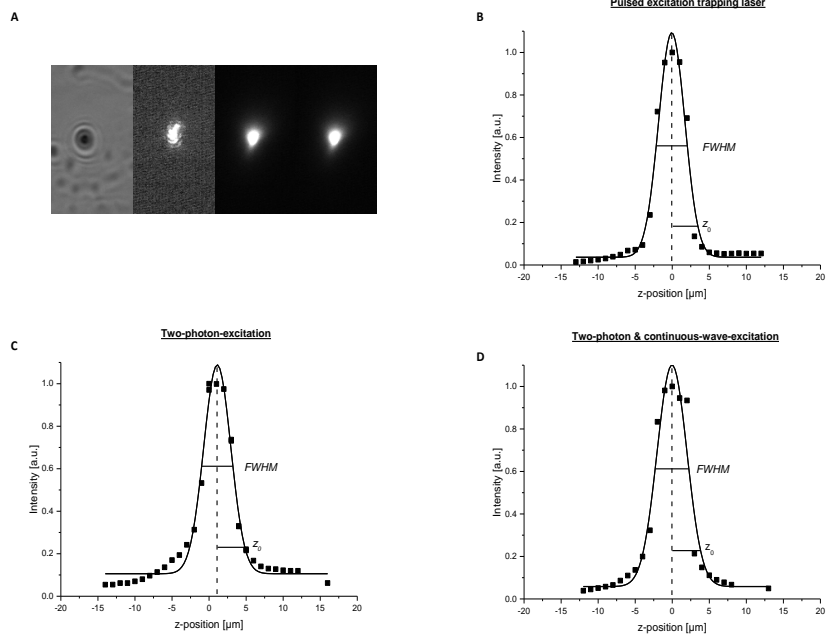


Figure 4.18: Characterization of the molecular detection function (MDF) in z-direction. (A) The picture to the very left hand side shows a single 1 μm fluorescent bead. This bead is excited with the pulsed trapping laser beam (second left), a TPE laser beam (third left) and with CW & TP excitation beams (right hand side). The originating fluorescence intensity distributions are represented as follows: (B) Trapping laser in pulsed mode, (C) TP excitation, (D) CW & TP excitation. Here, only the *FWHM* and the beam waist in z-direction  $z_0$  are shown.

The resulting intensity distribution can be approximated by a Gaussian distribution, leading to values for the full width half maximum (*FWHM*) and the actual length of the detection volume in z-direction [37]. The Gaussian function in axial direction can be expressed as [28]:

$$I(z) = I_0 \cdot \exp\left(-\frac{(z - z_c)^2}{z_0^2}\right) + C_0 \quad (4.5)$$

Here,  $I_0$  is the peak intensity of the Gaussian curve,  $z_c$  is the axial centroid,  $z_0$  is the axial intensity distribution width and  $C_0$  the background fluorescence signal. For the sake of clarity only the *FWHM* and the beam waist in z-direction  $z_0$  are shown in figure 4.18. The Gaussian fit is set free to converge without any constraints. Table 4.10 lists all relevant parameters deduced from

Table 4.10: Characterizing the focal volume for the trapping laser operating in pulsed mode, TP- and CW & TP excitation. The wavelength of both lasers is 800 nm. The power leaving the objective is set to 100 mW for the CW beam and 20 mW for the TPE beam.

parameter	Trapping laser	TPE	CW & TPE
<i>FWHM</i>	4.17 $\mu\text{m}$	4.31 $\mu\text{m}$	4.76 $\mu\text{m}$
$\sigma_z$	1.77 $\mu\text{m}$	1.83 $\mu\text{m}$	2.02 $\mu\text{m}$
$z_0$	$3.65 \pm 0.16 \mu\text{m}$	$3.66 \pm 0.14 \mu\text{m}$	$4.04 \pm 0.29 \mu\text{m}$
$r_{0,xy}$	$428 \pm 5.49 \text{ nm}$	$434 \pm 9.35 \text{ nm}$	$449 \pm 9.45 \text{ nm}$
$V_{eff}$	$1.32 \pm 0.09 \text{ fL}$	$1.35 \pm 0.14 \text{ fL}$	$1.61 \pm 0.22 \text{ fL}$
$\tau_{Diff,R6G}$	$55.23 \pm 0.075 \mu\text{s}$	$56.74 \pm 1.76 \mu\text{s}$	$60.95 \pm 1.83 \mu\text{s}$
$\tau_{life,R6G}$	$4.35 \pm 0.14 \text{ ns}$	$4.32 \pm 0.01 \text{ ns}$	$4.31 \pm 0.15 \text{ ns}$

these Gaussian curve fits. The  $R^2$  values in axial position are 0.97 for the trapping laser operating in pulsed mode, 0.98 for TP- and 0.94 for both excitation modes.

The corresponding Gaussian fit in 3D resembles a molecule detection function (MDF) which characterizes the position-dependent probability to excite and detect a fluorescence photon within a given space in the entire sample [56]. Thus, the MDF illustrates the shape and the size of the effective focal volume  $V_{eff}$ . To moreover determine the actual effective focal volume  $V_{eff}$  achieved under different excitation modes the diffusion time  $\tau_{Diff}$  of R6G is measured under the conditions described above. The diffusion time  $\tau_{Diff}$  of R6G is determined via FCS. The results of the corresponding auto-correlations are depicted in table 4.10. The diffusion coefficient  $D$  of R6G is known to be  $4.14 \cdot 10^{-10} \pm 0.05 \cdot 10^{-10} \text{ m}^2 \text{ s}^{-1}$  [81]. Hence, it is possible to calculate  $V_{eff}$  according to equation 2.32.

It has been reported elsewhere that photobleaching under 20 mW TPE conditions is not severe [24]. Here, the fluorescence lifetime  $\tau_{life}$  determined for TPE and the combined mode of CW & TPE are in agreement.

The error bars in table 4.10 result from the Gaussian fit presented in figure 4.18 for  $r_z$  and from the auto-correlation fit of R6G. Here,  $\sigma_z$  is the standard deviation which can be expressed in terms of  $\sigma_z = \frac{FWHM}{2\sqrt{2\ln 2}}$ . The error bars for  $r_{0,xy}$  are obtained via error analysis as can be deduced from chapter 7. The error for the effective focal volume is determined by addition of all relative errors of interest [115]. Given the fact that all calculated parameters comprise fitting errors, the results are still in good agreement.

### 4.2.3 Validation of optically trapped LUVs

It has been shown that it is possible to optically trap liposomes down to 50 nm in diameter with a CW laser operating in the near infrared regime (NIR) at 1064 nm [8]. To test whether LUVs can be trapped as well with 800 nm CW laser light, different bead and liposome samples are tested. As can be deduced from equation 2.28 the trappability depends on the ratio  $m = \frac{n_{object}}{n_{media}}$ . Hence, Texas red labeled LUVs containing various sucrose concentrations are prepared according to [43]. The refractive index of the 2 M sucrose buffer is determined as  $1.4381 \pm 0.0005$ . MilliQ water was measured as a reference yielding exactly 1.3330 and therefore resulting in a refractive index mismatch of  $\Delta n = 0.1051$ . Thus,  $m$  can be calculated as well, yielding  $m = 1.0788$ . Proper LUV preparation is confirmed by FCS.

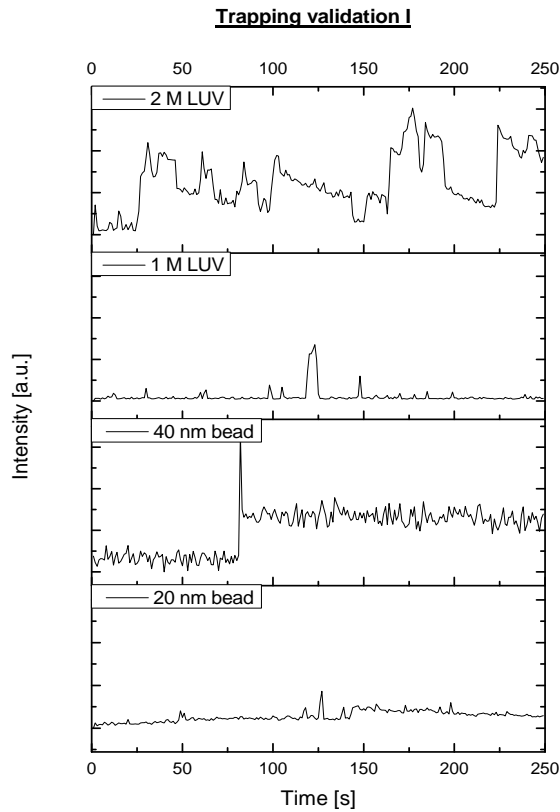


Figure 4.19: Time trace demonstrating the trappability of 20 nm and 40 nm beads and SUVs filled with either 1 M or 2 M sucrose.

Figure 4.19 represents the time traces for two distinct LUV populations filled with either 1 M or 2 M sucrose. Additionally, 20 nm and 40 nm beads are measured at concentrations around 10 nM. The CW power is set to 100 mW. As can be deduced from figure 4.19 the trappability of the beads increases with increasing size which is in line with the theory as depicted in subsection 2.3.4.

While 20 nm beads are not trapped at all, the 40 nm beads are already trappable. For the LUVs only the 2 M sucrose containing LUVs are sufficiently trapped up to 2 min. In order to furthermore prove that indeed a LUV is trapped, a time trace of a 2 M sucrose filled LUV sample is recorded and presented in figure 4.20. Upon rising intensity the shutter in the setup is closed for 1 s and opened again, as indicated by an arrow. The recorded fluorescence intensity goes down and does not rise until the next LUV is trapped again. Hence, figure 4.20 demonstrates the de-trapping of a LUV upon CW beam interruption.

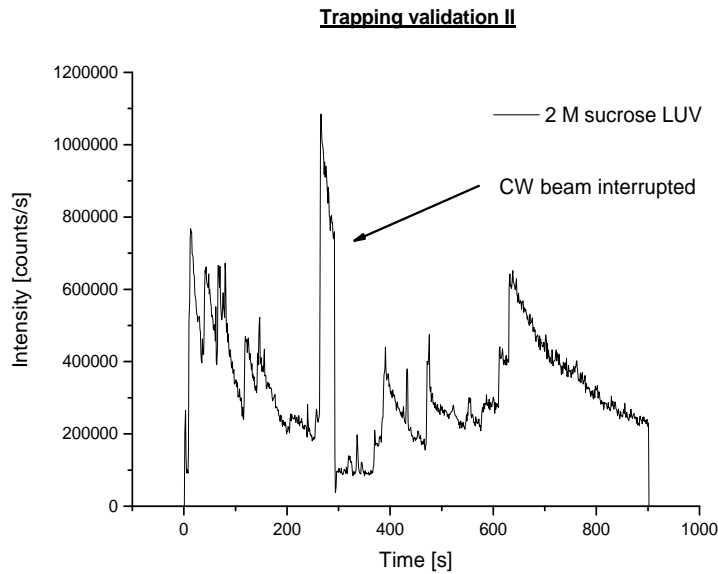


Figure 4.20: Time trace validating the trappability of LUVs filled with 2 M sucrose. The arrow indicates an interruption of the CW laser beam. The formerly trapped LUV is thus released.

Next, an adequate trapping power has to be evaluated in order to increase the trapping efficiency, but not to photobleach the Texas red dye within the LUV completely, especially because it has already been shown that Texas red photobleaching is quite severe under trapping conditions [8]. Figure 4.21 represents five different time traces of Texas red labeled LUVs. Each time trace is recorded with a different laser power of the CW beam. Here, 20, 50 and 75 mW do not provide enough radiation density to trap the LUV sufficiently and provide an adequate fluorescence intensity. The other time traces - recorded at 100 and 167 mW - indeed demonstrate several trapping events and a satisfactory fluorescence intensity. Nevertheless, a laser power of 167 mW already seems to increase photobleaching tremendously. Apparently the vast photobleaching does no longer permit to reliably monitor the trapping event over a longer period of time. Consequently the power is kept around 100 mW for the trapping beam for all further experiments. The TPE laser beam is kept at a power of 20 mW as previously described in chapter 3.

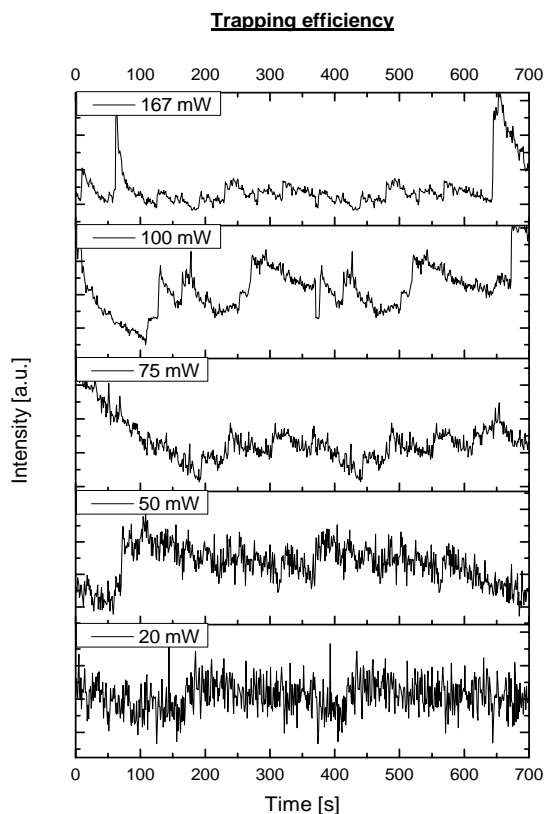


Figure 4.21: Trapping power evaluation. Trapping of LUVs with CW laser light works best around 100 mW. The higher the trapping power the greater the photobleaching of Texas red in the LUV.

#### 4.2.4 Oregon green lifetime

In order to apply this new approach of optical trapping in terms of docking and fusion reactions as described above, the influence of the different excitation modes on the lifetime of Oregon green has to be tested. Table 4.10 already depicts no significant difference in the fluorescence lifetime  $\tau_{life}$  of TP and CW & TP excited R6G. However, the application of Oregon green within this trapping approach in terms of photostability remains to be demonstrated. Although the wavelength of the trapping laser is far from the peak absorption of the fluorophore, a potential degradation of the dye can occur [8]. Since it is not possible to generate a liposome mixture that contains 100% docked liposomes, only the free diffusing (OGSUV) and fused state analogue (TR-OGSUV) are taken as a control. Figure 4.22 compares these two distinct liposome preparations. The first liposome contains 1.5% Oregon green, while the second contains 1.5% Oregon green and 1% Texas red mimicking the completely fused state of two distinct liposome populations. Both liposome preparations are measured under TPE

conditions (20 mW) either in the presence or the absence of an additional CW (100 mW) laser beam. It becomes clear that the non-interacting and fused state are distinguishable.

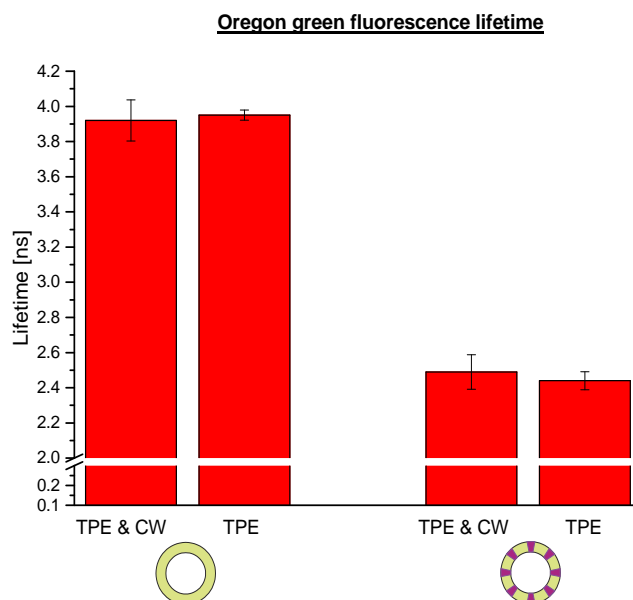


Figure 4.22: Two distinct liposome preparations, one containing 1.5% Oregon green the other containing 1.5% Oregon green and 1% Texas red, are measured under either solely TPE or TPE & CW conditions. A difference of the fluorescence lifetime of the non-interacting analogue and the fused analogue is demonstrated. The influence of the CW laser beam onto the Oregon green lifetime can be neglected.

While the Oregon green labeled SUVs alone reveal a fluorescence lifetime of about 3.9 ns, the fused state analogue shows a lifetime of 2.5 ns. There is no apparent difference in the fluorescence lifetime of Oregon green when additionally the trapping CW laser beam is coupled into the microscope. Here, error bars are higher for TP & CW excitation as for solely TP excitation. The diffusion time for a synaptotagmin-1 carrying SUV under TPE & CW excitation conditions is determined to be roughly 2.6 ms. This is in good agreement with about 2.2 ms under TPE conditions. As mentioned above, it is not possible to generate a control for the tethered state. Thus, it remains to be shown whether a FRET based on intermembrane distance shortening can be resolved in the context of optically trapped LUVs as well.

Having demonstrated the possibility of optically trapping LUVs and having characterized the related spectroscopic features, the question still remains what applications might emanate from this new approach. The following subsections are thus addressing a potential assignment in tethering or adsorption studies, in distance regulation studies and finally in studies of liposomal fusion events.

### 4.2.5 Adsorption isotherms of synaptotagmin-1 SUVs

The previous section 4.1 illustrates that upon rising  $\text{Ca}^{2+}$  concentrations, the amount of tethered liposomes increases. These steady state experiments do not provide any information about whether synaptotagmin-1 de-tethers at all. By trapping a LUV an immobile substitute for the plasma membrane is generated. Hence, diffusing SUVs carrying reconstituted synaptotagmin-1 should bind to the trapped LUV, thus exhibiting an increased diffusion time  $\tau_{Diff}$  which corresponds to a prolonged retention time within the focal volume. In the opposite case of not de-tethering, the tightly tethered liposomes do not contribute to the diffusion time  $\tau_{Diff}$ . Whereas, the diffusion time  $\tau_{Diff}$  of the remaining, freely diffusing SUVs is not affected by increasing  $\text{Ca}^{2+}$  concentrations.

LUVs and SUVs are prepared as described in chapter 3. LUVs are prepared with either containing no or 15% PS. Both liposome types are mixed in a 1:10 ratio with the LUV concentration being 0.2 particles within the focal volume. The liposome mixture is then incubated for 30 min to achieve equilibrium state. Hence, there should be no net change in tethering. The sample mixture is then measured under optical trapping conditions. Upon recording a trapping event of a LUV, the analysis of the inherent diffusion time of the SUVs is performed as explained in chapter 3. Here, mean values from different sample preparations are taken for further data analysis. For better comparison, the recorded diffusion times are normalized to a start value.

Figure 4.23 depicts the diffusion time  $\tau_{Diff}$  of the Oregon green labeled SUVs recorded under trapping conditions and depending on the  $\text{Ca}^{2+}$  concentration. As can be seen, in the absence of any anionic lipids in the LUV (gray) the diffusion time of the synaptotagmin-1 carrying SUVs is not altered significantly. Hence, demonstrating that tethering can be neglected, which is in line with the finding that synaptotagmin-1 only binds to anionic lipids [121]. In contrast, with 15% PS (black) present in the LUV membrane, the diffusion time of the SUVs is increased with increasing concentrations of calcium ions. The more calcium ions are present the stronger synaptotagmin-1, reconstituted into the SUVs, binds to the anionic lipid surface provided by the trapped LUV. The equilibrium for synaptotagmin-1 binding to anionic lipids is shifted towards the bound state upon rising  $\text{Ca}^{2+}$  concentrations. Here, a certain fraction of SUVs may indeed bind permanently to the LUV, but they do not contribute to the recorded diffusion time. Only those that either freely diffuse through the focus, or those that tether and de-tether determine the calculated diffusion time. Thus, an increased diffusion time may be interpreted as an increased retention time in the focal volume. Binding to a surface, as provided by the trapped LUV, may furthermore be seen as an equivalent process to adsorption. Especially, because tethering and de-tethering can be thought of as equivalent processes to adsorption and desorption. If this is the case then the recorded alterations in the diffusion time may as well be interpreted in terms of adsorption isotherms. Here, adsorption isotherms may provide a first measure for comparing tethering behaviour.

Since liposomes are mixed in a 1:10 ratio and LUVs only exhibit a 13 times

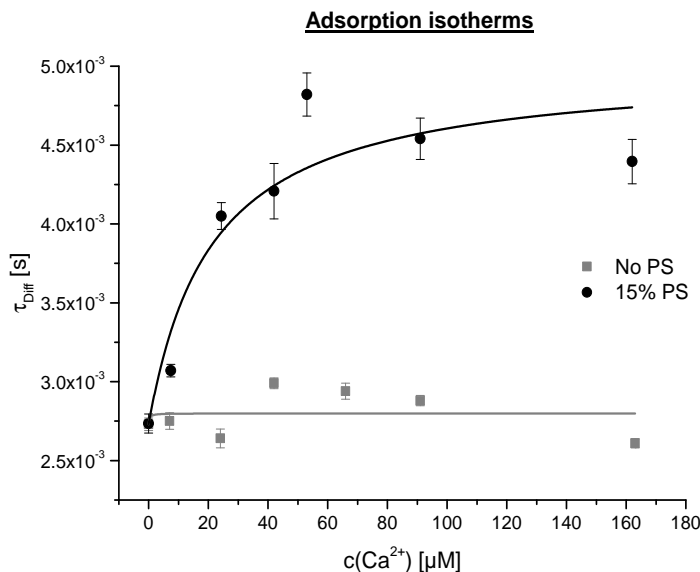


Figure 4.23: Adsorption isotherms of synaptotagmin-1 carrying SUVs to an optically trapped LUV containing either no PS (gray) or 15% PS (black). A Langmuir adsorption model fit is applied to the data. Error bars for the measurement containing 15% PS represent standard deviations from distinct sample preparations. Error bars for the negative control represent the fitting error.

greater surface than SUVs, Langmuir adsorption isotherms may no longer represent an appropriate fit model. Moreover, LUVs are round and not perfectly flat as claimed in the Langmuir model [5]. Therefore, models like those introduced by Freundlich [36] or Gunary [40] - owing to hindered adsorption - seem to display a more reasonable description (compare 2.5.3).

Hence, three different adsorption isotherms are applied to the data presented in figure 4.23, namely: Langmuir, Freundlich and Gunary. Here, the recorded diffusion time may be interpreted as  $\Theta = \frac{\tau_{Diff}}{\tau_{max}}$  according to equation 2.41. Here,  $\tau_{max}$  represents the maximum diffusion time that is achieved when the maximum LUV coverage with SUVs is reached. The fits are set free to converge, with the only restraint that the fit parameters have to be  $\geq 0$ . All models yield a sophisticated  $R^2$  for the adsorption of synaptotagmin-1 to 15% PS as can be deduced from table 4.11. Figure 4.23 exemplarily depicts fits according to the Langmuir model. As an optical guide for the reader the Langmuir isotherm model is also applied to the diffusion times recorded in the presence of the PS-less LUV (figure 4.23 (gray line)). As a matter of fact, no further interpretation of the achieved fit parameters is valid in this case.

Table 4.11: Three different adsorption isotherms are applied to the diffusion time of synaptotagmin-1 carrying SUVs. The constant  $K$  for the Langmuir adsorption as well as  $K_2$  from the Gurney adsorption isotherm are given in  $\mu\text{M}^{-1}$ ,  $K_3$  is given in  $\mu\text{M}^{-\frac{1}{2}}$ , whereas the remaining constants are dimensionless [10].

parameter	15% PS
<b>Langmuir</b>	
$K$	$0.048 \pm 0.027$
$R^2$	0.99
<b>Freundlich</b>	
$K$	$2.60 \cdot 10^{-3} \pm 3.03 \cdot 10^{-4}$
$n$	$0.13 \pm 0.03$
$R^2$	0.99
<b>Gurney</b>	
$K_1$	$258.91 \pm 652.46$
$K_2$	$201.38 \pm 34.21$
$K_3$	$159.97 \pm 331.92$
$R^2$	0.99

To further describe the tethering and de-tethering behaviour of synaptotagmin-1 the data shown in figure 4.23 is plotted according to the Langmuir as well as according to the Freundlich isotherms introduced above in subsection 2.5.3.

For the first approach the calcium concentration divided by the diffusion time is plotted against the calcium concentration. For the latter the logarithm of the diffusion time is plotted against the logarithm of the calcium concentrations. Although the Freundlich approach reveals an  $R^2$  of 0.99, the corresponding Freundlich plot nevertheless fails. Plotting the data according to the Freundlich model does not reveal a straight line with a satisfying  $R^2$  (data not shown here). In fact, plotting the data for the liposome containing 15% PS according to the Langmuir model reveals a straight line in the form of  $y = 542.06 \cdot x + 5094.18$  with an  $R^2$  of 0.94, as can be deduced from figure 4.24. Calculating the constant  $K$  on the basis of the linear Langmuir plot yields to  $K = 0.11 \pm 0.01 \mu\text{M}^{-1}$ , which is in the range of  $K$  determined beforehand (table 4.11). This demonstrates that the Langmuir adsorption isotherms depicted in figure 4.24 may indeed be applicable to describe tethering in the context of optical trapping.

An increased diffusion or retention time may also be interpreted as a reduced diffusion coefficient  $D$ . According to equation 2.15, the diffusion coefficients can

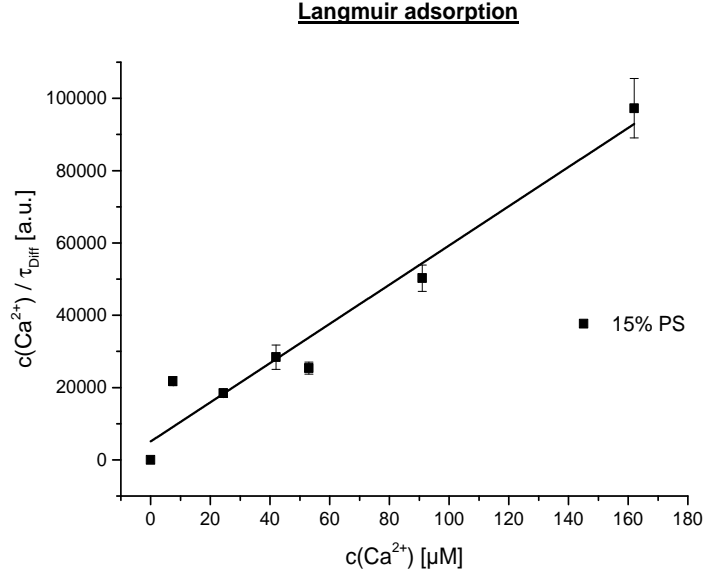


Figure 4.24: Langmuir plot of synaptotagmin-1 carrying SUVs to an optically trapped LUV containing 15% PS (black). Error bars represent the relative error.

be calculated from the increased diffusion time  $\tau_{Diff}$  as depicted in figure 4.25.

Here,  $r_{xy}$  and its error are known from the characterization of the focal volume presented in subsection 4.2.2. Again, the Langmuir adsorption model is applied. While the diffusion time of synaptotagmin-1 carrying SUVs does not change significantly in the absence of PS (gray), it is indeed reduced in the presence of 15% PS (black) in the LUV membrane. Here, the resulting fit parameters are presented in table 4.12. Here  $K$  slightly varies from the constant depicted in table 4.11. This is because the error of the underlying data is increased due to the error in  $r_{xy}$ .

Table 4.12: A Langmuir fit model is applied to the diffusion coefficient data resulting from the diffusion time of synaptotagmin-1 carrying SUVs. The constant  $K$  is given in  $\mu\text{M}^{-1}$ .

parameter	15% PS
<b>Langmuir</b>	
K	$0.074 \pm 0.032$
$R^2$	0.89

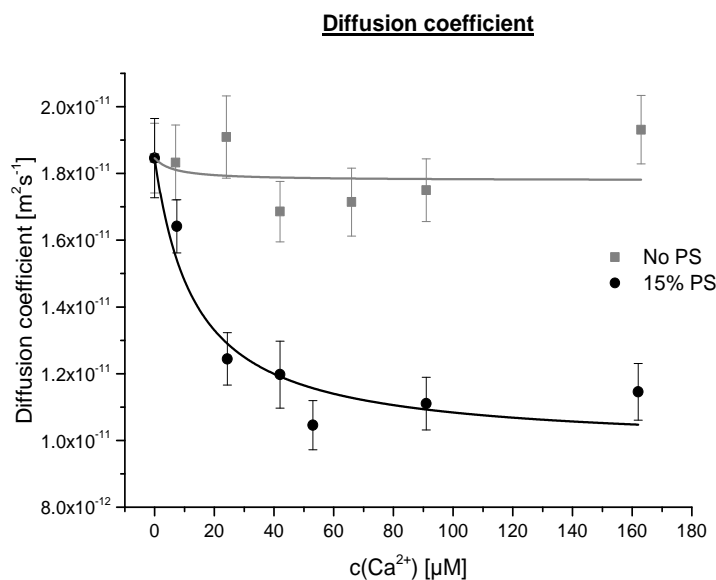


Figure 4.25: Diffusion coefficient of synaptotagmin-1 carrying SUVs depending on the presence of an optically trapped LUV either containing no PS (gray) or 15% PS (black). A Langmuir adsorption model fit is applied to the data. Error bars are calculated via error analysis.

The present section indicates that indeed optically trapped LUVs can be used to measure and characterize tethering. A critical discussion of the application of adsorption isotherms in this context is given in chapter 5. Having focussed on distance regulation in the previous section 4.1, the next step is to test whether it is also possible to gain any information about membrane distance shortening in terms of optical trapping.

## 4.2.6 Distance regulation in optical trapping

It has been shown that synaptotagmin-1 docking and SNARE fusion depend on the size of the liposomes prepared [43]. The reason for this is thought to be the varying curvature, which results in a varying lipid bilayer tension and availability of the involved proteins. Therefore, it is furthermore necessary to make sure that distance regulation based FRET also appears when mixing an Oregon green labeled SUV, having synaptotagmin-1 reconstituted, with a Texas red labeled LUV. A simple bulk experiment as in [119] is shown in figure 4.26. The liposomes are mixed in a 1:1 ratio and incubated for 30 min at RT in HP150

buffer. Here the Oregon green SUVs contain reconstituted synaptotagmin-1, while the Texas red labeled LUVs contain either no or 1% PiP<sub>2</sub>.

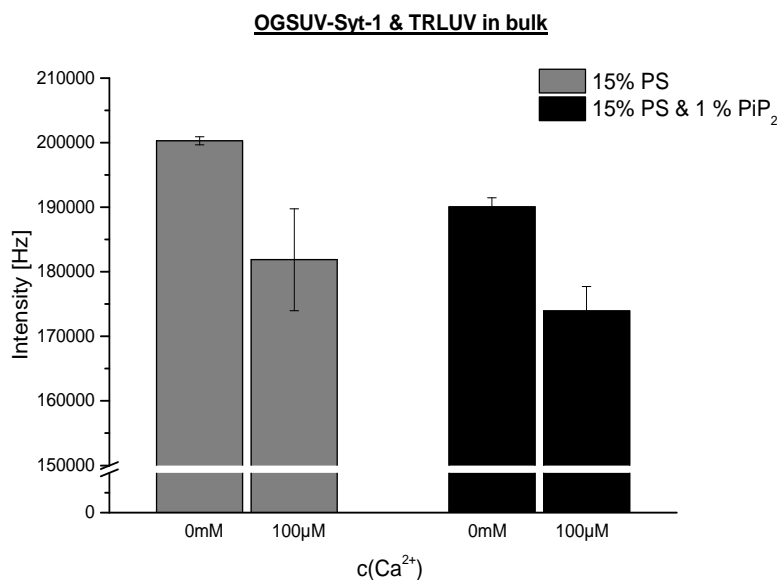


Figure 4.26: Bulk experiment with Texas red labeled LUV containing either no PiP<sub>2</sub> (gray) or 1% PiP<sub>2</sub> (black) and Oregon green labeled SUVs having synaptotagmin-1 reconstituted. Both liposome types additionally contain 15% PS.

Interestingly, for both liposome combinations a decrease in the fluorescence intensity is recorded upon addition of Ca<sup>2+</sup> ions. Formerly, in the SUV/SUV mixture, only the presence of PiP<sub>2</sub> was able to cause such a pronounced shift. The fact that in the presence of PiP<sub>2</sub> the intensity is in general a little smaller should not be over-interpreted as it may be a result from variations within the sample preparation. Thus, once more demonstrating the benefit of fluorescence lifetime instead of using the fluorescence intensity. Nonetheless, the present experiment demonstrates an apparent FRET, which can be interpreted as a reduction of intermembrane distance.

It is obvious from figure 4.26 that a lifetime shift as reported in section 4.1 should also occur for a SUV/LUV combination. Hence, LUVs carrying 15% PS alone or 15% PS and 1% PiP<sub>2</sub> are prepared. The SUVs contain 15% PS and reconstituted full-length synaptotagmin-1. The samples are mixed in a 1:1 ratio and incubated for 30 min at different Ca<sup>2+</sup> concentrations in HP150 buffer. Subsequently, the sample combinations are measured under optical trapping conditions. Interestingly, a much lower fluorescence lifetime is observed for all liposome combinations as compared to figure 4.22 (left hand side). Here, even in the absence of calcium ions the lifetime for both sample mixtures - either containing no or 1% PiP<sub>2</sub> - is located around 3.55 ns. This is even lower than the lowest lifetime reported in section 4.1. Except for the second last

measurement shown, which has been recorded in the presence of 3 mM  $\text{Ca}^{2+}$  the fluorescence lifetimes do not vary significantly at all. Of course, the second last bar may as well result from spontaneous fusion. The error bars are relatively high compared to those presented in section 4.1. Moreover, if there is a trend at all, the solely PS containing liposome combination shows a shorter lifetime than the one including 1%  $\text{PIP}_2$ . This is in contrast to what has been depicted in figure 4.26. Thus, it seems impossible to detect tethering based fluorescence lifetime changes under CW & TPE conditions.

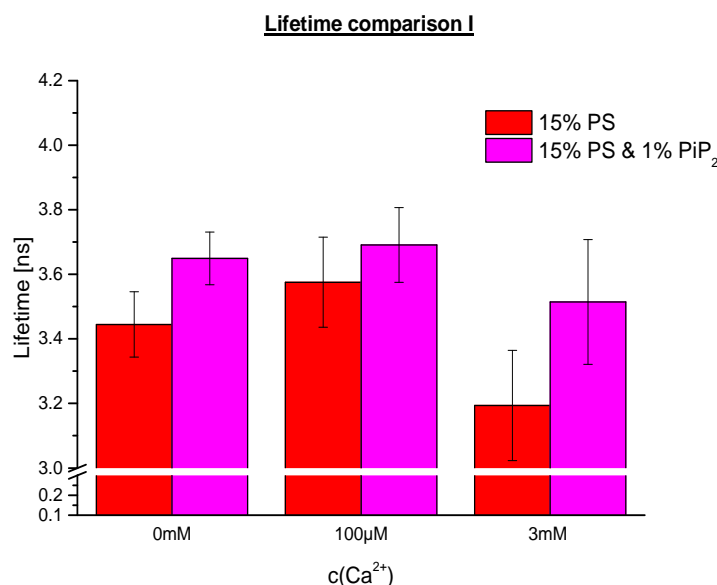


Figure 4.27: Oregon green fluorescence lifetimes recorded for different lipid compositions of the LUV membrane. The LUV membrane either contains no  $\text{PIP}_2$  (magenta bars) or 1%  $\text{PIP}_2$  (red bars). Varying  $\text{Ca}^{2+}$  concentrations, ranging from no, 100  $\mu\text{M}$  to excess concentrations are measured.

However, the concentration of 1% Texas red as the acceptor may be too low for recording a distance based FRET under the optical trapping conditions described above. Since Texas red photobleaching is quite severe it is unclear whether under these conditions it is possible to see a change in the fluorescence lifetime of an Oregon green labeled SUV attached to the Texas red LUV similar to the FRET reported in section 4.1. Especially, because for tethering we do not expect a great decrease of the fluorescence lifetime at all. Again, photobleaching of Oregon green labeled SUVs is less critical as demonstrated in subsection 4.2.4 and [8]. Hence, LUVs containing either no dye or 5% Texas red are prepared as a control. Both LUV preparations additionally contained 1%  $\text{PIP}_2$ . The unlabeled LUV is detected through a rise of fluorescence intensity on the green channel owing to Oregon green labeled SUVs which tether to the LUV.

Figure 4.28 depicts the effect of the concentration of Texas red in the LUV membrane on the lifetime of Oregon green located in the SUV membrane. Both

liposome mixtures do not show a difference in the recorded fluorescence lifetime unless excess amounts of  $\text{Ca}^{2+}$  (3 mM) are added. Again, spontaneous fusion can not be excluded here. Thus, this experiment demonstrates that membrane distance shortening studies are not possible under optical trapping conditions. Nonetheless, fusion may still be detectable since the resulting FRET is considerably greater. Hence, the following subsection delineates the exertion of fusion in the context of optical trapping.

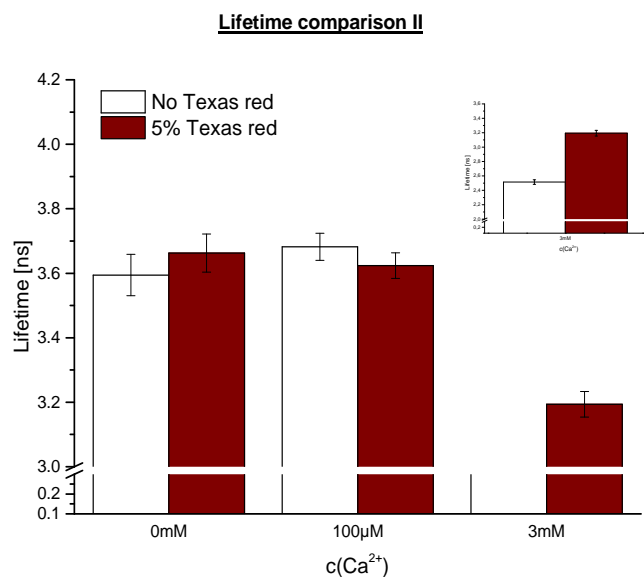


Figure 4.28: Fluorescence lifetimes recorded for different dye compositions of the LUV membrane. The LUV membrane either contains no dye (black stripes) or 5% Texas red (deep red). Varying  $\text{Ca}^{2+}$  concentrations, ranging from 0, 100  $\mu\text{M}$  to excess concentrations are measured.

### 4.2.7 Fusion of SUVs to optically trapped LUVs

Although it is not possible to reliably assign a distance based FRET between an Oregon green carrying SUVs and a Texas red carrying LUV, a significant decrease in the fluorescence lifetime is indeed expected in case of full fusion (compare figure 4.22). Currently, two fusion models are discussed. The first states that, although synaptotagmin-1 can trigger fast and efficient fusion, SNARE mediated fusion itself does not require any synaptotagmin-1 or calcium ions [29, 43, 11, 106] per se. A second hypothesis though states that synaptotagmin-1 is capable to arrest the SNARE complex in a partially zippered state, thus preventing fusion in the absence of  $\text{Ca}^{2+}$  [60, 14, 19]. Therefore the scope of work of this subsection is to investigate whether fusion can be observed under optical trapping conditions and if so, which of the two fusion models discussed can be supported. Since optical trapping is a process occurring accidentally, a

way of selectively triggering fusion has to be developed. A technique to control the fusion process is given by either injecting the SUVs or calcium ions after recording a trapping event. This in turn raises the challenge of not de-trapping the LUV due to an external flow.

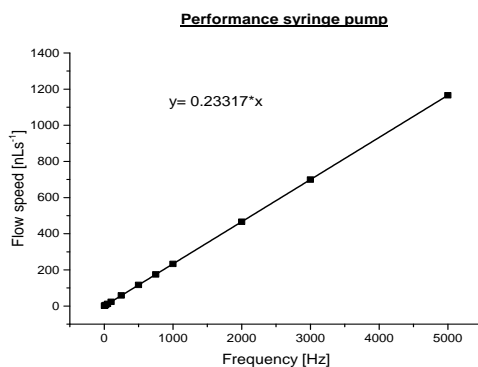


Figure 4.29: Performance of self-built syringe pump. The frequency of the rotation of the screw is linearly connected to the applied flow speed. The flow speed is determined by the volume pumped out of the syringe.  $R^2$  is calculated to be 0.99.

Several approaches are tested with the one described below being the most successful one. Here a self-built chamber comprising about 500  $\mu\text{L}$  of LUV sample is sealed to a cover slip and put on top of the objective. A 500  $\mu\text{L}$  Hamilton syringe is filled with sample and a sleeve is connected to the head of the syringe. The remaining end of the sleeve is positioned to the corner of the sample chamber. A self-built syringe pump made of a picomotor permits to pump the SUVs into the chamber. The rotation of the screw in the picomotor is to be set in Hz. In order to determine the flow speed obtained at a given frequency, several frequencies are applied for a fixed amount of time. Consequently, the volume pumped out of the syringe is deduced from the scale of the syringe. Thus, making it possible to assign a distinct flow speed to the set frequency of screw rotation as depicted in figure 4.29. Figure 4.30 illustrates a time trace taken from a LUV sample. Buffer influx is started after having trapped a LUV ( $\sim 230$  s). The LUV is not de-trapped by the induced flow but only by closing the shutter ( $\sim 325$  s). Interestingly, between 275 and 300 s the fluorescence intensity of the trapped LUV increases once more, which is eventually due to fluctuations within the laser intensity. Trapping of a second LUV can be excluded, since the intensity does not decrease exponentially afterwards due to photobleaching, but returns to its former value. Generally, an influx speed of 2000 Hz does not have to be exceeded in order to not de-trap the LUV.

Since figure 4.30 demonstrates that an applied influx does not necessarily de-trap a LUV there are two possible scenarios of how fusion can be observed. Thus, accounting for the two previously mentioned fusion models. In the first approach the LUV is trapped in an environment already containing a sufficient amount of calcium ions (100  $\mu\text{M}$ ). The SUVs are then injected after having trapped a LUV. This approach is referred to as "Fusion experiment I". In the second approach the LUVs are pre-incubated with SUVs in a  $\text{Ca}^{2+}$ -free environment as published in [60]. Upon trapping a LUV calcium ions are injected. This approach is referred to as "Fusion experiment II" and refers to an experiment including fluorescently labeled, immobilized liposomes carrying the plasma

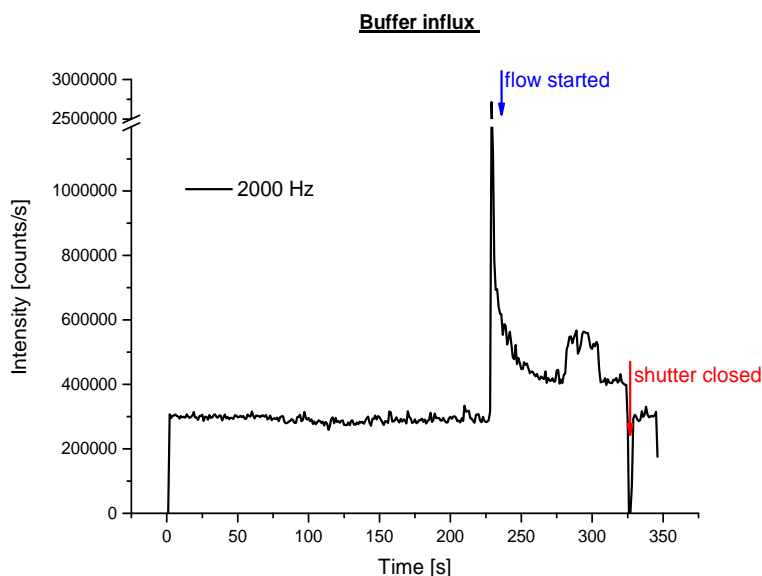


Figure 4.30: Time trace representing a trapping event of a LUV. Right after the LUV is trapped the syringe pump is started to pump buffer into the chamber. After 100 s the LUV is still not de-trapped. The fluorescence signal returns to its original intensity upon interrupting the CW laser beam by closing the shutter.

membrane part of the fusion machinery. These liposomes are pre-incubated then with their free diffusing counterpart. Both liposome populations are labeled differently. Undocked liposomes are washed away and the fluorescence intensity of both liposome populations is recorded upon  $\text{Ca}^{2+}$  influx [60]. Optical trapping provides another beneficial tool to either prove or rebut the above exposed findings. In order to monitor fusion of liposomes SNARE-complex formation is required (see section 2.2). Hence the following two paragraphs depict measurements performed with LUVs having the so called  $\Delta\text{N}$  complex reconstituted, as well as with SUVs having synaptotagmin-1 and synaptobrevin reconstituted in a 1:4 ratio. The  $\Delta\text{N}$  complex consists of the fusion machinery including syntaxin and SNAP25 and a shorter version of synaptobrevin 2. Upon fusion this shorter synaptobrevin 2 variant is replaced by the full length synaptobrevin 2 reconstituted into the SUV membrane. Fusion then takes place within a few minutes [43]. LUVs and SUVs are mixed in a 1:10 ratio for "Fusion experiment II". The LUV concentration is kept below 1 particle.

### Fusion experiment I

This paragraph focuses on the first approach, namely the SUV influx into a sample chamber where LUVs have already been trapped. Both samples find themselves in HP150 buffer containing  $100 \mu\text{M}$   $\text{Ca}^{2+}$ . A time trace in both

channels - red (channel 1) and green (channel 2) - is recorded as depicted in figure 4.31. Different events within the time trace are marked with capital letters. Here, (A) describes the initial fluorescence signal recorded for LUVs diffusing through the focal volume which is about 300.000 counts/s. (B) shows the rise in fluorescence intensity that is recorded upon trapping a LUV. Trapping of a Texas red labeled LUV even induces a rise in fluorescence intensity on the green channel. SUVs are subsequently injected via the syringe pump (C). Hence, the fluorescence on channel 2 rises while the intensity on channel 1 decreases a bit due to additionally untrapped, diffusing LUVs being washed away from the focal volume. (D) depicts the furthermore recorded fluorescence intensity of both channels during trapping. While the Texas red fluorescence remains stable, the Oregon green fluorescence corresponds to the amount of SUVs flown through the focus. After a rise in Oregon green intensity the fluorescence decreases again due to dilution within the sample chamber.

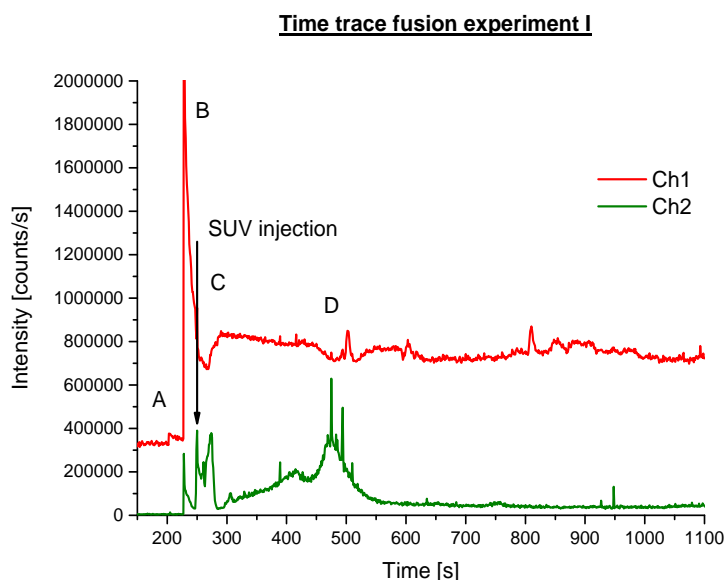


Figure 4.31: Time trace representing a trapping event of a LUV. Right after the LUV is trapped the syringe pump is started to pump SUVs into the chamber. The following capital letters mark distinct stages within the time trace: (A) original fluorescence intensity, (B) a LUV is trapped, (C) SUV injection, (D) the LUV is still trapped, SUVs heterogeneously diffuse through the focal volume.

From the time point of SUV influx onwards, the fluorescence lifetime is calculated in 30 s steps. A monoexponential tail fit is applied to the generated fluorescence lifetime histograms. As a quality control, the diffusion times of the SUVs within the particular time frames are calculated as well. In case of diffusion times being in the high ms- and s-range, the corresponding time frame is disregarded. This permits to exclude fluorescence lifetime data originating from possibly aggregated SUVs. Figure 4.32 depicts the fluorescence lifetime

development of Oregon green labeled SUVs upon fusion to a Texas red labeled LUV. As can be deduced from the corresponding time trace depicted in figure 4.31 the lifetime decreases right after SUV injection. The fluorescence lifetime is in general lower than the unaffected fluorescence lifetime of Oregon green measured under solely TP and TP & CW excitation conditions as presented in figure 4.22. This is may be due to the fact that some SUVs are already partially fused at  $t= 600$  s. Moreover, also the distance regulation experiments shown in figure 4.28 also reveal fluorescence lifetimes significantly below 4 ns. One data point is omitted, since the corresponding diffusion time in this time frame indicated the existence of an aggregated particle. Beyond all this, data points generated after 4 min of the initial fusion reaction are deleted (850 - 950s). Here, the excess amount of freely diffusing liposomes being heterogeneously diluted in the sample chamber may have caused an increase in the recorded fluorescence lifetime. Additionally, the contribution of the fusiogenic SUVs to the fluorescence lifetime recorded on channel 2 decreases, while - at the same time - the relative contribution of false photons originating from Texas red then increase . Thus, it is more difficult to reliably determine the fluorescence lifetime of Oregon green. Indeed, the corresponding fluorescence lifetime histograms do not appear as smooth monoexponential decay functions any longer (data not shown here). Three more data points at the very end of the time trace are taken into account as well, in order to receive a reasonable fit. Here, all fusiogenic SUVs are expected to be fused. According to earlier publications [43] fusion should be completed after a few minutes, with the first two minutes showing the most prominent FRET. Hence, the fluorescence lifetime development presented in figure 4.32 still includes the time frame that is of most interest.

Assuming  $1^{st}$  order kinetics and applying a monoexponential decay function to the data points presented in figure 4.32 does not yield a sophisticated fit (compare subsection 2.5.1). Furthermore plotting the natural logarithm of the fluorescence lifetime does not succeed in a linear function (data not show here). It has been described earlier that SNARE fusion kinetics may reveal multicomponent fusion reactions [29]. The authors consider a model with two types of fusion sites, which are each characterized by a different number,  $m$ , of elementary activating particles that activate fusion at different rates,  $k$ . Although the fluorescence signal of the different fusiogenic components follow a monoexponential decay, the resulting decline has to be characterized as follows:

$$N(t) = N_1(1 + e^{-k_1 t})^{m_1} + N_2(1 + e^{-k_2 t})^{m_2} \quad (4.6)$$

Here,  $N$  is the number of fusion events of either species 1 or 2. The total number of fusion events at a given time point  $t$  is then calculated as the sum of both species. In the present fusion experiment the number of liposomes which fuse is unknown. However, the number of fusiogenic liposomes is proportional to the recorded fluorescence lifetime alterations. An optically trapped LUV furthermore provides equal binding sites for a SUV, which makes  $m_1=m_2$ .

Once the liposomes are docked, the fusion reaction proceeds in an identical manner. The fit is set free to converge without any further constraints but the above mentioned one,  $m_1=m_2$ . As can be deduced from figure 4.32, the

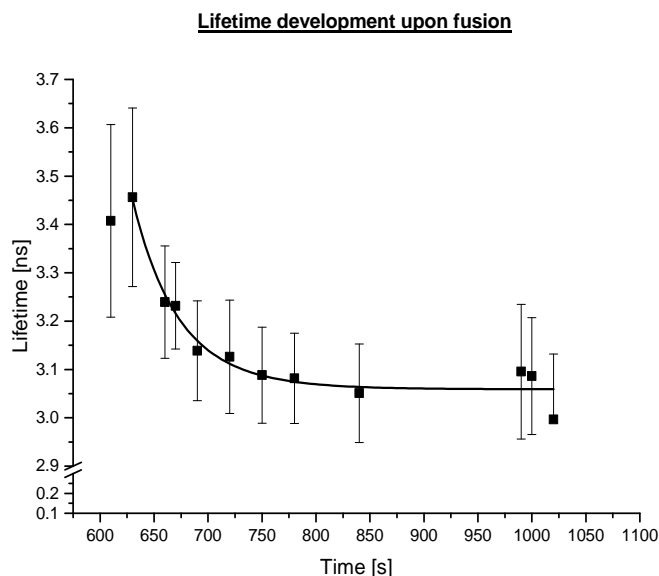


Figure 4.32: Fluorescence lifetime development of Oregon green in a SUV influx. A Texas red labeled LUV is trapped beforehand. Upon fusion of the SUV to the LUV the Oregon green lifetime is quenched. Error bars result from a monoexponential fit to the generated lifetime histograms.

applied fit function reveals a proper match to the data points. Although the fit identifies a fast ( $k_1 = 34$  s) and a slower ( $k_2 = 55$  s) fusiogenic liposome population the corresponding error bars are certainly too large for a trustworthy further interpretation of the achieved fit values. Here,  $N$  reflects an arbitrary amplitude. Regardless, a comparison of generally distinct fusion machineries comprising either slow or fast fusion kinetics should be applicable for future studies.

It would be beneficial though to apply the above described model function 4.6 to a homogeneously mixed sample, thus permitting for a more sophisticated interpretation of the resulting data. This in turn anticipates the existence of a tightly docked state as a prerequisite, which can then be triggered to fuse upon  $\text{Ca}^{2+}$  influx. This remains to be manifested, though. The next paragraph therefore focuses on the incubation of LUVs and SUVs prior to trapping. Calcium ion injection serves as an external trigger to stimulate fusion.

## Fusion experiment II

As mentioned earlier, it has been reported that synaptotagmin-1 may arrest the SNARE fusion complex and permits for full fusion only after binding  $\text{Ca}^{2+}$  [60, 14, 19]. However, others state that SNARE dependent fusion does not require synaptotagmin-1 and/or  $\text{Ca}^{2+}$  [29, 43, 11, 106]. In fact, although

synaptotagmin-1 effectively triggers SNARE mediated fusion, it does not block fusion per se. To test both hypotheses SUVs and LUVs containing the above described reconstituted proteins are incubated in a 10:1 ratio in HP150 buffer for 30 min. The presence of calcium ions is prohibited by excess amounts of EGTA (1 mM). Afterwards a time trace of the pre-incubated liposome mix is taken. Upon trapping a LUV the syringe pump is started. A total amount of 50  $\mu\text{L}$  of 40 mM  $\text{CaCl}_2$  is pumped into a 500  $\mu\text{L}$  sample mix.

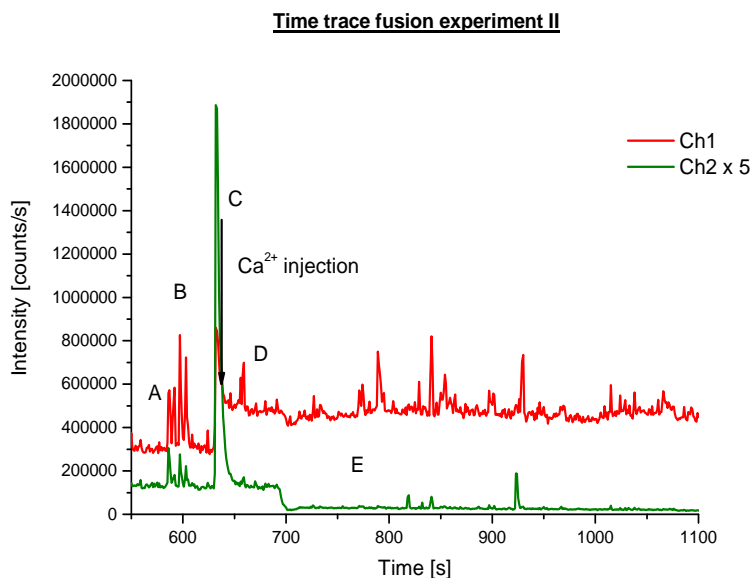


Figure 4.33: Time trace presenting a trapping event of a LUV. Right after the LUV is trapped the syringe pump is started to pump calcium ions into the chamber. The following capital letters mark distinct stages within the time trace: (A) original fluorescence intensity, (B) aggregations, (C) a LUV is trapped, (D) the LUV is still trapped, (E) freely diffusing SUVs are washed away by the applied  $\text{Ca}^{2+}$  influx.

The capital letters depicted in figure 4.33 characterize different events within the recorded fluorescence time trace. The initial Texas red fluorescence intensity is about 300.000 counts/s (A). Some random aggregated particles emerge as well (B). Although larger than the actual LUVs, they are not optically trapped. After 10.5 min of recording time a LUV is trapped (C). Consequently,  $\text{Ca}^{2+}$  is injected. Upon injection the trapped particle is not de-trapped (D). Freely diffusing SUVs are washed away by the applied buffer influx (E). The fluorescence lifetime is determined in 30 s steps starting from 600 s of total recording time. Again, auto-correlations are calculated as well in order to exclude time frames comprising aggregated particles diffusing through the focal volume.

As can be deduced from figure 4.34, no alteration of the fluorescence lifetime upon  $\text{Ca}^{2+}$  influx is recorded, either within a time frame of seconds or within a time frame of several minutes. Hence, the application of equation 4.6

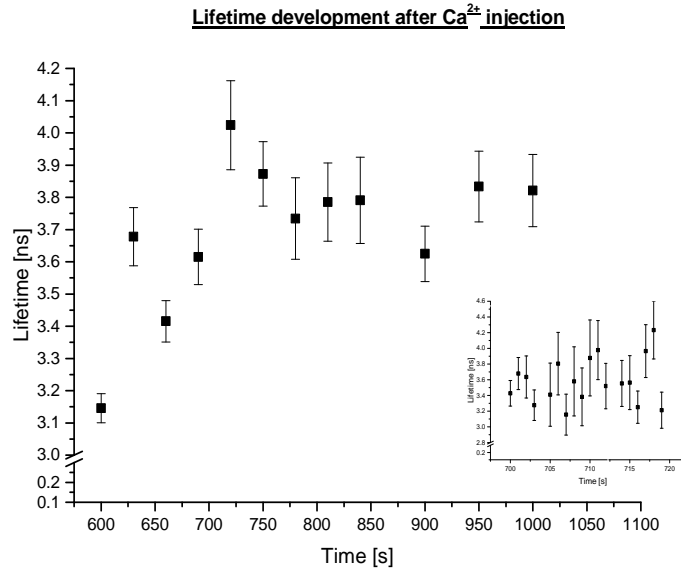


Figure 4.34: Fluorescence lifetime development of Oregon green upon  $\text{Ca}^{2+}$  influx. A Texas red labeled LUV is trapped beforehand. No significant alterations of the fluorescence lifetime are recorded. Error bars result from a monoexponential fit to the generated lifetime histograms.

can be rendered. The fluorescence lifetime is larger than the lifetime presented in figure 4.32. Taking a closer look at the time trace in figure 4.33(E) it becomes obvious that the Oregon green intensity is too low even for only one liposome in focus. The counts per particle (cpp) for one SUV should be around 30.000. It has to be noted that the cpp recorded on channel 2 and presented in figure 4.33 is multiplied by a factor of five. Thus, already revealing a too low intensity even for only one single SUV. According to the intensity profile depicted in figure 4.33(A), statistically one liposome diffuses through the focal volume. Possibly fusion already took place beforehand during incubation. Thus, only freely diffusing liposomes as well as "SUV relicts" that already underwent fusion are present in the sample mixture. Since the freely diffusing SUVs are washed away by the  $\text{Ca}^{2+}$  influx, the calculated fluorescence lifetime may thus be a result of photons originating from Texas red being detected on the green channel (Ch 2). The experiment is repeated with varying SUV:LUV ratios as well as with different amounts of  $\text{Ca}^{2+}$ . In none of the experiments performed under pre-incubating conditions a decrease in the fluorescence lifetime is observed. Contrary, for "Fusion experiments I", performed with SUV influx, a decrease of the fluorescence lifetime is observed in about 80% of all experiments. As mentioned earlier, this finding supports studies showing that indeed, synaptotagmin-1 can trigger fast fusion of the SNARE machinery, but does not prevent fusion per se [29, 43, 11, 106].

# Chapter 5

## Discussion

### 5.1 Synaptotagmin-1 is a distance regulator

A multitude of variations in sample preparation and measurement conditions are investigated via FCCS in this study. In order to avoid confusion the samples measured and the corresponding measurement conditions are listed for once more in this section, especially because in the context of the present study the technique used to characterize a potential distance regulation effect of synaptotagmin-1 does not change. In fact, the sample preparation and the measurement conditions are the parameters that permit for analyzing the functionality of synaptotagmin-1 and thus have to be put emphasis on. Thus, the following subsections 5.1.1 to 5.1.7 address these influences individually.

#### 5.1.1 The influence of ionic strength conditions and liposome concentration

The first step of this study, aiming to investigate a potential distance regulation function of synaptotagmin-1, is performed by taking a closer look at the influence the ionic strength of the media may have on tethering and the liposomal distance. Therefore, full length synaptotagmin-1 is reconstituted into Texas red labeled liposomes. Oregon green labeled liposomes which contain either no or 1%  $\text{PiP}_2$  are prepared as well. Both liposomes are mixed in equimolar ratio either under low ionic strength (5 mM KCl) or physiological ionic strength (150 mM KCl) conditions. Previously published findings [119] state that  $\text{PiP}_2$  is capable of shortening the intermembrane distance between two liposomes. These experiments were carried out under low ionic strength conditions in a bulk fluorescence assay and thus, have to be reproduced in terms of FCCS under low as well as under physiological buffer conditions.

Synaptotagmin-1 induced tethering and distance regulation under low ionic strength conditions measured either in bulk [119] or in terms of FCCS reveal dramatic differences. The previously published findings [119] demonstrate a FRET upon adding  $\text{Ca}^{2+}$  to the liposome mixture. FRET only occurs when  $\text{PiP}_2$  is present in the target liposome, though. The  $\text{Ca}^{2+}$  titration curve depicted in figure 4.1(B), resulting from FCCS experiments, only displays a very minor FRET at rather high  $\text{Ca}^{2+}$  concentrations. Here, the liposomes are diluted to the nM-level prior to incubation and subsequent measuring.

Of course, in a bulk fluorescence assay the concentration of liposomes is in the  $\mu\text{M}$ -range. Therefore, liposomes are additionally mixed in the  $\mu\text{M}$ -range and diluted to the nM-level afterwards. FCCS measurements with varying calcium ion concentrations are then performed either under low or physiological ionic strength conditions as can be deduced from figure 4.2. In contrast to the observations depicted in figure 4.1, when liposome concentrations are in the  $\mu\text{M}$ -range indeed increased amounts of tethered liposomes are recorded under low ionic strength conditions as presented in figure 4.2. This increase is only reported in the presence of calcium ions and furthermore depends on the presence of  $\text{PiP}_2$  in the target membrane. Whereas in the absence of calcium ions no significant tethering is observed under low ionic strength conditions as depicted in figure 4.2.

A straightforward interpretation of this remarkable finding is given by a reduction of the rate constant  $k_1$  of the tethering reaction:



While the rate of dissociation given by  $k_{-1}$  is not affected, the rate of association is indeed tremendously reduced when incubating the liposomes in the nM-range under low ionic strength conditions, which results in a net-binding close to zero. Thus, the impact of the electrostatic contributions of synaptotagmin-1 tethering to anionic lipids additionally depends on the likelihood that two liposomes come together close enough, which is a direct result of the underlying liposome concentration. Unfortunately, the actual concentration of vesicles in the synapse is not known. In view of the fact that the synapse may host different vesicles pools [25], the concentration of the synaptic vesicles may indeed vary among these pools.

Furthermore, FCCS experiments performed under physiological buffer conditions as presented in figure 4.2 and 4.7, do not constitute any dependence on liposome concentration in terms of tethering. Indeed, the fluorescence lifetime of the liposomes that host 1%  $\text{PiP}_2$  and are mixed in the  $\mu\text{M}$ -range is decreased even in the absence of any calcium ions, which is fundamentally different from the observation made when incubating the samples in the nM concentration range.

Moreover, when mixing the liposomes in the  $\mu\text{M}$ -range,  $\text{PiP}_2$  binding becomes dominant over PS-binding under low ionic strength conditions, while the

corresponding differences are not as prominent under physiological conditions as can be deduced from figure 4.2.

It has been reported that  $\text{Ca}^{2+}$  dependent phospholipid binding by the  $\text{C}_2\text{A}$  domain is not only sensitive to ionic strength, but that the  $\text{C}_2\text{A}$  domain also mediates hydrophobic interactions, in particular via methionine 173. This indicates that  $\text{C}_2\text{A}$ 's interaction is stabilized by a hydrophobic mechanism that mirrors the amphipathic nature of the phospholipid bilayer [39, 82].  $\text{Ca}^{2+}$ -dependent phospholipid binding may thus proceed by a multimodal mechanism [39]. Increasing the ionic strength of the surrounding media emphasizes the hydrophobic interactions and reduces the electrostatic contribution to synaptotagmin-1 binding to an opposing lipid bilayer. Especially the poly-lysine patch with its positive charges is thought to prime synaptic vesicle fusion by binding to the negatively charged  $\text{PiP}_2$  [49, 6]. Moreover,  $\text{Ca}^{2+}$ , when bound to one of the  $\text{C}_2$  domains, is thought to be additionally coordinated by either PS or  $\text{PiP}_2$  [83]. An enhancement of the electrostatic environment might thus hamper these interaction which are also electrostatically driven. Under non-physiological buffer conditions the electrostatic interactions become dominant and hence lead to an all or nothing effect concerning the presence of calcium ions.

The observations made in this study lead to the conclusion that electrostatic effects mediate synaptotagmin-1 interaction. Nonetheless, previous publications demonstrate an analogous behaviour for synaptotagmin-1 binding to SNAREs [113, 20]. Up to now it still remains elusive whether there is a hierarchy of electrostatic interactions, either between synaptotagmin-1 and SNAREs or between synaptotagmin-1 and anionic lipids, that determine synaptic vesicle exocytosis.

In the context of this study a decrease in fluorescence lifetime is a measure for the actual intermembrane distance of the two distinctly labeled liposomes. The normalized fluorescence lifetime change, which is defined as  $NFLC = (\Delta Lifetime / \Delta Tethering)$ , does not depend significantly on the electrostatic environment as can be deduced from figure 4.4. The normalized fluorescence lifetime change is highest under low ionic strength conditions in the presence of  $\text{PiP}_2$  and the absence of calcium. Nevertheless, the error is rather high and thus, the increased normalized fluorescence lifetime change may result from the small amount of tethering as shown in figure 4.2. The only trend that can be deduced from these experiments is a slight enhancement in the normalized fluorescence lifetime change in the presence of  $\text{PiP}_2$  in the target liposome, measured under physiological ionic strength conditions. Hence, to investigate a potential distance regulation function of synaptotagmin-1 further detailed experiments are required, as discussed below.

### 5.1.2 The influence of anionic lipid concentration and ATP

In the experiments addressing the influence of the anionic lipid concentration and the presence of ATP, Texas red labeled liposomes, containing reconstituted synaptotagmin-1, are again mixed with Oregon green labeled target liposomes

which contain either no or 1%  $\text{PiP}_2$ . Additionally, Texas red and Oregon green liposomes contain either 20% or 15% PS. The amount of tethered liposomes as well as the resulting fluorescence lifetime of the donor dye upon increasing  $\text{Ca}^{2+}$  concentrations are recorded. The influence of different parameters, such as ATP, on tethering and on the fluorescence lifetime, reflecting the actual membrane to membrane distance, are analyzed. The experiments are performed with liposomes being mixed in the nM-range under physiological buffer conditions (150 mM KCl).

The FCCS experiments shown in figure 4.6 represent corresponding measurements to what has been published earlier [121]. Here, liposomes containing 20% PS were measured in the absence of ATP. A comparison of these earlier findings [121] with the ones depicted in figure 4.6 permits for investigating the influence ATP may have on liposome tethering. It becomes apparent that ATP does not have any significant effect when both liposomes carry 20% PS as can be deduced from figure 4.6(A) and (B). The amount of tethered liposomes measured in the presence of ATP is not altered, which is in line with earlier published tethering [121] and fusion studies [83]. In contrast 15% PS in both membranes and an ATP concentration of 3 mM lead to an enhancement of tethering as reported in section 4.1.2 and 4.1.3. Nonetheless, ATP does not permit for *trans*-binding per se. Since earlier studies have focussed on fusion of synaptotagmin-1 carrying liposomes, it still remains elusive whether or not ATP enhances *trans*-binding due to the proposed electrostatic screening model [83]. The model states that ATP chelates calcium ions and hence, competes with  $\text{Ca}^{2+}$ -dependent membrane binding of synaptotagmin-1 by shielding the coordination site of PS in the host membrane. This competition may then prevent synaptotagmin-1 from binding in *cis* to its own host membrane. Given the fact that binding to  $\text{PiP}_2$ , which is located in the target membrane, is favoured over PS binding, ATP may indeed indirectly support *trans*-binding. ATP supported synaptotagmin-1 loosening from its own host membrane provides an explanation for the findings presented in [83]. Nonetheless, an enhancement in *trans*-binding remains to be shown. This study demonstrates that ATP does not permit for *trans*-binding per se. Tethering still depends on the presence of  $\text{Ca}^{2+}$ , but is indeed enhanced at high concentrations of calcium ions as can be deduced from figure 4.6 and 4.7. Moreover, the simultaneously recorded fluorescence lifetime, depicted in figure 4.6, shows a significant decrease in the presence of calcium ions, indicating a shortening of the intermembrane distance with increasing  $\text{Ca}^{2+}$  concentrations.

Additionally, for the 15% PS containing liposomes, the presence of  $\text{PiP}_2$  in the target liposome results in a more pronounced fluorescence lifetime decrease as can be deduced from figure 4.6(D), while in the absence of  $\text{PiP}_2$  the total alterations in fluorescence lifetime are rather minor. This observation is in line with the findings presented in figure 4.2 and discussed above in subsection 5.1.1. As mentioned beforehand, the influence  $\text{PiP}_2$  has on the recorded fluorescence lifetime under physiological ionic strength conditions is rather moderate. Thus, the observations and interpretations made in this subsection have to be analyzed in further detail, leading to the application of a Hill model.

### 5.1.3 Analyzing the role of $\text{PiP}_2$ and ATP with the Hill model

Again, liposomes are prepared and measured as described above in subsection 5.1.2. Both liposome preparations, labeled either with Oregon green or Texas red, contain 15% PS. Titration experiments with varying  $\text{Ca}^{2+}$  concentrations are performed. The amount of tethered liposomes as well as the fluorescence lifetime of Oregon green are recorded. Again, in the absence of  $\text{PiP}_2$  and ATP the signal changes are rather minor. The exertion of Hill fits to the obtained titration curves depicted in figure 4.7 reveals a correlation of the dissociation constants for tethering and fluorescence lifetime in the presence of 1%  $\text{PiP}_2$  in the target membrane. Here, tethering increases synchronously to a decrease in fluorescence lifetime. This correlation is even maintained in the presence of further proteins such as synaptobrevin 2 as shown in figure 4.12.

In the absence of  $\text{PiP}_2$  no such correlation is determined, that means that a rise in the amount of tethered liposomes is not synchronously accompanied by a decrease in the recorded fluorescence lifetime. Although these findings are in line with previously published data [119, 58], in these earlier studies a direct connection between the amount of tethered liposomes and the actually measured FRET, as determined via FCCS, could have not been given. Thus, this consistent feature of  $\text{PiP}_2$  causing synchronous alterations in tethering and fluorescence lifetime furthermore points towards a substantial role of  $\text{PiP}_2$  in membrane distance regulation as depicted in figure 2.3 and described in [49]. Hence, evidence for the second priming and triggering model presented in figure 2.3 is identified. Here, synaptotagmin-1 binds to  $\text{PiP}_2$  in the presynaptic membrane. Upon  $\text{Ca}^{2+}$  influx the intermembrane distance is reduced, thus permitting for proper SNARE nucleation [49]. In the model this reduction is triggered by the presence of  $\text{Ca}^{2+}$ . Therefore, the experiments presented in this study show that tethering and membrane distance shortening do not only depend on the presence of calcium ions, but that they are furthermore controlled by the  $\text{Ca}^{2+}$  concentration (compare figure 4.7). These findings support priming modes 3-5 presented in subsection 2.2.2. However, with the FCCS experiments performed in this study it is not possible to rule out whether the lipid bilayer is destabilized at the fusion site [106, 64, 131], lipids are displaced due to curvature stress [72, 45] or simply a reduction of the intermembrane distance automatically leads to SNARE complex formation [2].

The argument of  $\text{PiP}_2$  being a prerequisite for intermembrane distance shortening is supported by several ways of analyzing the fluorescence lifetime decrease recorded in this study. The fluorescence lifetime of Oregon green incorporated into the target liposome containing either no or 1%  $\text{PiP}_2$  is analyzed by the  $f_{bound}$  (equation 4.3), a biexponential fit (equation 4.4), a burst analysis (figure 4.10) and a linear regression model (figure 4.9) as presented in section 4.1.3. Here, all four evaluation procedures lead to a reduced fluorescence lifetime of Oregon green in the presence of  $\text{PiP}_2$ . Thereby underlining the above characterized results of  $\text{PiP}_2$  being responsible for membrane distance shortening - as suggested elsewhere [58] - and contrariwise ATP preventing too close proximity of the two liposome membranes. This is in line with the findings reported above

in subsection 5.1.1. An increased electrostatic environment, as introduced by the addition of ATP, might hinder the electrostatic interaction of synaptotagmin-1, resulting in a greater membrane to membrane distance.

Besides the calculation of the  $f_{bound}$ , the biexponential fit and the burst analysis - which have already been described elsewhere [86, 24] - the possibility of applying a linear regression model has not been reported yet. In fact, determining precise amounts of tethered liposomes has been achieved only recently [121]. By plotting the actually measured fluorescence lifetime against the amount of tethered liposomes this study demonstrates that, in the presence of  $\text{PiP}_2$ , membrane distance shortening occurs proportionally to docking (compare figure 4.1.3). In the absence of  $\text{PiP}_2$  no linear regression could be applied to the data shown in figure 4.7. Synaptotagmin-1 possesses five  $\text{Ca}^{2+}$  binding sites binding calcium ions in a cooperative manner when synaptotagmin-1 is tethered to  $\text{PiP}_2$  [118]. Nonetheless, synaptotagmin-1 does not seem to act in a cooperative manner with regard to membrane distance shortening. The linear regression model applied in this study demonstrates a linear behaviour of fluorescence lifetime decrease depending on the amount of tethered liposomes with  $R^2$  values above 0.9. The slope of the resulting graph is a measure for the effectiveness of membrane distance shortening. Here, in case of ATP being present, the slope is always significantly shallower than that determined for the measurements performed in the absence of ATP. This may again be explained by an additional contribution of ATP to an increased electrostatic environment as discussed above in section 5.1.1.

In summary, all four evaluation methods demonstrate that indeed  $\text{PiP}_2$  is a fundamental prerequisite for distance regulation between liposome membranes. Moreover, ATP seems to prevent too short intermembrane distance. It still remains elusive though, whether ATP relieves synaptotagmin-1 to overcome *cis*-binding and promote fusion [83]. It has been shown as well that an additional protein density in the host liposome tremendously supports the fusiogenic effect ATP has on liposomes [83]. However, it is still unclear what the source of this observation is. Therefore, liposomes containing synaptotagmin-1 and synaptobrevin 2 are prepared. Titration experiments are performed analogously to those presented earlier in subsection 4.1.3.

The presence of synaptobrevin 2 shifts the dissociation constant for tethering to higher calcium concentrations as can be deduced by comparing figure 4.7 and figure 4.12. This indicates that an additional protein density in the host liposome does not prevent *cis*-binding per se. It rather demonstrates that more calcium ions are required to support *trans*-binding, but when the concentration of  $\text{Ca}^{2+}$  is in the higher  $\mu\text{M}$ -range the total amount of tethered liposomes is indeed greater. This observation can be explained by synaptobrevin 2 introducing steric hindrance for synaptotagmin-1 binding to an opposing lipid bilayer. Here, the presence of ATP as demonstrated in figure 4.12(C) and (D) does not tremendously affect the total amount of tethering that can be achieved. Again, synchronous alterations in tethering and fluorescence lifetime are reported in the presence of  $\text{PiP}_2$  as shown in figure 4.12(B) and (D). Moreover, the fluorescence lifetime is significantly reduced even in the absence of  $\text{PiP}_2$  in the target liposome. This shift is observed in the presence and the absence of ATP. Thus,

synaptobrevin 2 may indeed facilitate intermembrane distance shortening even in the absence of PiP<sub>2</sub>. However, this behaviour is not connected to the presence of ATP. This finding remains to be further characterized though. Microinjection experiments of a recombinant protein, corresponding to the cytoplasmic domain of synaptobrevin, have shown to produce a more rapid and reversible inhibition of synaptic vesicle exocytosis [46]. Here, the authors state that synaptobrevin participates in neurotransmitter release at a step between vesicle docking and fusion. Thus, identifying synaptobrevin 2 as one of the prime candidates to support synaptotagmin-1 based tethering especially in the context of ATP. However, no further influence of synaptobrevin2 on the tethering behaviour of synaptotagmin-1 is reported in this study.

In summary, the general tethering behaviour of synaptotagmin-1 as discussed in subsection 5.1.2 is not affected by the presence of ATP and synaptobrevin 2.

#### 5.1.4 The role of PiP<sub>2</sub> in distance regulation

The fact that synchronous alterations in tethering and fluorescence lifetime upon rising Ca<sup>2+</sup> concentrations as depicted in figure 4.7 are observed in the presence of PiP<sub>2</sub>, but not in its absence, provides evidence for the model of PiP<sub>2</sub> being essential for synaptotagmin-1 dependent distance regulation [119, 49]. The influence of the concentration of PiP<sub>2</sub> in the plasma membrane remains to be addressed though. It has been described elsewhere that Ca<sup>2+</sup> promotes PiP<sub>2</sub> clustering in lipid bilayers [95]. These clusters are thought to act as molecular beacons or liposome recruitment [44] and furthermore may provide a platform for a reduced liposome to membrane distance. This is then thought to support fast and efficient liposome exocytosis.

Therefore, liposomes including reconstituted synaptotagmin-1 are prepared as described above. Additionally, Oregon green labeled liposomes containing different amounts of PiP<sub>2</sub>, ranging from zero to 5%, are prepared as well. Again, all experiments are performed under physiological buffer conditions in the nM-range.

While binding in *trans* to an opposing target membrane including 1% PiP<sub>2</sub> requires a sufficient rise in the concentration of Ca<sup>2+</sup>, this strict calcium ion dependence is circumvented in case of higher PiP<sub>2</sub> concentrations of about 3% in the target membrane. Here, the base level of tethering is increased even in the absence of any calcium ions and thus, tethering becomes more independent from the present Ca<sup>2+</sup> concentration as can be deduced from figure 4.13. Nonetheless, in the presence of Ca<sup>2+</sup>, the amount of tethering is again increased even further. The normalized fluorescence lifetime change is not increased upon greater tethering. Moreover, in the absence of Ca<sup>2+</sup> the fluorescence lifetime is not altered significantly (figure 4.14) when compared to the total amount of tethering.

In summary, calcium generally increases tethering. The base level of tether-

ing is determined by the concentration of PiP<sub>2</sub>. Nonetheless Ca<sup>2+</sup> is a prerequisite for distance based FRET. Hence, the amount of PiP<sub>2</sub> significantly increases the amount of tethered liposomes, but does not bring the liposomes closer together. In fact, 1% PiP<sub>2</sub> is sufficient to assure membrane distance shortening upon an external triggering signal like Ca<sup>2+</sup>.

### 5.1.5 The role of the different functional domains of synaptotagmin-1

The putative functions of the three different domains of synaptotagmin-1 have been discussed extensively [16, 59, 129]. However, their distinct roles are still not entirely clear. Liposomes are prepared as described in subsection 4.1.3. The corresponding mutants of synaptotagmin-1 are reconstituted into the Texas red labeled liposome. 1% PiP<sub>2</sub> is present in the target liposomes. Again, titration curves with rising Ca<sup>2+</sup> concentrations are generated. The amount of tethered liposomes is calculated via FCCS. The recorded fluorescence lifetime of Oregon green reflects a measure for the membrane to membrane distance of host and target liposome. Again, a Hill equation is applied to the data points.

Comparing the resulting fits for the mutant data to the fits obtained for synaptotagmin-1 wt, the least modifications in tethering and fluorescence lifetime are observed, when mutating the poly-lysine patch (figure 4.16(A)). Here, the total decrease in fluorescence lifetime is less, although the total amount of tethered liposomes is increased compared to figure 4.7(B). This may be explained by the poly-lysine patch binding in *cis* to its own host membrane as reported in [123]. Upon mutating the patch *cis*-binding may be reduced and the competing *cis/trans* interactions of the poly-lysine patch are repealed. Thus, permitting for enhanced *trans*-binding via the C<sub>2</sub>B domain as discussed below. Hence, although PiP<sub>2</sub> binding of the fully functional poly-lysine patch is favoured over PS binding [118], the presence of PS in the host liposome may still reduce the tethering efficiency [6, 67]. Upon binding in *trans* the mutated poly-lysine patch may then no longer be capable of dipping into to the target membrane [6]. Thus minimizing the liposome distance to an extent as reported for the wild type protein (figure 4.7(B)) can not be achieved. Although PiP<sub>2</sub> binding in *trans* is thought to be mainly accomplished by the poly-lysine patch [6], *trans*-binding can be sufficiently achieved by the remaining two C<sub>2</sub> domains.

The dissociation constants obtained for tethering and fluorescence lifetime alterations in the titration experiments performed with the KAKA mutant still shift simultaneously as can be deduced from figure 4.16(A). This means that a rise in tethering is accompanied by a synchronous decrease in the recorded fluorescence lifetime. Here, the determined dissociation constants are equal within the error range. Thus, demonstrating that the poly-lysine patch is not directly responsible for the actual regulation of the membrane to membrane distance. Compared to the dissociation constants obtained for the titration experiments including synaptotagmin-1 wt (figure 4.7(B)) here, the dissociation constants are shifted to higher Ca<sup>2+</sup> concentrations. This indicates a less effective bind-

ing of synaptotagmin-1 to  $\text{PiP}_2$ , which has been suggested to be supported by the poly-lysine patch [119, 6]. In fact, the higher dissociation constants show that the poly-lysine patch increases the sensitivity of synaptotagmin-1 towards binding in *trans* to  $\text{PiP}_2$  upon rising calcium concentrations. This finding is furthermore in line with previous NMR studies demonstrating that mutating the poly-lysine patch does not cause any substantial structural changes, but decreases the neurotransmitter release probability [66].

Up to today a multitude of *in vitro* [131, 99] and *in vivo* [26, 68, 70, 80] studies have been performed demonstrating that mutating the  $\text{C}_2\text{B}$  domain is more severe for the functionality of synaptotagmin-1 than mutating the  $\text{C}_2\text{A}$  domain. Nonetheless, it still remains elusive why this is the case. The titration curves presented in figure 4.16 provide the first direct evidence for the  $\text{C}_2\text{B}$  domain being the only one that can bind in *trans* upon increasing  $\text{Ca}^{2+}$  concentrations. Here, reconstituted synaptotagmin-1 mutants carrying either a mutation in one of the  $\text{C}_2$  domains or in both of them have been used to study tethering and liposomal distance regulation. While *trans*-binding is still maintained when mutating the  $\text{C}_2\text{A}$  domain, an increase in tethering as a consequence of rising calcium concentrations is completely abolished when mutating the  $\text{C}_2\text{B}$  domain. Consequently, also the fluorescence lifetime is not altered upon rising  $\text{Ca}^{2+}$  concentrations. Contrariwise, it has been demonstrated earlier [121] that a functional  $\text{C}_2\text{A}$  domain is enough to achieve *trans*-binding. These experiments were performed with no anionic lipids present in the host membrane. Thus, the  $\text{C}_2\text{A}$  domain can not bind in *cis*. Furthermore, this study shows that both  $\text{C}_2$  domains bind to anionic lipids like PS [121]. Taken together, these findings show that although the  $\text{C}_2\text{A}$  domain is also capable of binding in *trans*, it may preferentially bind in *cis*. This is supported by the finding that the dissociation constant of tethering determined for the  $\text{C}_2\text{aB}$  mutant only experiences a minor shift when compared to the corresponding measurement with synaptotagmin-1 wt 4.7.

Hence, *cis*-binding may be favoured over *trans*-binding in case of the  $\text{C}_2\text{A}$  domain. Whereas, the  $\text{C}_2\text{B}$  domain preferentially binds in *trans*, thus supporting the idea of a split-binding mechanism as proposed earlier [106]. Here, a soluble fragments of the cytoplasmic domain of synaptotagmin-1, as well as reconstituted full length protein were used. The authors hypothesize that an interaction of the  $\text{C}_2\text{B}$  domain in *trans* by binding to a partially assembled SNARE complex may account for their results. In fact, the  $\text{C}_2\text{A}$  domain is thought to bind in *cis* to its own host membrane. This finding is partly based on the fact, that the soluble  $\text{C}_2\text{AB}$  domain accelerates liposome fusion in the presence of  $\text{Ca}^{2+}$  [106]. Moreover, the  $\text{C}_2\text{B}$  domain alone was dispensable, whereas the  $\text{C}_2\text{A}$  domain was absolutely required for fusion [106] mediated by the cytoplasmic domain of synaptotagmin-1. This may be explained by the poly-lysine patch binding to one and the  $\text{C}_2\text{A}$  domain binding to the other liposome. Whereas, upon mutating the  $\text{C}_2\text{A}$  domain, the remaining two functional domains are located in too close proximity in order to bridge opposing membranes.

Interestingly, upon introducing point mutations into both  $\text{C}_2$  domains, tethering is already increased, while the fluorescence lifetime is reduced accordingly even in the absence of any calcium ions (compare figure 4.16(D)). Again, no

further changes upon rising  $\text{Ca}^{2+}$  concentrations are recorded when both domains are mutated as can be deduced from 4.16(D). Since the poly-lysine patch is the only functional domain left, *trans*-binding even in the absence of calcium ions demonstrates the increased affinity of the poly-lysine patch to  $\text{PiP}_2$  over binding to PS [6]. Moreover, since with the mutated  $\text{C}_2\text{A}$  domain no significant tethering is observed in the absence of  $\text{Ca}^{2+}$ , this demonstrates that both  $\text{C}_2$  domains may bind in *cis* even in the absence of any calcium ions. This has only been suggested for the  $\text{C}_2\text{A}$  domain [7] so far. In fact, this  $\text{Ca}^{2+}$  independent back-binding may prevent the liposome from tethering to the target membrane in the absence of calcium ions, providing a potential negative control mechanism to maintain proper  $\text{Ca}^{2+}$  response. Moreover unpublished data of collaborators (Dr. Angel Perez-Lara)[51] indicate a tendency of the double mutant for aggregation. Thus, further control experiments including soluble fractions of the  $\text{C}_2\text{AB}$  domain and its mutants are required.

### 5.1.6 Circumvention of synaptotagmin-1 based distance regulation

All results provided and discussed so far, strengthen the idea that synaptotagmin-1 indeed acts as a distance regulator upstream of SNARE nucleation. This distance regulation mechanism is dependent on the presence of calcium ions and  $\text{PiP}_2$  in the target membrane. On the contrary, subsection 4.1.6 demonstrates that syntaxin 1A is capable to inhibit synaptotagmin-1 dependent distance regulation. Here, Texas red and Oregon green labeled liposomes containing 15% PS are prepared as described above. Additionally, 3%  $\text{PiP}_2$  and reconstituted syntaxin 1A are present in the target liposome thus, referring to earlier findings [44] which demonstrate that  $\text{PiP}_2$  clusters colocalize with syntaxin 1A in the presynaptic membrane. Again, with 3%  $\text{PiP}_2$  in the target membrane tethering is already about 30% in the absence of calcium ions as shown in figure 4.15. The addition of  $\text{Ca}^{2+}$  increases the amount of tethered liposomes even further. This observation is consistent in the presence as well as in the absence of syntaxin 1A in the target membrane. Hence, this implies that there is no additional synaptotagmin-1/syntaxin 1A interaction present that might either hinder or facilitate tethering. Although tethering of synaptotagmin-1 is not affected by the presence of syntaxin 1A, a different picture can be drawn from the recorded fluorescence lifetime. The present study shows that, in the presence of syntaxin 1A the requirement for calcium ions for shortening the intermembrane distance diminishes as can be deduced from figure 4.15. Here, the same decrease in the fluorescence lifetime is recorded in the presence or the absence of any  $\text{Ca}^{2+}$ .

Previous findings demonstrate that synaptotagmin-1 interacts with the polybasic linker region of syntaxin-1A independent of  $\text{Ca}^{2+}$  through  $\text{PiP}_2$  [44]. Thus, syntaxin 1A may not alter the amount of tethered liposomes, but it shortens the intermembrane distance through an interaction with synaptotagmin-1 via its polybasic linker region. Consequently, the question arises what the biological function of synaptotagmin-1 based distance regulation may be, when there are obviously mechanisms that easily circumvent this regulation. The functional

role of this striking antagonism may be explained by the existence of different pools of synaptic vesicles. Recent studies point towards a ready releasable pool that fast and efficiently releases its cargo into the synaptic cleft [93]. Moreover, the existence of a reserve pool of synaptic vesicles that fuse upon greater  $\text{Ca}^{2+}$  influx is predicted [25]. Nonetheless, the capability of synaptotagmin-1 to circumvent distance regulation upon binding to syntaxin 1A is hard to reconcile with earlier findings demonstrating that the interaction between synaptotagmin-1 and syntaxin is regulated by  $\text{Ca}^{2+}$  [9, 18]. Here the authors state that the calcium ion dependence of this interaction is composed of two components with  $\text{EC}_{50}$  values of 0.7 and 180  $\mu\text{M}$ .  $\text{Ca}^{2+}$ .

Although, the findings obtained in this work are in good agreement with the priming and triggering model II introduced by Jahn and Fasshauer [49] and presented in subsection 2.2.2, the original model may not represent the whole spectrum of regulating vesicle exocytosis. One explanation is indeed given by the existence of distinct vesicle pools, possessing different mechanistic features of regulating vesicle exocytosis.

### 5.1.7 Distance regulation in the recycling and/or reserve pool

The hypothesis that different synaptic vesicle pools exist and thus synaptic vesicles are not all functionally equivalent has been raised already decades ago [12] on the basis of the observation that some vesicles are more easily released than others [12]. Over the past years this model has become more and more important. So far, three major synaptic vesicle pools have been suggested.

1. A ready releasable pool, which permits for fast and efficient exocytosis.
2. A recycling pool, consisting of vesicles that recycle upon moderate stimulation and thus contribute to exocytosis.
3. A reserve pool, which hosts vesicles that are only released upon high-frequency stimulation.

However, a detailed picture of the functionality of these pools is still missing. Variations of the models including spatial separation within the synapse as well as recruitment mechanisms to an active zone of exocytosis have been discussed extensively [25]. Nonetheless, it is widely accepted that the ready releasable pool consists of synaptic vesicles docked to the active zone and primed for exocytosis [25, 44, 93], whereas the vesicles in the other two pools require much higher stimulus in order to be released into the synaptic cleft [25]. The present study supports the idea of the existence of different synaptic vesicle pools.

First, the ready releasable pool of synaptic vesicles is bound to an active zone, which is already discussed to be represented by  $\text{PiP}_2$  clusters [44]. Here, 3%  $\text{PiP}_2$  in the target membrane indeed cause significant liposome tethering of about 30% even in the absence of any calcium ions.

Second, the intermembrane distance is already reduced in these  $\text{PiP}_2$  clusters due to an interaction between synaptotagmin-1 and syntaxin 1A. Here, the synaptic vesicle is already docked in close proximity to the plasma membrane. Probably other proteins like Munc18 or complexin prevent the liposome from fusion [57, 134, 47]. Upon the arrival of an action potential these proteins are released from the pre-docked fusion machinery, thus leading to very fast exocytosis.

Third, the other two pools require a significant larger amount of calcium ions for triggering exocytosis. These pools may as well contain synaptic vesicles that bind to  $\text{PiP}_2$  via synaptotagmin-1 upon stimulus. Here, the concentration of  $\text{PiP}_2$  in the presynaptic membrane is rather dilute (about 1%), which supports the idea of spatial separation of the different pools. The spatial separation may thus be a result of local differences in the  $\text{PiP}_2$  concentration in the presynaptic membrane. With a  $\text{PiP}_2$  concentration about 1% no syntaxin 1A is recruited as demonstrated in [44]. As can be deduced from figure 4.7(B) and 4.12(B)  $\text{Ca}^{2+}$  concentrations in the  $\mu\text{M}$ -range are required to sufficiently shorten the intermembrane distance, which in turn may then permit for proper SNARE nucleation. Hence, the second priming and triggering model presented in figure 2.3 (right hand side) may be the case for either the recycling or the reserve pool, with the exception that in the present study no synaptotagmin-1 tethering to 1%  $\text{PiP}_2$  in the absence of calcium ions has been observed. However, this finding is in line with studies indicating that the synaptic vesicles of the recycling pool are mobile within the synapse [25]. In fact, the model introduced by Jahn and Fasshauer [49] suggests that synaptotagmin-1 binds to either  $\text{PiP}_2$  clusters being colocalized with syntaxin 1A or directly to the SNAREs. This assumption is hard to reconcile with the finding that syntaxin 1A inhibits synaptotagmin-1 based distance regulation though. Whereas, an additional contribution of e.g. Munc18 or other proteins contributing to the distance regulation mechanism can not be excluded.

Taken together, all the above described findings depict a mechanism of synaptotagmin-1 based distance regulation that may hold for a certain fraction of synaptic vesicles. Exocytosis may in fact be regulated in different manners depending on the pool they belong to. Here, even proteins like Munc18 or complexin may exhibit a hidden function [49]. For example, Munc18 is known to lock syntaxin 1A in a closed conformation, in which it can not enter SNARE complexes [49, 30, 77]. Therefore it may prevent synaptic vesicles from fusion, although they are already in close proximity to the presynaptic membrane due to the synaptotagmin-1/syntaxin 1A interaction. Even up to today the function of some proteins involved in exocytotic processes still remains unclear [49]. Hence, these proteins potentially could also enhance or hinder synaptotagmin-1 based shortening of the liposome to membrane distance.

### 5.1.8 Summary of findings

In the previous sections the following conclusions have been drawn from the experiments in this study, thus helping to get new insights in Synaptotagmin-1 dependent vesicle priming and triggering processes:

1. Synaptotagmin-1 can act as a distance regulator when bound to  $\text{PiP}_2$  by synchronous alterations in tethering and membrane distance shortening.
2. Despite the cooperative behaviour of synaptotagmin-1 in the presence of  $\text{PiP}_2$ , a reduction of the intermembrane distance occurs proportional to tethering.
3. Calcium ions are required for tethering and trigger  $\text{PiP}_2$  dependent distance regulation.
4. High  $\text{PiP}_2$  concentrations increase the base level of tethering, though.
5. Circumvention of distance regulation by syntaxin 1A may reflect the situation in the ready releasable pool.
6. The distance regulation function of synaptotagmin-1 may thus be relevant for the recycling and/or reserve pool.
7. The  $\text{C}_2\text{B}$  domain of synaptotagmin-1 mediates *trans*-binding, whereas the  $\text{C}_2\text{A}$  domain accomplishes *cis*-binding.

## 5.2 Optical trapping

So far, different techniques have been used to study tethering and fusion to membranes. Nonetheless, any of these techniques has its advantages and drawbacks. Planar lipid bilayers as e.g. black lipid membranes exhibit an altered surface tension. Here, the lipid bilayer is fixed between two teflon partitions, creating a solvent annulus at either end [79]. Others used liposomes immobilized to a pacified PEG-coated surface in order to imitate the plasma membrane [60]. Here, it can not be excluded that injected, freely diffusing liposomes do not interact with the PEG surface, or that the shape of the liposomes may be modified. FCCS experiments with freely diffusing liposomes avoid such deficits [24, 121]. The surface tension of the liposomal membrane is not affected at all. A disadvantage of this approach is though that the individually diffusing particles, either bound to one another or not, can not be investigated for longer than several ms. Such short time scales obviously do not permit to study elementary processes in real-time. Depending on the system under investigation the drawbacks of the different approaches can lead to conflicting observations. Thus, an optically trapped liposome provides a possibility to circumvent these drawbacks. Here, the advantages of both approaches can be combined. The liposomes are still free in solution without any attachment to a coated surface that may introduce artificial surface tension. Furthermore, processes such fusion can be observed in real-time over a larger period of time. It has been reported earlier that with laser light in the NIR (1064 nm) at high power (850 mW) large unilamellar vesicles ( $d=130$  nm) with 1 M sucrose inside can be trapped. Nonetheless, this study exclusively focussed on the force that keeps such a liposome in focus and on its motion in x,y-direction [8]. It does not address potential methodical applications arising from the trappability of these liposomes. The present study shows that indeed trapping of large unilamellar vesicles ( $d=110$  nm) is also possible at a wavelength of 800 nm in case of bearing 2 M sucrose inside. Furthermore, the combination of two lasers operating at 800 nm provides new prospects in terms of studying membrane interactions, because one can super-impose the trapping center with the focal volume created under TPE conditions.

### 5.2.1 Optical trapping conditions

Trapping at this rather low wavelength of 800 nm comprises a striking advantage: An 800 nm CW beam can be combined with an 800 nm TPE beam. Although an achromatic objective is used in this study, refraction can still vary among different wavelength. With this setup it is now possible to not only excite green and red fluorescence dyes within exactly the same focal volume, but furthermore the position of the trapping area is super-imposed on the excitation volume.

In fact, the trapping beam and the TPE beam may still be shifted by one another of a few nm. This is because super-position in x,y-direction is achieved with the help of a wide-field camera with a limited resolution. The pixel length of

the monitor reflects a distance of about 108 nm. Moreover, z-scan is performed in 1  $\mu\text{m}$  steps as can be deduced from figure 4.18. A smaller step size could indeed reveal a shift also in z-direction, although both lasers operate at the same wavelength. Since with 800 nm CW light Oregon green is not excited noteworthy, the trapping laser light does not evoke the requirement of an additional pinhole. Oregon green excitation still occurs within a defined focal volume as typical for TPE.

Nonetheless, super-position permits to selectively trap LUVs and observe processes like docking and fusion of a second, distinctly labeled liposome species to the trapped LUV in real-time. This provides access to kinetic parameters on a molecular level without the typical drawbacks of surface tension of supported membranes or immobilized liposomes.

A challenge raised by measuring under optical trapping conditions is to avoid photobleaching of the species under investigation [8]. Depending on the dye used photobleaching due to the enhanced irradiation density of the CW laser beam may indeed considerably reduce the actual fluorescence lifetime of the dye. The present study illustrates that the fluorescence lifetime of Oregon green is not affected by photobleaching as can be deduced from figure 4.22. Here, Oregon green labeled SUVs are prepared with or without additional Texas red or not. Both samples are measured under TPE or under TPE & CW conditions. In both cases the fluorescence lifetime does not alter upon additional CW excitation. SUVs can still traverse the focal volume within the lower ms-range. It should be noted that slower diffusing particles may indeed encounter photobleaching. In fact, Texas red being incorporated into the trapped LUV displays quite tremendous photobleaching (compare figure 4.20), underlining the requirement for more photostable dyes like quantum dots. Quantum dots possess a high extinction coefficient combined with a quantum yield comparable to common organic fluorescence dyes [75], which yields to a brightness roughly 20 times and a photostability being 100 times larger than conventional fluorescence dyes [127]. Nonetheless, they fail to be used under the above described conditions, because of their actual size which varies from 2 - 10 nm. Labeling the LUV membrane with these rather large particles, compared to common organic dyes, would of course result in a hampered access to the plasma membrane substitute. A way to circumvent this inherent drawback could be the incorporation of quantum dots inside the LUV, rather than connecting them to the phospholipid head group as in Texas red PE. However, this creates the challenge of quantum dots exclusively being located inside the LUV, which is an issue of preparation that remains to be solved.

A benefit of encapsulating sucrose is that the liposome is preserved due to very low membrane permeability [8]. Furthermore with sucrose inside no deformation of the liposome itself is expected [8]. Here, 2 M sucrose filled LUVs are in the majority of cases trapped for about 2 min. In order to extend the trapping period one could test other buffer additives than sucrose which might increase the refractive index mismatch. Sucrose concentrations higher than 2 M are thus not feasible. Although the solubility product of sucrose, which is  $1970 \text{ gL}^{-1}$  at 293 K [38], theoretically permits for an almost 3 times higher sucrose concentration, the preparation of the LUVs, as described in chapter 3, causes

limitations. Therein especially the onset of organic solvents and the employment of a rotary evaporator cause the sucrose to precipitate at concentrations higher than 2 M.

Another way to extend the trapping period consists of the preparation of larger LUVs, e.g. with a diameter of 400 nm instead of 110 nm. Nonetheless, sucrose encapsulation efficiency has been demonstrated to decrease with liposome size [69]. As can be deduced from table 4.10,  $r_{0,xy}$  is in the range of 450 nm whereas  $z_0$  is about 4  $\mu\text{m}$ , thus allowing for larger objects to be trapped.

Nonetheless, trapping particles for about 2 min constitutes a tremendous benefit in terms of studying protein to membrane interactions.

## 5.2.2 Applications of optical trapping

For analyzing a potential application of optical trapping in terms of tethering, Texas red labeled LUVs containing 2 M sucrose are incubated in a 1:10 ratio with Oregon green labeled SUVs containing reconstituted synaptotagmin-1. The liposome mixture is measured under optical trapping conditions including different amounts of calcium ions. The measurement containing the PS-less LUV demonstrates that without any anionic lipids present in the LUV membrane, the diffusion time of the Oregon green labeled SUVs is not altered significantly. When there are 15% PS present in the LUV membrane, the recorded diffusion time is indeed increased (figure 4.23). Thus, pointing towards a prolonged retention time of the synaptotagmin-1 carrying SUVs in the focal volume.

The present study demonstrates that adsorption isotherms such as Langmuir may be applied in order to describe reduced or prolonged retention times of molecules being docked or not to a plasma membrane substitute, especially because the analysis of the diffusion time according to Langmuir as presented in figure 4.24, reveals a straight line. Referring to the experiments presented in subsection 4.2.5, more data points would be a benefit in order to further analyze the tethering behaviour on the basis of adsorption. Thus, making it a very time consuming study. Therefore, the obtained values for the constant  $K$  should not be over-interpreted, although they reveal a sophisticated consistency. Nevertheless, the application of adsorption isotherms also exhibits some critical aspects. For example, adsorption isotherms disregard the biological functionality of the protein reconstituted into the SUV. In case of synaptotagmin-1, the protein can also bind in *cis* to its own host membrane [121], or to other anionic lipids embedded into a second SUV hence, leading to a competing binding mode. In fact, the underlying tethering and de-tethering processes may be even more complicated depending on the biological system under investigation. Moreover, a thorough analysis of tethering under optical trapping conditions requires pronounced control experiments, as well as a more theoretical analysis of the underlying physics and biological nature of the samples used. Although the basic concept of tethering to an immobilized surface resembles an adsorption process, the classical adsorption isotherms apparently do not provide a precise

description. This underlines the requirement for an elaborate analysis of the molecular processes determining the tethering behaviour in this context. As a matter of course, this is beyond the scope of this work. However, the application of the Langmuir adsorption concept is rather convenient for this study in order to demonstrate that a modified model of the classical adsorption isotherms may indeed reflect the ongoing processes.

Distance regulation measurements fail to be applicable in the context of optical trapping. With the method described above in chapter 3 and section 4.1 the obtained fluorescence lifetimes exhibit a larger error. Since the expected decrease in fluorescence lifetime is anyway rather low, when compared to e.g. fusion studies, the FRET already lies within the error. Furthermore reduced photostability under optical trapping conditions may impede reliable assignment of a potential FRET effect. Taken together these drawbacks prohibit the application of optical trapping in terms of intermembrane distance analysis.

In order to study fusion events under optical trapping conditions two distinct approaches of sample handling are possible. In the first approach, also referred to as "Fusion experiment I", the 15% PS containing LUV sample and the SUVs are both separately incubated at 100  $\mu\text{M}$   $\text{Ca}^{2+}$  ion concentration. Upon recording a trapping event SUV influx to the LUV sample is started. In "Fusion experiment II", the 15% PS containing LUV sample is pre-incubated with SUVs. Calcium ion influx is then thought to trigger vesicle fusion. In both cases the  $\Delta\text{N}$ -complex is reconstituted into the LUV, whereas the SUV contains reconstituted synaptotagmin-1 and synaptobrevin 2.

Fusion can be monitored under "Fusion experiment I" conditions, since here the observed FRET is more prominent than that for distance regulation. Again, the fluorescence lifetime decay presented in figure 4.32 may as well comprise additional photobleaching of Oregon green beyond the actual FRET based on fusion. This is, because under "Fusion experiment I" conditions, the whole fusion process takes several minutes to be completed. As previously mentioned photobleaching has to be taken into account in case of retention times significantly above the ms-range. Hence, underlining the demand for more photostable dyes in the dimensions of traditional, organic fluorescent ones. Nonetheless, equation 4.6 provides a sophisticated fit model to the obtained data. This indicates that indeed fusion is detected. Upon "Fusion experiment II" conditions no such fluorescence lifetime decrease is observed.

Moreover, the performed fusion experiments explicitly provide evidence for fusion model I and thus rebut fusion model II. The present study demonstrates that pre-incubation of SUVs containing reconstituted synaptotagmin-1 does not prevent fusion in the absence of calcium ions. While upon  $\text{Ca}^{2+}$  influx to the pre-incubation mixture no significant Oregon green signal is detected within the focal volume, a plain fluorescence lifetime decrease is detected upon SUV influx. This leads to the interpretation that synaptotagmin-1 does indeed trigger fast and efficient fusion by binding to  $\text{Ca}^{2+}$ , but the protein itself does not prevent fusion per se in the absence of calcium ions as stated elsewhere [19], especially because  $\text{Ca}^{2+}$  triggered fusion is completed after one or two seconds. In case of pre-incubation for 20 to 30 min as described in [60], all liposomes have already

been fused. This idea is furthermore supported by earlier findings demonstrating that synaptotagmin accelerates  $\text{Ca}^{2+}$  independent fusion [106], thus underlining the multitude of conflicting observations that have been reported concerning the role of synaptotagmin-1 in exocytosis.

A major drawback of the application of optically trapped LUVs in fusion processes is, of course, the coincidence and the instability of the trapping event. First, optical trapping is a process which occurs accidentally, thus making a high throughput study very time consuming. Second, photobleaching can not be neglected for the reasons described above. Third, external influx of triggering factors like  $\text{Ca}^{2+}$  may de-trap the LUV. Fourth, to make sure that the LUV is not de-trapped due to an external influx, the outlet of the pump has to be put further away from the focal volume. Thus, the time it takes for the triggering molecules to diffuse into the focal volume may already exceed the trapping period. In fact, although a FRET is reported in about 80% of all "Fusion I experiments", the actual time the LUV is trapped as shown in figure 4.32 and 4.34 is remarkably high. Rather an aggregate of LUVs seems to be trapped here, which nonetheless provides a substitute for the plasma membrane. This, again demonstrates the demand for longer and stronger trapped liposomes. Fifth, it is also not possible to wash away excess amounts of untethered liposomes prior to trigger signal influx, which may be a prerequisite for other studies.

In summary, for the above mentioned reasons, the employment of fusion in the context of optical trapping generally works, although it does not represent the method of choice.

### 5.2.3 Summary of findings

In the previous sections the following conclusions have been drawn from the experiments in this study:

1. Optical trapping of sucrose filled large unilamellar vesicles is possible.
2. The combination of a CW and a TPE laser beam, both operating at 800 nm, permits for super-position of the trapping center with the TPE-volume. Hence, trapping and FCS can be combined.
3. Optical trapping of large unilamellar vesicles can be used to study retention times of liposomal tethering.
4. Intermembrane distance measurements are not possible.
5. Studying fusion of small unilamellar vesicles to optically trapped large unilamellar vesicles is in general possible.

## Chapter 6

# Outlook

The present study shows that synaptotagmin-1 may indeed act as a distance regulator upstream of SNARE nucleation [119]. A multitude of parameters influencing this intermembrane shortening attribute are characterized and discussed above. Since syntaxin-1 seems to inhibit the distance regulation function of synaptotagmin-1, it would be interesting to perform the above listed FCCS experiments with a non-fusiogenic SNARE (syb2  $\Delta$ 84, SNAP25A, sx1A) complex reconstituted into the target membrane. Here, the fusion reaction is quantitatively arrested at a tightly docked state [43]. This would be of particular interest since up to today it still remains elusive how assembly of the SNARE complex generates docking and other fusion intermediates [43].

Another prospect for following studies would be to test the influence of soluble proteins like Muncs and complexin on distance regulation. Earlier findings [30] indicate that syntaxin binds to Munc18 in a closed conformation, thereby suggesting that this conformation represents an essential intermediate in exocytosis. Furthermore, the authors of this study raise a model whereby, during exocytosis, syntaxin undergoes a large conformational switch that mediates the transition between the syntaxin-Munc18 complex and the core complex [30]. It would thus be interesting to investigate a potential inhibitory effect of Munc18 on syntaxin 1A induced distance regulation circumvention. These measurements could potentially answer questions arising from the conflicting findings reported elsewhere [105, 128, 130, 14, 27, 117]. This may then shed light on the role of  $\text{Ca}^{2+}$  in exocytosis as reported above in subsection 2.2.2.

In the context of optical trapping the application of tethering or adsorption studies can be supported with the constraints mentioned beforehand. Given the fact that future studies may provide a more elaborate theoretical concept, a multitude of applications emerges. In the context of this study, one could think of an investigation of different synaptotagmin-1 isoforms binding to a membrane that either includes  $\text{PiP}_2$  or not, especially because there are already 17 different isoforms of synaptotagmin known in humans [114]. Although synaptotagmin-1 and synaptotagmin-2 have been under extensive investigation much less is

known about the other synaptotagmins. Many of them are abundantly co-expressed with synaptotagmin-1 and synaptotagmin-2 in brain and are evolutionarily conserved [104]. Moreover, different synaptotagmin isoforms exhibit distinct calcium ion affinities, suggesting that plasma membrane and vesicular synaptotagmins may function as complementary  $\text{Ca}^{2+}$  sensors in exocytosis with a hierarchy of  $\text{Ca}^{2+}$  affinities [16, 107, 108].

Furthermore, referring to the considerations concerning the electrostatic nature of synaptotagmin-1 tethering, that have been made in subsection 5.1.1, an investigation of the corresponding differences between distinct synaptotagmin-1 isoforms may be investigated. It has been shown earlier, that dissociation from membranes of synaptotagmin-7, but not synaptotagmin-1, is slowed by  $\text{Na}_2\text{SO}_4$  and trehalose [13]. These components enhance the hydrophobic nature of the proteins. Thus, varying buffer conditions in the context of optical trapping could potentially reveal hidden mechanistic functions.

Here, research is of course not limited in terms of protein to membrane interaction. One could also think of studies of pharmacological relevance. Here, e.g. docking of fluorescently labeled drugs to G-protein coupled membrane receptors may depict an interesting aspect for further research studies.

# Chapter 7

## Appendix

### 7.1 Error analysis

#### 7.1.1 Fraction bound $f_{bound}$

$$\Delta\tau_{bound} = \left| \frac{\partial\tau_{bound}}{\partial\tau_{measured}} \right| \Delta\tau_{measured} + \left| \frac{\partial\tau_{bound}}{\partial f_{bound}} \right| \Delta f_{bound} + \left| \frac{\partial\tau_{bound}}{\partial f_{unbound}} \right| \Delta f_{unbound} =$$

$$\Delta\tau_{bound} = \frac{1}{f_{bound}} \Delta\tau_{measured} + \frac{\tau_{measured} - f_{unbound} \cdot \tau_{unbound}}{f_{bound}^2} \Delta f_{bound} + \frac{\tau_{unbound}}{f_{bound}} \Delta f_{unbound}$$

#### 7.1.2 Linear regression

$$\Delta\tau_{bound} = \left| \frac{\partial\tau_{bound}}{\partial slope} \right| \Delta slope + \left| \frac{\partial\tau_{bound}}{\partial intercept} \right| \Delta intercept =$$

$$\Delta\tau_{bound} = x \cdot \Delta slope + \Delta intercept$$

#### 7.1.3 Normalized fluorescence lifetime changes

$$\Delta NFLC = \left| \frac{\partial NFLC}{\partial \Delta Lifetime} \right| \Delta \Delta Lifetime + \left| \frac{\partial NFLC}{\partial \Delta Tethering} \right| \Delta \Delta Tethering =$$

$$\Delta NFLC = \frac{1}{\Delta Tethering} \Delta \Delta Lifetime + \frac{-1}{\Delta Tethering^2} \Delta \Delta Tethering$$

### 7.1.4 Characterization of the setup

$$\Delta r_{xy} = \left| \frac{\partial r_{xy}}{\partial \tau_{Diff}} \right| \Delta \tau_{Diff} + \left| \frac{\partial r_{xy}}{\partial D} \right| \Delta D =$$

$$\Delta r_{xy} = \frac{8D}{2 \cdot \sqrt{8D\tau_{Diff}}} \Delta \tau_{Diff} + \frac{8\tau_{Diff}}{2 \cdot \sqrt{8D\tau_{Diff}}} \Delta D$$

### 7.1.5 Langmuir coefficient

$$\Delta K = \left| \frac{\partial K}{\partial \tau_{max}} \right| \Delta \tau_{max} + \left| \frac{\partial K}{\partial \left( \frac{1}{\tau_{max}K} \right)} \right| \Delta \left( \frac{1}{\tau_{max}K} \right) =$$

$$\Delta K = (\tau_{max}K) \Delta \tau_{max} + \frac{1}{(\tau_{max}K)^{-2}} \Delta \left( \frac{1}{\tau_{max}K} \right)$$

### 7.1.6 Diffusion coefficient

$$\Delta D = \left| \frac{\partial D}{\partial r_{xy}} \right| \Delta r_{xy} + \left| \frac{\partial D}{\partial \tau_{Diff}} \right| \Delta \tau_{Diff} =$$

$$\Delta D = \frac{2 \cdot r_{xy}}{4 \cdot \tau_{Diff}} \Delta r_{xy} + \frac{r_{xy}^2}{\tau_{Diff}^2} \Delta \tau_{Diff}$$

## 7.2 Matlab codes

### 7.2.1 MatLab codes for displaying time trace

```

%[trace,base]=spcTrace(file,base)
%-----
%
%Extract the intensity trace from an SPC file.
%
% file   File name
% base   Bin time [s]      {10us}
%
% trace  Intensity trace
%
function [tra,base]=spcTrace64(file,base)
if nargin < 2 || isempty(base)
    base=10e-6;
end
%trace=uint8(0); <- Das auskommentieren

tra=[];

[c,t,f,s]=readSPCpart(file);
while ~isempty(t)
    t=t(c == 1);
    clear('c');

    if ~isempty(t)
        t=ceil(1 + s/base*t);
        if isempty(tra)
            tra = zeros(t(end),1);
        elseif t(end) > numel(tra)
            tra(t(end))=0;
        end

        %inc(trace,t); <- Das auch weg
        tra=tra + accumarray(t, 1, []);

    end
    clear('t');
    if isempty(f)
        break;
    else
        [c,t,f]=readSPCpart(f);
    end
end
end

```

Figure 7.1: Time trace analysis.

## 7.2.2 MatLab codes for FCS

Matlab algorithm is kindly provided by M. Leutenegger and programmed based on [125].

## 7.2.3 MatLab codes for fluorescence lifetime analysis

```
function [ ctime, counts ] = readSPCrageHist( file, range, chan, shift)
%readSPCrageHist Reads a certain time range of Becker & Hickl DPC-230 SPC
%FIFO files.
%
% file      File name
% range     Time range to load from SPC trace
%
% type      Event channel/type
% time      Event time [tick]
% step      Tick interval [s]

if nargin < 2
    error('Need more input parameter.');
```

```
end

[type,time,f,step]=readSPCpart(file);
%syncT=0;
first = 1;
syncT=syncPeriod(time(type==12));
range = range ./ step;

while ~isempty(time) && time(end) < range(1)

    if isempty(f)
        break;
    else
        [type,time,f]=readSPCpart(f);
    end
end

if isempty(time)
    error('End of file reached befor specified time point.');
```

```
end

type(time<range(1)) = [];
time(time<range(1)) = [];
t=0;
zeroIt = 1;
while ~isempty(time) && t(end) < range(2)
    if isempty(f)
        break;
    else
        [c,t,f]=readSPCpart(f);
        if zeroIt
            type = [type ; c];
            time = [time ; t];
            zeroIt = 0;
        end
        type(time>range(2)) = [];
        time(time>range(2)) = [];

        tc = time(type==chan);
        sync = time(type==12);

        if first == 1
            %syncT=syncPeriod(sync(1:min(end,1e6)));
            first = 0;
            ctime = [0:2:syncT]'.*step;
            counts = zeros(numel(ctime),1);
        end
        if ~isempty(tc) && ~isempty(sync)
            [~,dt]=histc(tc,[0;sync;inf]);
            dt=min(dt,numel(sync));
            dt=mod(shift+tc-sync(dt),syncT);
            counts = counts + histc(dt,[0:2:syncT]);
        end
    end
end

if isempty(t)
    error('End of file reached befor specified time point.');
```

```
end
```

Figure 7.2: Fluorescence lifetime histogram analysis.

### 7.3 Abbreviations and Symbols

$\alpha$ -SNAP	N-Ethylmaleimide-sensitive factor attachment protein, $\alpha$
Abs	Absorption
aa	Amino acids
APS	Ammonium persulfate
ATP	adenosine triphosphate
CG	Chromaffin granules
CHAPS	3-[(3-Cholamidopropyl)dimethylammonio]-1-propanesulfonate
Cys	Cysteine
ddH <sub>2</sub> O	Double distilled water
DC	Dichroic Mirror
DHPE	Dihexadecanoylphosphoethanolamine
DTT	Dithiothreitol
EDTA	Ethylenediaminetetraacetic acid
fl	Femtoliter
FRET	Förster Resonance Energy Transfer
h	Host
HEPES	4-(2-Hydroxyethyl)piperazine-1-ethanesulfonic acid
IEXC	Ion Exchange Chromatography
IPTG	Isopropyl- $\beta$ -D-thiogalactopyranosid
IRF	Instrument response function
KCl	Potassium chloride
LUVs	Large unilamellar vesicles
MDF	Molecule detection function
MeOH	Methanol
Milli-Q	Ultrapure water
min	Minutes
MOPS	3-(N-morpholino)propanesulfonic acid
ms	Milliseconds
$\mu$ M	Micromolar
NA	Numerical aperture
NFLC	Normalized fluorescence lifetime change
ns	Nanoseconds
NSF	N-Ethylmaleimide-sensitive factor
OG	Oregon green
OPE	One-photon excitation
PC	L- $\alpha$ -Phosphatidylcholine
PE	L- $\alpha$ -Phosphatidylethanolamine
PI	L- $\alpha$ -Phosphatidylinositol
PiP <sub>2</sub>	Phosphatidylinositol-4,5-bisphosphate
PLM	Plasma membrane
PMSF	Phenylmethanesulfonylfluoride
PS	L- $\alpha$ -Phosphatidylserine
RT	Room temperature

---

SDS	Sodium dodecyl sulfate
SDS-PAGE	Sodium dodecyl sulfate polyacrylamide gel electrophoresis
SNAPs	Soluble NSF attachment proteins
SNAP25A	Synaptosomal-associated protein 25A
SNARE	Soluble N-ethylmaleimide-sensitive-factor attachment receptor
SUVs	Small unilamellar vesicles
Sx1A	Syntaxin 1A
Syt1	Synaptotagmin-1
t	Target
$\tau_D$	Donor fluorescence lifetime
$\tau_{Diff}$	Diffusion time
$\tau_{Life}$	Fluorescence lifetime
TCSPC	Time Correlated Single Photon Counting
TEMED	N,N,N,N-Tetramethylethylenediamine
TPE	Two-photon excitation
TMD	Trans membrane domain
Tricine	N-(Tri(hydroxymethyl)methyl)glycine
TR	Texas Red
TTL	Transistor-Transistor-Logic
v/v	volume/volume
w/v	weight/volume

# Curriculum Vitae

## Personal Details

Surname: Schröder  
 Name: Sabrina  
 Address: Apoldaer Weg 6, 37085 Göttingen  
 Date of birth: 03/20/1985  
 Place of birth: Bünde  
 Citizenship: german  
 Marital status: single

## Education

Summer 2014	End of PhD
Summer 2010	Admission to the doctoral excellence program of the GGNB)
July 2010	Receipt of a Max-Planck stipend for a PhD thesis at the Max-Planck-Institute for biophysical chemistry in Göttingen
April 2010	Master of Science
October 2009-	Master thesis at the Max-Planck-Institute
April/May 2010	for biophysical chemistry in Göttingen
August 2009-	Research internship at the Max-Planck-Institute
October 2009	for biophysical chemistry in Göttingen
September 2008-	Research internship at the Notre Dame University, Indiana, USA
March 2009	
2008:	Receipt of a DAAD stipend for a research internship abroad
2007	Bachelor of Science
2004- 2009	Study of biochemistry at the University of Bielefeld
June 2004-	Internship at the Herz- und Diabeteszentrum Bad Oeynhausien
October 2004	
2004	Abitur
2002	Diplome d'études en langue française (DELF) ; 1er degré
1995-2004	Freiherr-vom-Stein Gymnasium Bünde
1991-1995	Elementary school Quernheim

# Publications

## 2014

1. Schröder S, Perez AL, Jahn R, Walla PJ, Synaptotagmin-1 primes and triggers vesicle fusion, Manuscript in preparation
2. Halder P, Perez AL, Schröder S, Jahn R, Walla PJ, Biochemical reconstitution of late endosomal pathway using full-length SNAREs: Syntaxin7, VTI1b, Syntaxin8, VAMP 8 and VAMP 7, Manuscript in preparation

## 2012

1. Munari F, Soeroes S, Zenn HM, Schomburg A, Kost N, Schröder S, Klingberg R, Rezaei-Ghaleh N, Stützer A, Gelato KA, Walla PJ, Becker S, Schwarzer D, Zimmermann B, Fischle W, Zweckstetter M., Methylation of lysine 9 in histone H3 directs alternative modes of highly dynamic interaction of heterochromatin protein hHP1 with the nucleosome, *J Biol Chem.* 2012 Sep 28;287(40):33756-65
2. Vennekate W, Schröder S, Lin CC, van den Bogaart G, Grunwald M, Jahn R, Walla PJ. Cis- and trans-membrane interactions of synaptotagmin-1, *Proc Natl Acad Sci U S A.* 2012 Jul 3;109(27):11037-42

# Acknowledgement

I would like to thank Professor Peter Jomo Walla and Professor Reinhard Jahn for supporting me to complete my PhD thesis with many pleasant discussions and many important suggestions. I also would like to thank Professor Ulf Diederichsen and Professor Jörg Enderlein for joining my thesis committee and giving me lots of useful suggestions.

My collaboration partners, Dr. Geert van den Bogaart, Dr. Yongsoo Park, Dr. Angel Perez and Halenur Yavuz, have to be named not only for offering an active working atmosphere, but also for the growing friendships with them during the past four years.

I would like to give special thanks to Dr. Wensi Vennekate, Dr. Jianhua Chen, Matthias Grunwald and Chao-Chen Lin for sharing a great time with me. Additionally, I would like to thank Inge Dreger for always being a reliable associate.

A very special thank goes to Dr. Silvio Weber.

# List of Figures

2.1	Structure of SNARE complex . . . . .	4
2.2	Structure of synaptotagmin-1 . . . . .	5
2.3	Two models of priming and triggering . . . . .	7
2.4	Jablonski diagram . . . . .	8
2.5	Fluorescence lifetime histogram . . . . .	9
2.6	Absorption and emission spectra of Oregon green . . . . .	11
2.7	auto-correlation . . . . .	12
2.8	Generation of continuous wave excitation (CW) . . . . .	17
2.9	Two photon excitation . . . . .	18
3.1	The TP-setup . . . . .	31
4.1	Synaptotagmin-1 tethering and fluorescence lifetime under low ionic strength conditions . . . . .	35
4.2	Synaptotagmin-1 tethering III . . . . .	36
4.3	Synaptotagmin-1 fluorescence lifetime III . . . . .	37
4.4	Normalized fluorescence lifetime changes . . . . .	38
4.5	EGTA control experiment . . . . .	39
4.6	Synaptotagmin-1 tethering and fluorescence lifetime I . . . . .	42
4.7	Synaptotagmin-1 tethering and fluorescence lifetime II . . . . .	45
4.8	Empty liposome control . . . . .	46

---

4.9	Linear regression model . . . . .	48
4.10	Burst analysis method . . . . .	50
4.11	Western Blot of synaptotagmin-1 and synaptobrevin 2 . . . . .	52
4.12	Synaptobrevin 2 influence . . . . .	54
4.13	PiP <sub>2</sub> influence n tethering . . . . .	56
4.14	PiP <sub>2</sub> influence o fluorescence lifetime . . . . .	57
4.15	Syntaxin 1A influence . . . . .	59
4.16	Mutant analysis . . . . .	62
4.17	Optical trapping setup . . . . .	66
4.18	z-scan . . . . .	67
4.19	Trapping validation I . . . . .	69
4.20	Trapping validation II . . . . .	70
4.21	Trapping efficiency . . . . .	71
4.22	Oregon green fluorescence lifetime under trapping conditions . . . . .	72
4.23	Adsorption isotherms . . . . .	74
4.24	Langmuir plot . . . . .	76
4.25	Diffusion coefficient . . . . .	77
4.26	Bulk measurement . . . . .	78
4.27	Oregon green fluorescence lifetime in distance regulation under trapping conditions I . . . . .	79
4.28	Oregon green fluorescence lifetime in distance regulation under trapping conditions II . . . . .	80
4.29	Syringe characterization . . . . .	81
4.30	Buffer influx test . . . . .	82
4.31	Time trace fusion experiment I . . . . .	83
4.32	Fluorescence lifetime development I . . . . .	85
4.33	Time trace fusion experiment II . . . . .	86

4.34 Fluorescence lifetime development II . . . . . 87

7.1 Time trace analysis . . . . . 110

7.2 Fluorescence lifetime histogram analysis . . . . . 111

# List of Tables

3.1	Summary of all proteins used in this study. . . . .	23
3.2	Summary of all antibodies used in this study. . . . .	23
3.3	Summary of all lipids and cholesterol used in this study. . . . .	24
3.4	Summary of all additionally used dyes/fluorescent components in this study. . . . .	25
3.5	Summary of all buffers used in this study. . . . .	25
3.6	Summary of all instruments used in this study. . . . .	26
3.7	Summary of SUV composition . . . . .	29
4.1	Summary of Hill fit values determined for synaptotagmin-1 wt presented in figure 4.7. . . . .	45
4.2	Summary of linear regression fit values. . . . .	48
4.3	Summary of Oregon green fluorescence lifetimes. . . . .	51
4.4	Summary of Hill fit values determined for synaptotagmin-1 wt and synaptobrevin 2 presented in figure in 4.12. . . . .	54
4.5	Summary of Oregon green fluorescence lifetimes in case of synaptobrevin 2 being reconstituted into the host liposome. . . . .	55
4.6	Summary of Oregon green fluorescence lifetimes in case different PiP <sub>2</sub> concentrations in the target liposome. . . . .	58
4.7	Summary of Oregon green fluorescence lifetimes in case of 3% PiP <sub>2</sub> and syntaxin 1A being reconstituted into the target liposome. . . . .	60
4.8	Summary of Hill fit values determined for synaptotagmin-1 mutants presented in figure 4.16. . . . .	62

---

4.9	Summary of Oregon green fluorescence lifetimes of all four synaptotagmin-1 mutants. . . . .	64
4.10	Characterizing the focal volume in CW-, TP- and both excitation modes. . . . .	68
4.11	Three different adsorption isotherms are applied to the diffusion time of synaptotagmin-1 carrying SUVs. The constant $K$ for the Langmuir adsorption as well as $K_2$ from the Gurney adsorption isotherm are given in $\mu\text{M}^{-1}$ , $K_3$ is given in $\mu\text{M}^{-\frac{1}{2}}$ , whereas the remaining constants are dimensionless [10]. . . . .	75
4.12	A Langmuir fit model is applied to the diffusion coefficient data resulting from the diffusion time of synaptotagmin-1 carrying SUVs. The constant $K$ is given in $\mu\text{M}^{-1}$ . . . . .	76

# Bibliography

- [1] Antonin, W, Fasshauer, D, Becker, S, Jahn, R, Schneider, T R, *Crystal structure of the endosomal SNARE complex reveals common structural principles of all SNAREs*, *Nat.Struct.Biol*, 2001, 9, 107
- [2] Araç D, Chen X, Khant H A, Ubach J, Ludtke S J, Kikkawa M, Johnson A E, Chiu W, Südhof T C, Rizo J, *Close membrane-membrane proximity induced by Ca(2+)-dependent multivalent binding of synaptotagmin-1 to phospholipids*, *Nat Struct Mol Biol.*, 2006, 13, 3, 209-17
- [3] Ashkin D, *Acceleration and trapping of particles by radiation pressure*, *Phys. Rev. Lett*, 1970, 24, 156-159.
- [4] Ashkin A, Dziedzic J M, Bjorkholm J E, Chu S, *Observation of a single-beam gradient force optical trap for dielectric particles*, *Optics Letters*, 1986, 11, 288-290.
- [5] Atkins P W, *Physikalische Chemie*, 3. Aufl, Wiley-VHC, Weinheim, 2001
- [6] Bai J, Tucker W C, Chapman E R, *PiP2 increases the speed of response of synaptotagmin and steers its membrane-penetration activity toward the plasma membrane*, *Nat Struct Mol Biol.*, 2004, 11, 36- 44
- [7] Bai J, Earles C A, Lewis J L, Chapman E R, *Membrane-embedded Synaptotagmin Penetrates cis or trans Target Membranes and Clusters via a Novel Mechanism*, *The Journal of Biological Chemistry*, 2000, 275, 25427-25435
- [8] Bendix P M, Oddershede L B, *Expanding the optical trapping range of lipid liposomes to the nanoscale*, *Nano Lett.*, 2011, 11, 12, 5431-7
- [9] Bennett M K, Calakos N, Scheller R H, *Syntaxin: a synaptic protein implicated in docking of synaptic vesicles at presynaptic active zones*, *Science*, 1992, 257, 5067, 255-259
- [10] Bhal G S, Toor G S, *Influence of poultry manure on phosphate availability and the standard phosphate requirement of crop estimated from quantity intensity relationship in different soils*, *Bio-resource Tech.*, 2002, 85, 317-322.
- [11] Bhalla A, Chicka M C, Tucker W C, Chapman E R, *Ca(2+)-synaptotagmin directly regulates t-SNARE function during reconstituted membrane fusion*, *Nat Struct Mol Biol.*, 2006, 13, 4, 323-30
- [12] Birks R, MacIntosh F C, *Acetylcholine metabolism of a sympathetic ganglion*, *Can. J. Biochem. Physiol.* 1961, 39, 787-827

- [13] Brandt D S, Coffman M D, Falke J J, Knight J D, *Hydrophobic contributions to the membrane docking of synaptotagmin 7 C2A domain: mechanistic contrast between isoforms 1 and 7*, *Biochemistry*, 2012, 51, 7654-64
- [14] Brunger A T, Weninger K, Bowen M, Chu S, *Single-molecule studies of the neuronal SNARE fusion machinery*, *Annu Rev Biochem.*, 2009, 78, 903-28.
- [15] Burkhardt P, Hattendorf D A, Weis W I, Fasshauer D, *Munc18a controls SNARE assembly through its interaction with the syntaxin N-peptide*, *EMBO J.*, 2008, 27, 7, 923-33
- [16] Butz S, Fernandez-Chacon R, Schmitz F, Jahn R, Südhof T C, *The subcellular localizations of atypical synaptotagmins III and VI. Synaptotagmin II is enriched in synapses and synaptic plasma membranes but not in synaptic vesicles*, *J. Biol. Chem.*, 1999, 274, 18290-18296
- [17] Chapman E R, *How does synaptotagmin trigger neurotransmitter release?*, *Annu Rev Biochem.*, 2008, 77, 615-41
- [18] Chapman E R, Hanson P I, An S, Jahn R, *Ca<sup>2+</sup> regulates the interaction between synaptotagmin and syntaxin 1*, *J Biol Chem.* 1995, 270, 40, 23667-71
- [19] Chicka M C, Hui E, Liu H, Chapman E R, *Synaptotagmin arrests the SNARE complex before triggering fast, efficient membrane fusion in response to Ca<sup>2+</sup>*, *Nat Struct Mol Biol.*, 2008, 15, 8, 827-35
- [20] Choi U B, Strop P, Vrljic M, Chu S, Brunger AT, Weninger KR *Single-molecule FRET-derived model of the synaptotagmin 1-SNARE fusion complex*, *Nat Struct Mol Biol*, 2010, 17, 3, 318-24
- [21] Chung C, Raingo J, *liposome dynamics: how synaptic proteins regulate different modes of neurotransmission*, *J Neurochem.*, 2013, 126, 2, 146-54
- [22] Clegg R M, *Förster resonance energy transfer - FRET what is it, why do it, and how it's done*. In: Theodoros W. J. Gadella (Hrsg.): *FRET and FLIM techniques*. Elsevier, Amsterdam 2009, ISBN 0-08-054958-6
- [23] Collini M, Caccia M, Chirico G, Barone F, Dogliotti E, Mazzei F, *two-photon fluorescence cross-correlation spectroscopy as a potential tool for highthroughput screening of DNA repair activity*, *Nuc. Acid Res*, 2005, 33, e165
- [24] Cyionka, A, Stein, A, Hernandez, J M, Hippchen, H, Jahn, R, Walla, P. J, *Discrimination between docking and fusion of liposomes reconstituted with neuronal SNARE-proteins using FCS*, *Proc Natl Acad Sci U S A* 2009, 106, 44, 18575-18580
- [25] Denker A, Rizzoli S O, *Synaptic liposome pools: an update*, *Front Synaptic Neurosci*, 2010, 2, 135
- [26] Desai R C, Vyas B, Earles C A, Littleton J T, Judith A. Kowalchuck J A, Martin T F J, Chapman E R, *The C2b Domain of Synaptotagmin Is a Ca<sup>2+</sup>-Sensing Module Essential for Exocytosis*, *Journal of Chemical Biology*, 2000, 150, 1125-1136
- [27] Diao J, Ishitsuka Y, Bae W R, *Single-molecule FRET study of SNARE-mediated membrane fusion*, *Biosci Rep.*, 2011, 31, 6, 457-63

- [28] Dong C Y, Koenig K, So P, *Characterizing point spread functions of TPE microscopy in turbid medium*, *Journal of Biomedical Optics*, 2003, 8, 3, 450-459
- [29] Domanska M K, Kiessling V, Stein A, Fasshauer D, Lukas K, *Single liposome millisecond fusion kinetics reveals number of SNARE complexes optimal for fast SNARE-mediated membrane fusion*, *J Biol Chem*, 2009, 284, 32158-32166
- [30] Dulubova I, Sugita S, Hill S, Hosaka M, Fernandez I, Südhof T C, Rizo J, *A conformational switch in syntaxin during exocytosis: role of munc18*, *EMBO J.*, 1999, 18, 4372-4382
- [31] Eagle S, Scott J W, *Liquid phase adsorption equilibria and kinetics*, *Industrial and Engineering chemistry*, 1950, 42, 7
- [32] Elson E L, Madge D, *Fluorescence spectroscopy I: Conceptual basis and theory*, *Biopolymers*, 1974, 13, 1-27
- [33] Einstein A, *Über die von der molekularkinetischen Theorie der Wärme geforderten Bewegung von in ruhenden Flüssigkeiten suspendierten Teilchen*, *Ann. Phys*, 105, 17, 549-560
- [34] Förster T, *Zwischenmolekulare Energiewanderung und Fluoreszenz*, *Ann. Phys*, 1948, 437, 55-75
- [35] Förster T, *Experimentelle und theoretische Untersuchung des zwischenmolekularen Übergangs von Elektronenanregungsenergie*, *Z. Naturforsch.*, 1949, 4a, 321-327
- [36] Freundlich H, *Über die Adsorption in Lösungen*, *Z. Phys. Chem.*, 1907, 57, 385- 470
- [37] Gendron P O, Avaltroni F, Wilkinson K J, *Diffusion coefficients of several rhodamine derivatives as determined by pulsed field -nuclear magnetic resonance and fluorescence correlation spectroscopy*, *J Fluoresc.*, 2008, 18, 6, 1093-101
- [38] *GESTIS-Stoffdatenbank des IFA*
- [39] Gerber S H, Rizo J, Südhof T C, *Role of electrostatic and hydrophobic interactions in Ca(2+)-dependent phospholipid binding by the C(2)A-domain from synaptotagmin I*, 2002, 51
- [40] Gunary D, *A new adsorption isotherm for phosphate in soil*, *Journal of soil science*, 1970, 21 ,1
- [41] Haustein E, Schwille P, *Fluorescence Correlation Spectroscopy: Novel variations of an established technique*, *Annu. Rev. Biophys. Struct*, 2007, 36, 151-169.
- [42] Hecht E, *Optics*, Addison-Wesley, 4th edition, 2001
- [43] Hernandez, J M, Stein, A, Behrmann, E, Riedel, D, Cypionka, A, Farsi, Z, Walla, P J, Raunser, S, Jahn, R, *Membrane fusion intermediates via directional and full assembly of the SNARE complex*, *Science* 336, 2012 6088, 1581- 1584
- [44] Honigmann, A, van den Bogaart, G, Iraheta, E, Risselada, H J, Milovanovic, D, Mueller, V, Mueller, S, Diederichsen, U, Fasshauer, D, Grubmüller, H, Hell, S W, Eggeling, C, Kühnel, K, Jahn, R, *Phosphatidylinositol 4,5-Bisphosphate Clusters Act as Molecular Beacons for liposome Recruitment*, *Nat.Struct.Mol.Biol*, 2013, 20, 679

- [45] Hui E, Johnson C P, Yao J, Dunning F M, Chapman E R, *Synaptotagmin-mediated bending of the target membrane is a critical step in Ca(2+)-regulated fusion*, *Cell*. 2009, 138, 4, 709-21
- [46] Hunt J M, Bommert K, Charlton M P, Kistner A, Habermann E, Augustine G J, Betz H, *A post-docking role for synaptobrevin in synaptic vesicle fusion*, *Neuron*, 1994, 12, 6, 1269-79
- [47] Huntwork S, Littleton J T, *A complexin fusion clamp regulates spontaneous neurotransmitter release and synaptic growth*, *Nat Neurosci.*, 2007, 10, 1235- 1237
- [48] Jahn R, Scheller R H, *SNAREs—engines for membrane fusion*, *Nat Rev Mol Cell Biol.*, 2006, 631-43
- [49] Jahn R, Fasshauer D, *Molecular machines governing exocytosis of synaptic vesicles*, *Nature*, 2012, 490, 7419, 201-7
- [50] <http://rsb.info.nih.gov/ij/>
- [51] Reinhard Jahn Department
- [52] Jahn R, Lang T, Südhof T C, *Membrane fusion*. *Cell*, 2003, 112, 4, 519-533.
- [53] Kerker M, *The Scattering of Light and other Electromagnetic radiation*, 1969, New York, NY, 32-37
- [54] Klopper T H, Kienle C N, Fasshauer D, *An elaborate classification of SNARE proteins sheds light on the conservation of the eukaryotic endomembrane system*, *Mol Biol Cell.*, 2007, 18, 9, 3463-71
- [55] Kohl T, Heinze K G, Kuhlemann R, Koltermann A, Schwille P, *A protease assay for two-photon crosscorrelation and FRET analysis based solely on fluorescent proteins*, *Proc. Natl. Acad. Sci. USA*, 2002, 99, 12161-12166.
- [56] Korlann Y, Detring T, Michalet X, Weiss S, Enderlein J, *Measuring diffusion with polarized-modulation dual-focus fluorescence correlation spectroscopy*, *Optics express*, 2008, 16, 146
- [57] Krishnakumar S, Radoff D, Kuemmel D, Giraudo C, Li F, Khandan L, Wood Baguely S, Coleman J, Reinisch K, Pincet F, Rothman J, *A conformational switch in complexin is required for synaptotagmin to trigger synaptic fusion*, *Nature Structural & Molecular Biology*, 2011, 18, 934-940
- [58] Kuo W, Herrick D Z, Cafiso D S, *Phosphatidylinositol 4,5-bisphosphate alters synaptotagmin 1 membrane docking and drives opposing bilayers closer together*, *Biochemistry*, 2011, 50, 2633-2641
- [59] Kuo W, Herrick D Z, Ellena J F, Cafiso D S, *The calcium-dependent and calcium-independent membrane binding of synaptotagmin 1: two modes of C2B binding*, *J Mol Biol.*, 2009, 387, 284-294
- [60] Kyoung M, Zhang Y, Diao J, Chu S, Brunger A T, *Studying calcium-triggered liposome fusion in a single liposome-liposome contact and lipid-mixing system*, *Nat Protoc.*, 2013, 8, 1, 1-16.
- [61] Laage R, Ungermann C, *The N-terminal domain of the t-SNARE Vam3p coordinates priming and docking in yeast vacuole fusion*, *Mol Biol Cell.*, 2001, 12, 11, 3375-85

- [62] Laemmli U K, *Cleavage of structural proteins during the assembly of the head of bacteriophage T4*. *Nature*, 1970, 227, 5259, 680-685.
- [63] Lakowicz J R, *Principles of Fluorescence Spectroscopy*, Plenum Publishers, 1999
- [64] Lee H K, Yang Y, Su Z, Hyeon C, Lee T S, Lee H W, Kweon D H, Shin Y K, Yoon T Y, *Dynamic Ca<sup>2+</sup>-dependent stimulation of liposome fusion by membrane-anchored synaptotagmin 1*, *Science*, 2010, 328, 5979, 760-3
- [65] Nelson D L, Cox M M, *Lehninger Principles of Biochemistry*, 2012, 6th ed.,
- [66] Li T, *Fundamental test of physics with optically trapped microspheres*, Springer, 2013
- [67] Li L, Shin O, Rhee J-S, Arac D, Rah J-C, Rizo J, Südhof T, Rosenmund C, *Phosphatidylinositol Phosphates as Co-activators of Ca<sup>2+</sup> Binding to C2 Domains of Synaptotagmin 1*, *The Journal of Biological Chemistry*, 2006, 281, 15845-15852
- [68] Littleton J T, Bai J, Vyas B, Desai R, Baltus A E, Garment M B, Carlson S D, Ganetzky B, Chapman E R, *Synaptotagmin Mutants Reveal Essential Functions for the C2B Domain in Ca<sup>2+</sup>-Triggered Fusion and Recycling of Synaptic Vesicles In Vivo*, *The Journal of Neuroscience*, 2001, 21, 1421-1433
- [69] Lohse B, Bohlinger P-Y, Stamou D, *Encapsulation efficiency measured on single small unilamellar vesicles*, *J. Am. Chem. Soc.*, 2008, 130, 44, 14372
- [70] J. M. Mackler J M, Drummond J A, Loewen C A, Robinson I M, Reist M E, *The C2B Ca<sup>2+</sup>-binding motif of synaptotagmin is required for synaptic transmission in vivo*, *Nature*, 418, 340-344
- [71] Madge D, Webb W W, Elson D L, *Fluorescence Correlation Spectroscopy II: An experimental realization*, *Biopolymers*, 1974, 13, 29-61
- [72] Martens S, Kozlov M M, McMahon H T, *How synaptotagmin promotes membrane fusion*, *Science*, 2007, 316, 5828, 1205-8
- [73] <http://maxchelator.stanford.edu>
- [74] McGuigan J A, Kay J W, Elder H Y, Luthi D, *Comparison between measured and calculated ionised concentrations in Mg<sup>2+</sup>/ATP, Mg<sup>2+</sup>/EDTA and Ca<sup>2+</sup>/EGTA buffers; influence of changes in temperature, pH and pipetting errors on the ionised concentrations*, *Magnesium Research*, 2007, 20, 1, 72-81
- [75] Michalet X, Pinaud F F, Bentolila L A, Tsay J M, Doose S, Li J J, Sundaresan G, Wu A M, Gambhir S S, Weiss S, *"Quantum dots for live cells, in vivo imaging, and diagnostics"*, *Science*, 2005, 307, 538- 44
- [76] Min D, Kim K, Hyeon C, Cho Y H, Shin Y K, Yoon T Y, *Mechanical unzipping and reziping of a single SNARE complex reveals hysteresis as a force-generating mechanism*, *Nat Commun.*, 2013, 4, 1705
- [77] Misura K M, Scheller R H, Weis W I, *Three-dimensional structure of the neuronal-Sec1-syntaxin 1a complex*, *Nature*, 2000, 404, 355-362

- [78] Mohrmann R, de Wit H, Connell E, Pinheiro P S, Leese C, Bruns D, Davletov B, Verhage M, Sørensen J B, Synaptotagmin Interaction with SNAP-25 Governs liposome Docking, Priming, and Fusion Triggering, *J Neurosci.*, 2013, 33, 36, 14417-14430
- [79] Mueller P, Rudin D O, Tien H I, Wescott W C, Reconstitution of cell membrane structure in vitro and its transformation into an excitable system, *Nature*, 1962, 194, 979- 980
- [80] Nishiki T, Augustine G J, Dual Roles of the C2B Domain of Synaptotagmin I in Synchronizing Ca<sup>2+</sup>-Dependent Neurotransmitter Release, *The Journal of Neuroscience*, 2004, 24, 8542-8550
- [81] Müller C B, Loman A, Pacheco V, Koberling K, Willbold D, Richtering W, Enderlein J, Precise measurement of diffusion by multi-color dual-focus fluorescence correlation spectroscopy, *EPL (Europhysics Letters)*, 2008, 83, 4
- [82] Paddock B E, Wang Z, Biela L M, Chen K, Getzy M D, Striegel A, Richmond J E, Chapman E R, Featherstone D E, Reist N E, Membrane penetration by synaptotagmin is required for coupling calcium binding to vesicle fusion in vivo., *J Neurosci.*, 2011, 31, 6, 2248-57.
- [83] Park Y, Hernandez J M, van den Bogaart G, Ahmed S, Holt M, Riedel D, Jahn R, Controlling synaptotagmin activity by electrostatic screening, *Nat Struct Mol Biol.*, 2012, 19, 10, 991-7
- [84] Perin M S, Fried V A, Mignery G A, Jahn R, Südhof TC, Phospholipid binding by a synaptic vesicle protein homologous to the regulatory region of protein kinase C., *Nature*, 1990, 345, 260-263
- [85] Pobatti V, Stein A, Fasshauer D, N- to C-terminal SNARE complex assembly promotes rapid membrane fusion, 2006, *Science* 313, 5787, 673-676
- [86] Pohl W H, *Entwicklung und Anwendung spektroskopischer Korrelationsverfahren zur Beantwortung biomolekularer Fragestellungen*, Dissertation
- [87] Radhakrishnan A, Stein A, Jahn R, Fasshauer D, The Ca<sup>2+</sup> affinity of synaptotagmin 1 is markedly increased by a specific interaction of its C2B domain with phosphatidylinositol 4,5-bisphosphate, *J Biol Chem.*, 2009, 284(38), 25749-60
- [88] Rasband W S, *ImageJ*, U. S. National Institutes of Health, Bethesda, Maryland, 1994-2014
- [89] Rigler R, *Fluorescence correlations, single molecule detection and large number screening: Applications in biotechnology*, *J. Biotechnology*, 1995, 41, 177-186.
- [90] Rigler R, Földes-Papp Z, Meyer-Almes F J, Sammet C, Völcker M, Schnetz A, *Fluorescence cross-correlation: a new concept for polymerase chain reaction*, *J Biotechnol*, 1998, 63, 2, 97-109
- [91] Rizo J, Chen X, Araç D, *Unraveling the mechanisms of synaptotagmin and SNARE function in neurotransmitter release*, *Trends Cell Biol.*, 2006, 16, 7, 339-50
- [92] Rizo J, Rosenmund C, *Synaptic vesicle fusion*, *Nat Struct Mol Biol.*, 2008, 15, 7, 665-74

- [93] Rizzoli S O, Betz W O, *Synaptic vesicle pools*, *Nature Reviews Neuroscience* 6, 2005, 57-69
- [94] Pobbati A V, Stein A, Fasshauer D, *N- to C-terminal SNARE complex assembly promotes rapid membrane fusion*, *Science*, 2007, 313, 5787, 673-676.
- [95] Sarmiento M J, Coutinho A, Fedorov A, Prieto M, Fernandes F, *Ca(2+) induces PI(4,5)P2 clusters on lipid bilayers at physiological PI(4,5)P2 and Ca(2+) concentrations*, *Biochim Biophys Acta.*, 2014 , 1838, 822-830
- [96] Seven A B, Brewer K D, Shi L, Jiang Q X, Rizo J, *Prevalent mechanism of membrane bridging by synaptotagmin-1.*, *Proc Natl Acad Sci USA*, 2013, 110, 34
- [97] Schwille P, Rigler R, Elson E L, *Fluorescence correlation spectroscopy: Theory and applications*, Springer, Berlin, 2001 S. 360.
- [98] Schuette C G, Hatsuzawa A K, Margittai M, Stein A, Riedel D, Küster P, König M, Seidel L C, Jahn R, *Determinants of liposome fusion mediated by synaptic SNARE proteins.* *Proc Natl Acad Sci U S A*, 2004, 101, 9, 2858-2863
- [99] Shin O, Xu J, Rizo J, Südhof T C, *Differential but convergent functions of Ca2+ binding to synaptotagmin-1 C2 domains mediate neurotransmitter release*, *Proc Natl Acad Sci*, 2009, 106, 16469-16474
- [100] Stein A, Radhakrishnan A, Riedel D, Fasshauer D, Jahn, R. *Synaptotagmin activates membrane fusion through a Ca2+-dependent trans interaction with phospholipids.* *Nat Struct Mol Biol* 14, 2007, 10, 904-911.
- [101] Südhof T C, *The synaptic vesicle cycle*, *Annu Rev Neurosci.*, 2004, 27, 509-47
- [102] Südhof T C, Rizo J, *Synaptic vesicle exocytosis*, *Cold Spring Harb Perspect Biol.* 2011, 3, 12
- [103] Südhof T C, Rothman J E, *Membrane fusion: grappling with SNARE and SM proteins*, *Science*, 2009, 323, 5913, 474-477
- [104] Südhof T C, *Synaptotagmins: Why So Many?*, *JBC*, 2002, 277, 7629-7632
- [105] Sørensen J B, Wiederhold K, Müller E M, Milosevic I, Nagy G, de Groot B L, Grubmüller H, Fasshauer D, *Sequential N- to C-terminal SNARE complex assembly drives priming and fusion of secretory liposomes*, *EMBO J.* 2006, 25(5), 955-66
- [106] Stein A, Radhakrishnan A, Riedel D, Fasshauer D, Jahn R, *Synaptotagmin activates membrane fusion through a Ca2+-dependent trans interaction with phospholipids*, *Nat Struct Mol Biol.* 2007, 14(10), 904-11
- [107] Sugita S, Han W, Butz S, Liu X, Fernandez-Chacon R, Lao Y, Südhof T C, *Synaptotagmin VII as a plasma membrane Ca(2+) sensor in exocytosis*, *Neuron*, 2001, 30, 459-473
- [108] Sugita, S, Shin, O-K, Han, W, Lao, Y, Südhof, T C, *Synaptotagmins form a hierarchy of exocytotic Ca(2+) sensors with distinct Ca(2+) affinities*, *EMBO J.*, 2002, 21, 3, 270- 280

- [109] Sutton R B, Fasshauer D, Jahn R, Brunger A T, *Crystal structure of a SNARE complex involved in synaptic exocytosis at 2.4 Å resolution*, *Nature*, 1998, 395(6700), 347-53
- [110] Svelto O, *Principle of Lasers*, 4th edition, 1998
- [111] Svoboda K, Block S M, *Biological applications of optical forces*, *Annu. Rev. Biophys. Biomol. Struct.* 23, 247-285, 1994
- [112] Takamori S, Holt M, Stenius K, Lemke E A, Grønborg M, Riedel D, Urlaub H, Schenck S, Brügger B, Ringler P, Müller SA, Rammner B, Gräter F, Hub J S, De Groot B L, Mieskes G, Moriyama Y, Klingauf J, Grubmüller H, Heuser J, Wieland F, Jahn R, *Molecular anatomy of a trafficking organelle*, *Cell*, 2006, 127, 4, 831-46
- [113] Tang J, Maximov A, Shin OH, Dai H, Rizo J, Südhof T C, *A complexin/synaptotagmin-1 switch control fast synaptic vesicle exocytosis*, *Cell*, 2006, 126(6), 1175-87
- [114] <http://www.uniprot.org>
- [115] [www.physik.uni-jena.de/FFehlerrechnungLeichtGemacht.pdf](http://www.physik.uni-jena.de/FFehlerrechnungLeichtGemacht.pdf)
- [116] <http://www.uni-leipzig.de/pwm/web/?section=introduction&page=opticaltraps>
- [117] van den Bogaart G, Holt M G, Bunt G, Riedel D, Wouters F S, Jahn R, *One SNARE complex is sufficient for membrane fusion*, *Nat Struct Mol Biol.*, 2010, 17, 3, 358-64.
- [118] van den Bogaart G, Meyenberg K, Diederichsen U, Jahn R, *Phosphatidylinositol 4,5-bisphosphate increases Ca<sup>2+</sup> affinity of synaptotagmin-1 by 40-fold*, *J Biol Chem.* 2012, 287, 20, 16447-53
- [119] van den Bogaart G, Thutupalli S, Risselada J H, Meyenberg K, Holt M, Riedel D, Diederichsen U, Herminghaus S, Grubmüller H, Jahn R, *Synaptotagmin-1 may be a distance regulator acting upstream of SNARE nucleation*, *Nat Struct Mol Biol.*, 2011, 18, 7, 805-12
- [120] van den Bogaart G, Meyenberg K, Risselada J H, Amin H, Willig K I, Hubrich B E, Dier M, Hell S W, Grubmüller H, Diederichsen U, Jahn R, *Membrane protein sequestering by ionic protein-lipid interactions*, 2011, *Nature* 479, 552- 555
- [121] Vennekate W, Schröder S, Lin C C, van den Bogaart G, Grunwald M, Jahn R, Walla P J, *Cis- and trans-membrane interactions of synaptotagmin-1*, *Proc Natl Acad Sci U S A.*, 2012, 109(27), 11037-42
- [122] Vennekate W, *Investigation of neuronal membrane fusion using fluorescence correlation spectroscopy*, *Dissertation*
- [123] Ochoa W F, Corbalan-Garcia S, Eritja R, Rodriguez-Alfaro J A, Gomez-Fernandez J C, Fita I, Verdaguer N, *Additional binding sites for anionic phospholipids and calcium ions in the crystal structures of complexes of the C2 domain of protein kinase  $\alpha$* , *Journal of Molecular Biology*, 2002, 320, 2, 277-91
- [124] Vrljic, M, Strop, P, Ernst, J, Brunger, A.T, *Molecular mechanism of the synaptotagmin-SNARE interaction in Ca<sup>2+</sup>-triggered liposome fusion*, *Nat.Struct.Mol.Biol.*, 2010, 17, 325-331

- [125] Wahl M, Gregor I, Patting M, Enderlein J, Fast calculation of fluorescence correlation data with asynchronous time-correlated single photon-counting, *Opt. Express*, 2003, 11, 2583- 2591
- [126] Walla P. J, *Modern Biophysical Chemistry*, Wiley-VCH, 2009
- [127] Walling M A, Novak J A, Shepard J R, "Quantum Dots for Live Cell and In Vivo Imaging", *Int. J. Mol. Sci.*, 2009, 10, 441-491
- [128] Walter A M, Wiederhold K, Bruns D, Fasshauer D, Sørensen J B, Synaptobrevin N-terminally bound to syntaxin-SNAP-25 defines the primed liposome state in regulated exocytosis, *J Cell Biol.* 2010, 188, 3, 401-13
- [129] Wang P, Wang C T, Bai J, Jackson M B, Chapman E R, Mutations in the effector binding loops in the C2A and C2B domains of synaptotagmin I disrupt exocytosis in a nonadditive manner., *J Biol Chem.*, 2003, 278, 47030-7.
- [130] Wiederhold K, Kloepper TH, Walter AM, Stein A, Kienle N, Sørensen JB, Fasshauer D, A coiled coil trigger site is essential for rapid binding of synaptobrevin to the SNARE acceptor complex, *J Biol Chem.* 2010, 285, 28, 21549-59
- [131] Xue M, Ma C, Craig T K, Rosenmund C, Rizo J, The Janus-faced nature of the C(2)B domain is fundamental for synaptotagmin-1 function, *Nat Struct Mol Biol.*, 2008, 15, 11, 1160-8
- [132] Yang X, Kaeser-Woo Y J, Pang Z P, Xu W, Südhof T C, Complexin clamps asynchronous release by blocking a secondary Ca(2+) sensor via its accessory  $\alpha$  helix, *Neuron.*, 2010, 68, 5, 907-20
- [133] Yu R C, Jahn R, Brunger A T, NSF N-terminal domain crystal structure: models of NSF function, *Mol Cell.* 1999, 4, 1, 97-107
- [134] Zilly F E, Sørensen J B, Jahn R, Lang T, Munc18-bound syntaxin readily forms SNARE complexes with synaptobrevin in native plasma membranes, *PLoS Biol.*, 2006, 4